Old Dominion University Research Foundation

DEPARTMENT OF MECHANICAL ENGINEERING
COLLEGE OF ENGINEERING AND TECHNOLOGY
Old DOMINION UNIVERSITY
NORFOLK, VIRGINA 23529

FABRICATION OF THERMOPLASTIC COMPOSITE LAMINATES HAVING FILM INTERLEVES BY AUTOMATED FIBER PLACEMENT

By,
A.B. Hulcher, Graduate Research Assistant
S.N. Tiwari, Principal Investigator
and
J.M. Marchello

Final Report for the period ending December 31, 2001

Prepared for:
National Aeronautics and Space Administration
Langley Research Center
Hampton, VA 23681-2199

Under
Cooperative Agreement NCC1-227
Dr. Norman J. Johnston, Technical Monitor
Materials Division
ODURF #150101

April 2001

DEPARTMENT OF MECHANICAL ENGINEERING
COLLEGE OF ENGINEERING AND TECHNOLOGY
Old DOMINION UNIVERSITY
NORFOLK, VIRGINA 23529

FABRICATION OF THERMOPLASTIC COMPOSITE LAMINATES HAVING FILM INTERLEVES BY AUTOMATED FIBER PLACEMENT

By,
A.B. Hulcher, Graduate Research Assistant
S.N. Tiwari, Principal Investigator
and
J.M. Marchello

Final Report for the period ending December 31, 2001

Prepared for:
National Aeronautics and Space Administration
Langley Research Center
Hampton, VA 23681-2199

Under
Cooperative Agreement NCC1-227
Dr. Norman J. Johnston, Technical Monitor
Materials Division
ODURF #150101

April 2001

DEPARTMENT OF MECHANICAL ENGINEERING
COLLEGE OF ENGINEERING AND TECHNOLOGY
Old DOMINION UNIVERSITY
NORFOLK, VIRGINA 23529

FABRICATION OF THERMOPLASTIC COMPOSITE LAMINATES HAVING FILM INTERLEVES BY AUTOMATED FIBER PLACEMENT

By,
A.B. Hulcher, Graduate Research Assistant
S.N. Tiwari, Principal Investigator
and
J.M. Marchello

Final Report for the period ending December 31, 2001

Prepared for:
National Aeronautics and Space Administration
Langley Research Center
Hampton, VA 23681-2199

Under
Cooperative Agreement NCC1-227
Dr. Norman J. Johnston, Technical Monitor
Materials Division
ODURF #150101

April 2001

FOREWARD

This is a final report on the research work completed on the project "Investigation of Advanced Composite Materials and Automated Processes". The work was done under the subcategory "Automated Processes" and attention was directed on "Fabrication of Thermoplastic Composite Laminates Having Film Interleaves By Automated Fiber Placement."

This work was supported by the NASA Langley Research Center through the Cooperative Agreement NCC1-227. The Cooperative Agreement was monitored by Dr. Norman J. Johnston, Materials Division, Mail Stop 226, NASA Langley Research Center, Hampton, Virginia 23681-2199

FABRICATION OF THERMOPLASTIC COMPOSITE LAMINATES HAVING FILM INTERLEAVES BY AUTOMATED FIBER PLACEMENT

ABSTRACT

Experiments were carried out at the NASA Langley Research Center automated fiber placement facility to determine an optimal process for the fabrication of composite materials having polymer film interleafs. A series of experiments was conducted to determine an optimal process for the composite prior to investigation of a process to fabricate laminates with polymer films. The results of the composite tests indicated that a well-consolidated, void-free laminate could be attained. Preliminary interleaf processing trials were then conducted to establish some broad guidelines for film processing. The primary finding of these initial studies was that a two-stage process was necessary in order to process these materials adequately. A screening experiment was then performed to determine the relative influence of the process variables on the quality of the film interface as determined by the wedge peel test method. Parameters that were found to be of minor influence on specimen quality were subsequently held at fixed values enabling a more rapid determination of an optimal process. Optimization studies were then performed by varying the remaining parameters at three film melt processing rates. The resulting peel data were fitted with quadratic response surfaces. Additional specimens were fabricated at levels of high peel strength as predicted by the regression models in an attempt to gage the

accuracy of the predicted response and to assess the repeatability of the process. The overall results indicate that quality laminates having film interleaves can be successfully and repeatably fabricated by automated fiber placement.

TABLE OF CONTENTS

Section Page

LIST OF SYMBOLS

Symbol

ASTM	American Society for Testing and Materials
DCB	Double cantilever beam
ENF	End-notched flexure
G_{IC}	Strain energy release rate in opening mode fracture
G_{IIC}	Strain energy release rate in shearing mode fracture
IITRI	Illinois Institute of Technology Research Institute
IR	Infrared
MODE I	Opening mode due to normal stresses
MODE II	Sliding mode due to in-plane shear stresses
NASA	National Aeronautics and Space Administration
PEEK	Poly ether ether ketone
RT	Room temperature
SEM	Scanning Electron Microscope
SI	International system of units
SS_e	Sum-of-squares of error
SS_m	Sum-of-squares error for the model
T_g	Glass transition temperature
T_m	Melt temperature

Units of Measure

C	Celsius
cm	Centimeter
J	Joules
K	Kelvin
kN	Newtons x 10^3
ksi	Pounds per square inch x 10^3
m	Meter
mm	Millimeter
Pa, kPa	Pascals, kiloPascals
s	Seconds
ssc	Standard cubic centimeters
W, mW	Watts, milliWatts
μm	Meters x 10^{-6}

LIST OF TABLES

Table Page

LIST OF FIGURES

Figure Page

Figure Page

Figure Page

SECTION 1

INTRODUCTION

Fiber-reinforced polymer-matrix composite materials offer significant advantages over metals in aerospace and other applications. Properties such as high strength-to-weight ratio, low thermal expansion coefficient, excellent fatigue behavior and solvent resistance make these materials attractive alternatives to more conventional materials in both structural and non-structural applications. Additionally, these materials may be highly tailored to maximize their mechanical properties. Variations such as fiber orientation, laminate stacking sequence, and modifications of the composite matrix resin component can yield a variety desired of material and structural properties.

1.1 Automated Fabrication Technologies for Composite Materials

Fabrication of laminated composite materials may be accomplished by various processing methods. Traditional fabrication technologies such as hand lay-up are both labor and time intensive. In an attempt to increase productivity, improve quality, and reduce costs, much effort has been focused in recent years toward the development of automated fabrication methods for composites. Specific advantages of such methods include the reduction or elimination of manual labor, increases in fabrication speed and quality, and increases in part complexity. Automated processes include such methods as filament winding, automated tape lay-up, and automated fiber placement.

Filament winding is a method of fabrication currently in widespread use in the composites industry. This method consists of the winding of pre-impregnated fibers onto a rotating tool surface. The desired part thickness is obtained and the mandrel is removed from the part prior to autoclave or oven post-processing. The filament winding process is limited in that fibers are held in place by tension in the tow, allowing only positive curvature part geometry to be fabricated. This processing method is used extensively and with great success, however, in the fabrication of such components as rocket motor nozzles, pressure vessels, storage tanks, pipes, and shafts.

Automated tape lay-up has a distinct advantage over filament winding in that both positive and negative curvature components may be successfully fabricated. Material in tape form is fed to a robotic placement head and tacked onto a placement tool. The machine is preprogrammed to fabricate the entire component, ply-by-ply, to the required thickness and shape. Thermosetting materials are typically used in tape lay-up fabrication. These materials are usually tacky at room temperature and therefore must be fed to the placement head at low temperatures to maintain material stiffness and to ease material feeding operations. The material is heated just prior to lay-down to increase tack and promote light adhesion to the substrate material. The completed laminate must then undergo final processing in either an autoclave or oven to achieve full cure [1].*

Automated fiber placement shares many of the key characteristics of automated tape lay-up. The important distinction is that with fiber placement, thermoplastic matrix

---

* The model used for formatting this work was the Journal of Composite Materials.

resins, instead of thermosetting materials, are used. Fully consolidated thermoplastic tape or ribbon is fed to a heated placement head where the temperature of both the incoming material and the upper substrate surface are brought to above the matrix melt temperature. A compaction device is employed to effect intimate contact and consolidation between plies. Ideally, the optimization of placement parameters such as consolidation force, placement speed, and processing temperatures results in fully consolidated composite components needing no post-processing treatment. This is an important advantage in that very large structures and components may be fabricated in-situ. Prior to the development of fiber placement technology, the size of such composite parts was limited to the physical dimensions of the autoclave, where final processing was necessary. The ability to fabricate very large structures without the need for large expensive autoclaves has made possible new and important applications for composite materials [2-6].

1.2 Interleaving of Composites for Mechanical Property Enhancement

The enhancement of the mechanical properties of composite materials through various methods has been investigated in some detail over the past several years. Most of these methods have focused on improving the damage tolerance, interlaminar fracture toughness, and fatigue life of these materials. Design approaches for optimization of composite material mechanical properties include laminate stacking sequence, z-axis stitching, modifications to the matrix resin, and hybrid laminate concepts including resin and metal interleaves [7].

The most important material property that governs the fatigue behavior of composite materials is the toughness of the matrix resin component. Most methods of fabrication of laminated composites result in resin-rich regions between plies. Most composite material failures occur as the result of ply delamination, especially in mechanical fatigue. Attention has been directed toward the toughening of this inter-ply region. This may be achieved by modification of the matrix resin or by the incorporation of thin discrete layers of tough, ductile resin between the composite plies. The addition of such interleaves has been shown to improve fatigue and impact properties by increasing the interlaminar fracture toughness. Ideal materials for use as interleaves are tough, high strain-to-failure thermoplastic matrix resins that reduce shear stress concentrations at the ply interfaces.

Sela and Ishai present a review of the state of the art in interlaminar fracture toughness and its relationship to structural performance and damage tolerance in composites. One such method reported is the use of adhesive interleaving, which may significantly improve the interlaminar fracture toughness of composites. G_{IC} and G_{IIC} fracture toughness were reportedly increased nine-fold and seven-fold, respectively, using AS4/3502 composite and FM73 and FM300 adhesive strips. The optimal adhesive thickness for both fracture modes was reported to be 0.1-mm [8].

Dolan and Masters performed a study on carbon/bismaleimide composites interleaved with a 0.0127-mm thick thermoplastic film. The study centered on the characterization of these materials with respect to impact and delamination resistance. Tests performed included IITRI compression, open-hole compression, DCB, and ENF. Damage tolerance and compression fatigue tests were also conducted. Improvements in delamination and

impact resistance were reported. Increases in G_{IC} values of from 25% - 45% were also reported for the interleaved systems [9].

Analytical investigations of the effect of interleaves on the fracture behavior of laminated composites were conducted by Kaw and Goree. A fracture and crack growth model was developed and predictions of the model were presented. The results indicate that the interleaf provides a significant reduction in the stresses adjacent to the crack regions and that proper selection of interleaf material and thickness should improve the damage tolerance of these materials [10].

Lagace et al. conducted testing of interleaved composites to determine the effectiveness of such layers in preventing delaminations. Several different lay-ups of AS1/3501-6 graphite/epoxy composite with and without the FM300M adhesive film were fabricated and tested in tension. The interleaved specimens were fabricated with the film layer present only between plies having different angular orientations. The results of the study indicate that the addition of the film layer was successful in preventing delamination which correlated well with predictions. These results were attributed to the redistribution of interlaminar stresses in the test panels [11].

A study of the effect of resin interleaving on the fatigue properties of unidirectional epoxy composites was conducted by Partrige, Jaussaud, and Neyrat. Tension-tension fatigue tests were carried out, followed by mode II ENF static fracture testing on 913/E-glass and 920/T300 materials. The fatigue durability in both materials is reported. Mode II static toughness is reported to double, and the fatigue crack propagation rate reduced five-fold, with the inclusion of a 0.051-mm thick resin layer in the 920/T300 systems [12].

Interleaved graphite/epoxy prepregs were evaluated as part of a study by Hirschbuehler to investigate the toughness of composites. Laminates having a low modulus, high strain resin layer, and a high modulus matrix resin were fabricated and tested for interlaminar mode I fracture toughness and compressive strength after impact. Increases in fracture toughness of 20% and compressive strength after impact of 40-55% were reported [13]. Several other studies have been conducted on interleaving of composites for damage tolerance with similar improvements in performance reported [14-21].

1.3 Propellant Tank Barrier Films

The design and application of very large, novel composite structures and components is key to the successful development of the next generation of single-stage, reusable launch vehicles. Incorporated into these vehicles are very large cryogenic propellant tanks. In current designs, these tanks must serve an additional role as integral structural components of the launch vehicle. Laminated composite materials are being seriously considered for such tanks. An important materials issue concerning composite tanks in this application is the permeation resistance of the tank material to cryogenic liquid hydrogen. Thermal and mechanical cycling of the tank material during tank filling operations may lead to microcracking of the matrix resin and the loss of integrity within the tank wall material. Tailored matrix resin systems or film barrier layers designed to be capable of withstanding such fatigue loading cycles and having favorable permeation resistance to specific fuels are being investigated for these applications.

Though the addition of barrier film interleaves into composite laminates increases the fatigue properties and impact damage resistance of the composite, they also reduce the specific strength of the material due to increased part weight, which is unacceptable in weight-critical applications such as launch vehicles. Currently under development for barrier film and composite matrix resin applications are novel nano-composite materials made from organo-clay materials [22]. Such materials form lamellar structures that both increase the modulus of the polymer and provide additional barrier properties. The use of these materials may actually increase the overall specific strength of the material, while providing the permeation resistance needed in cryogenic fuel tank applications. These materials may be used as barrier film or as matrix resin systems. Additionally, some studies indicate that thermoplastic interleaving materials may be superior to thermosetting materials in low-temperature, cryogenic applications [23].

1.4 Objectives and Format of Presentation

As mentioned previously, automated fiber placement technology is necessary for the fabrication of very large-scale composite structures. In the case of fuel tank applications, it may be further desired to incorporate a discrete barrier layer or layers that are impermeable to specific fuels. The issue then becomes one of determining if the fiber placement method may be used to successfully process composite laminates having these interleaf barrier films.

The fundamental objective, therefore, of the current study is to determine the viability of fabricating composite laminates having film interleaves by fiber placement. The

strength of the film-to-composite bond, as measured by the wedge peel test, will be the primary quality indicator in determining a set of processing parameters. Film-to-composite consolidation quality (interfacial void content), as-processed film thickness, and film layer integrity will also be used as indicators to determine the adequacy of the process.

A brief description of the NASA Langley Fiber Placement Facility is presented in Section 2, with discussions of the heated-head placement machine and associated machine control software. Section 3 provides information on the thermal and processing properties of the materials used in the study. A description of the fiber placement process development for the PEEK/IM7 composite and the PEEK film interleaf laminates are given in Section 4 and Section 5, respectively. A summary of the study, including conclusions and suggestions for future work, is presented in Section 6. A description of the wedge peel test, including a short literature study on wedge and peel test methods is given in Appendix A. The design of a fiber placement trailing shoe system is detailed in Appendix B. Finally, presented in Appendix C, are the results of a study on the hydrogen permeability characteristics of PEEK matrix resin systems and other selected composite materials.

SECTION 2

NASA LANGLEY FIBER PLACEMENT FACILITY

2.1 Placement Machine Hardware

The NASA Langley Research Center Fiber Placement Facility was designed as a research tool to investigate processing and machine hardware design issues relating to fiber placement fabrication methods and to conduct studies on the feasibility of fabricating novel material forms, including high-temperature matrix resin systems and hybrid laminates, by this method. The placement machine consists of an Asea Brown Boveri (ABB) Model IRB 6000, six-axis fully articulating robot. The robot heated placement head end-effector was designed and fabricated by the Automated Dynamics Corporation, Schenectady, NY. A fully programmable rotating spindle is included which provides a seventh axis of motion for fabrication of cylindrical components. Aluminum cylindrical placement tooling mandrels of 14.6-cm, 45.7-cm, and 61.0-cm in diameter are available for fabrication of cylindrical shell articles. A heated flat tool is also available for fabrication of open-section flat panels for material property specimen evaluations [24].

The fiber placement heated-head as used in the present study is shown in Figure 2.1. The head consists of a servo-actuated tape dispensing system that feeds material from the spool creel, through a guide chute, and onto the placement surface. The head is capable of placement of up to five 0.635-cm wide composite ribbons or one 3.17-cm wide composite tape. A combination of hot gas and radiant energy heat sources are available to preheat both the incoming and substrate materials prior to laminate compaction and consolidation.

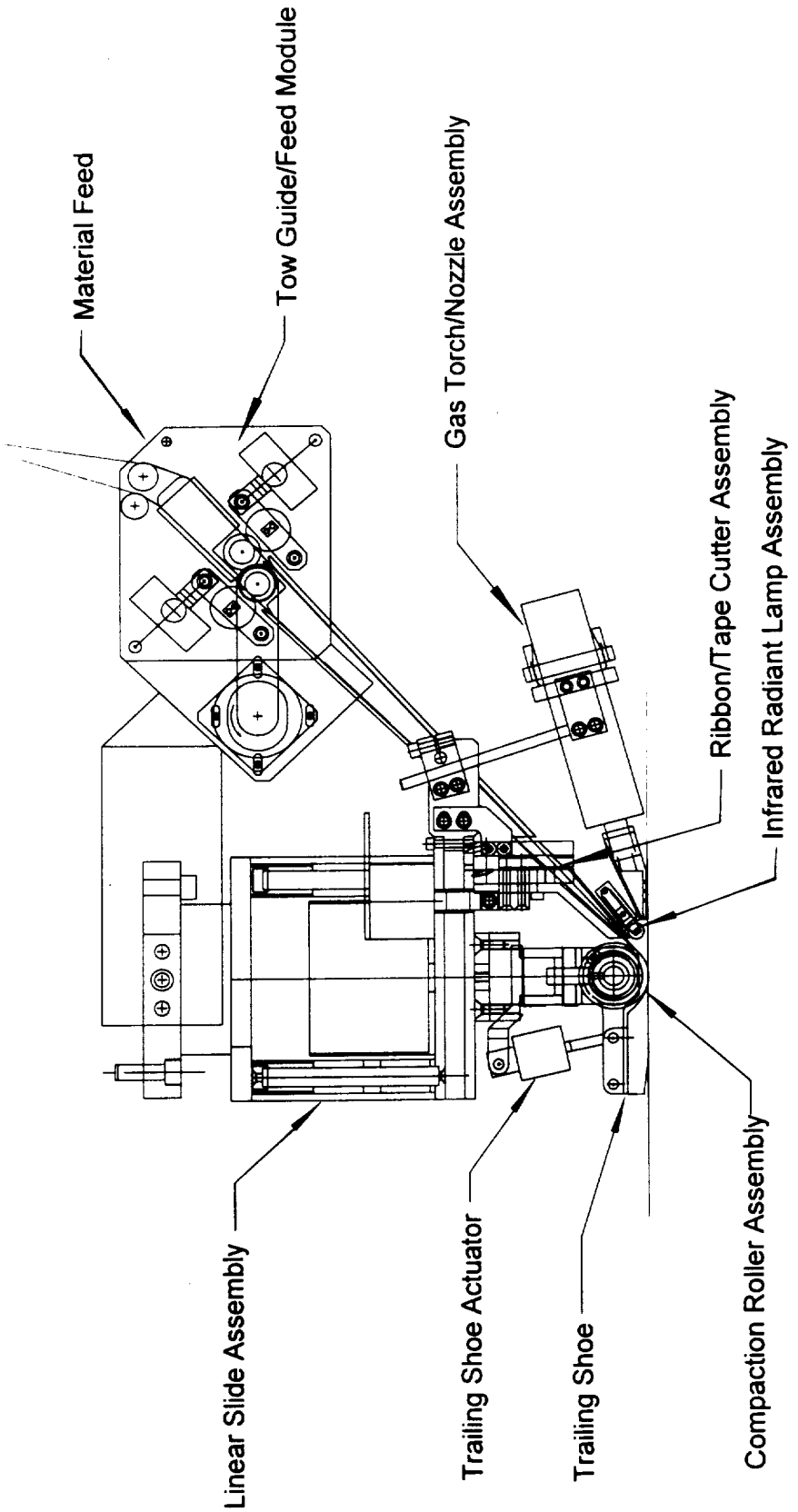

Figure 2.1. *NASA Langley fiber placement machine heated-head assembly.*

The gas source consists of two nitrogen torches that are capable of heating the gas to 900°C. The heated gas is directed into the nip-point region during placement via a single nozzle shared by the torches. The radiant heat source consists of a Ushio 1000W tungsten halogen infrared lamp [25]. The preheating sources may be implemented either individually or in tandem during processing, depending on the thermal properties of the composite and other placement parameters. The incoming preheated material is fed beneath a compaction roller that may be heated to up to 500°C by a cartridge resistance heater located within the roller. Gas torch and compaction roller temperature control are accomplished by means of closed-loop feedback control systems. Roller temperature is monitored by use of an infrared temperature sensor located behind the roller. Torch temperature is monitored by two thermocouples that are exposed to the gas stream within the shared gas exit nozzle. Laminate consolidation is effected by a pneumatically actuated compaction roller and is capable of producing consolidation loads up to 1.47-kN.

Material adhesion to the compaction roller during fabrication at elevated roller temperatures results in roller fouling, ply wrinkling, and fiber damage in the placed material. This results in rough, uneven substrate surface and decreases the probability of complete intimate contact between this surface and the following ply, resulting in high void content at the ply interfaces. A trailing shoe attachment has been added to the placement head to reduce or eliminate ply damage. The addition of this shoe system has brought about a significant reduction in the adhesion of the material to the roller and thus a marked improvement in panel surface quality. The shoe is actuated pneumatically and is slave-controlled to the roller compaction force actuator solenoid valve. Shoe actuation

timing for both extend and retract modes is adjustable by use of electronic delay circuitry. A similar trailing shoe for fabrication of cylindrical parts has been designed and is detailed in Appendix B.

2.2 Control Software

The Langley fiber placement machine robot is computer-controlled through a personal computer interface. The creation of part placement files is accomplished by creating several intermediate files according to pre-defined program formats. These files are then combined via software commands to create actual placement run files.

The creation of an actual placement file begins with the creation a mandrel, or tool file, and a ply file. The mandrel file is created to define the spatial coordinates of the component to be fabricated relative to the robot joint coordinates. The ply file contains such information as composite tape strip width, required strip placement angle, and strip overlap and gap tolerances. The mandrel file and ply file are then combined via a command to a path generator program that creates a points file. The points file defines the fiber placement of strips in terms of the mandrel coordinates. A processing file which describes basic placement head functions such as ply placement rate, strip pre-feed length, off part machine speed, and head extension and retract timing is then created and combined with the points file. The combination of these files results in an executable placement file. This file contains all of the necessary information that allows the machine to carry out the fiber placement of a ply.

SECTION 3

MATERIALS

3.1 PEEK Neat Resin Processing Properties

The composite tape used in the present work was comprised of unidirectional IM7 intermediate modulus fibers in a PEEK (poly-ether-ether-ketone) matrix. The material was supplied from Cytec Fiberite Inc. in spools of 3.18-cm wide, 0.014-cm thick tape. The average resin content of the tape used in the study was 33% by weight. PEEK is a tough engineering thermoplastic having up to 48% crystallinity content. The percentage of crystallinity is dependent on the thermal history of the polymer, with higher percentages of crystallinity produced during lower material cool-down rates. High crystalline content increases the resistance of the resin to chemical and solvent attack and also increases the elastic modulus. The disadvantage of higher crystalline content is the accompanying reduction in fatigue and impact properties due to a reduction in matrix toughness. Additionally, automated processing methods such as fiber placement of these systems can result in crystallinity gradients in two or more directions relative to the laminate. This may result in unpredictable panel warpage due to resin volumetric changes associated with the development of crystalline structures [26-29]. Listed in Table 3.1 are some processing properties of PEEK resin [30].

Table 3.1 PEEK neat resin processing properties [30].

Property	Value
Glass Transition Temperature, T_g (°C)	143
Melt Temperature, T_m (°C)	343
Maximum Crystallinity (%)	48
Specific Gravity	
Amorphous	1.265
Fully Crystalline	1.320
Processing Temperature Range, (°C)	371-399
Melt Viscosity Range @400°C, 1/1000 s^{-1}, (Pa·s)	400-500

3.2 Film and Composite Thermal Properties

Thermal analysis by differential scanning calorimetry was carried out on a Shimadzu Model DSC-50 calorimeter on both the as-received 0.0076-cm PEEK film and the PEEK/IM7 composite tape. The temperature ramp was held constant for both runs at 20°C/min until a peak temperature of 400°C was reached. The resulting thermal scans for the composite and film are presented in Figures 3.1 and 3.2, respectively.

Analysis of the thermogram for the composite reveals a well-defined glass transition at 134°C, a crystallization exotherm at 178.5°C, and a melt endotherm at 342°C. The exothermic peak at 178.5°C is characteristic of the cold-crystallization behavior of PEEK. Such crystallization behavior occurs when the polymer chains attain sufficient mobility at just above the glass transition temperature to begin formation of crystallites [31].

The thermogram for the film shows a glass transition at 141°C and a crystallization exotherm at 179°C. The endotherm at 226°C is most probably solvent; this peak was not present after a second DSC run of the specimen.

3.3 Composite Tape Physical Properties

The as-received PEEK/IM7 composite tape was tested to determine void content by both acid-digestion and optical image analysis. Results from digestions indicate a void content of less than 1%. Void content by optical image analysis was performed on an Olympus BH-2 laboratory microscope using an Olympus Cue 2 image acquisition and analysis system. Thirty screen images totaling 0.06-cm^2 of area were analyzed. The mean void content was found to be 0.45% with a standard deviation of 0.25%.

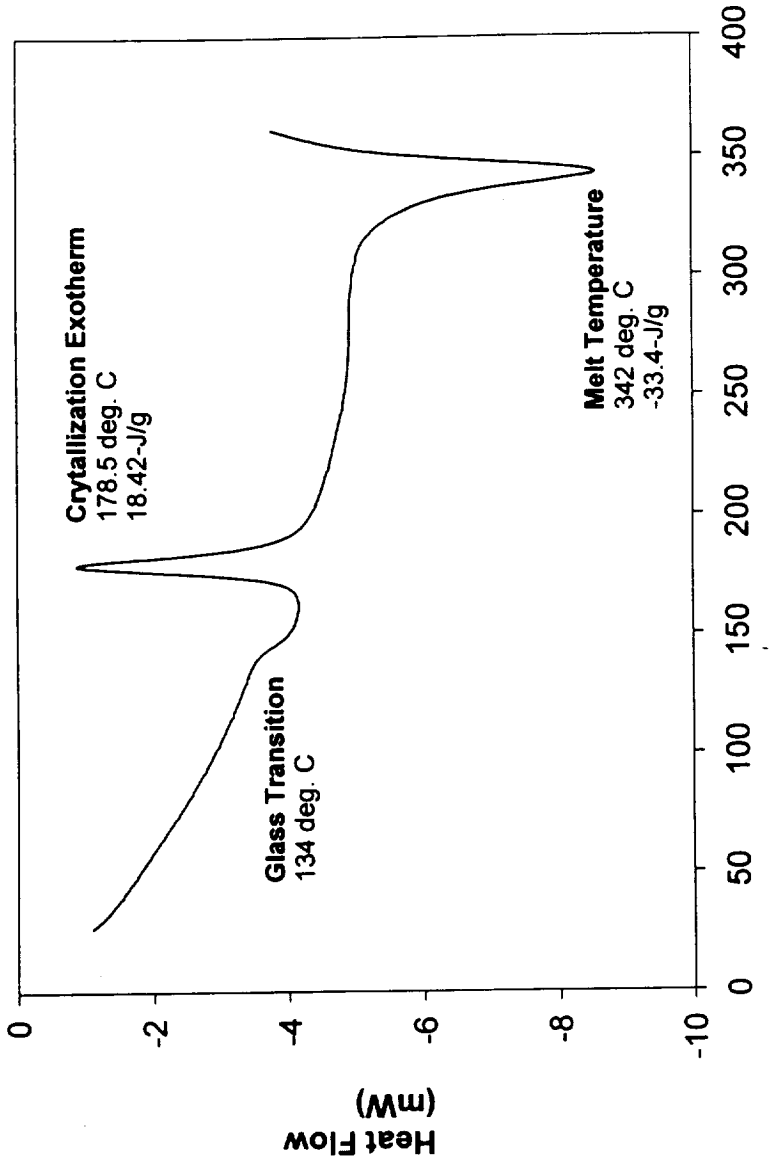

Figure 3.1. *Differential scanning calorimetry thermogram of as-received PEEK/IM7 composite tape.*

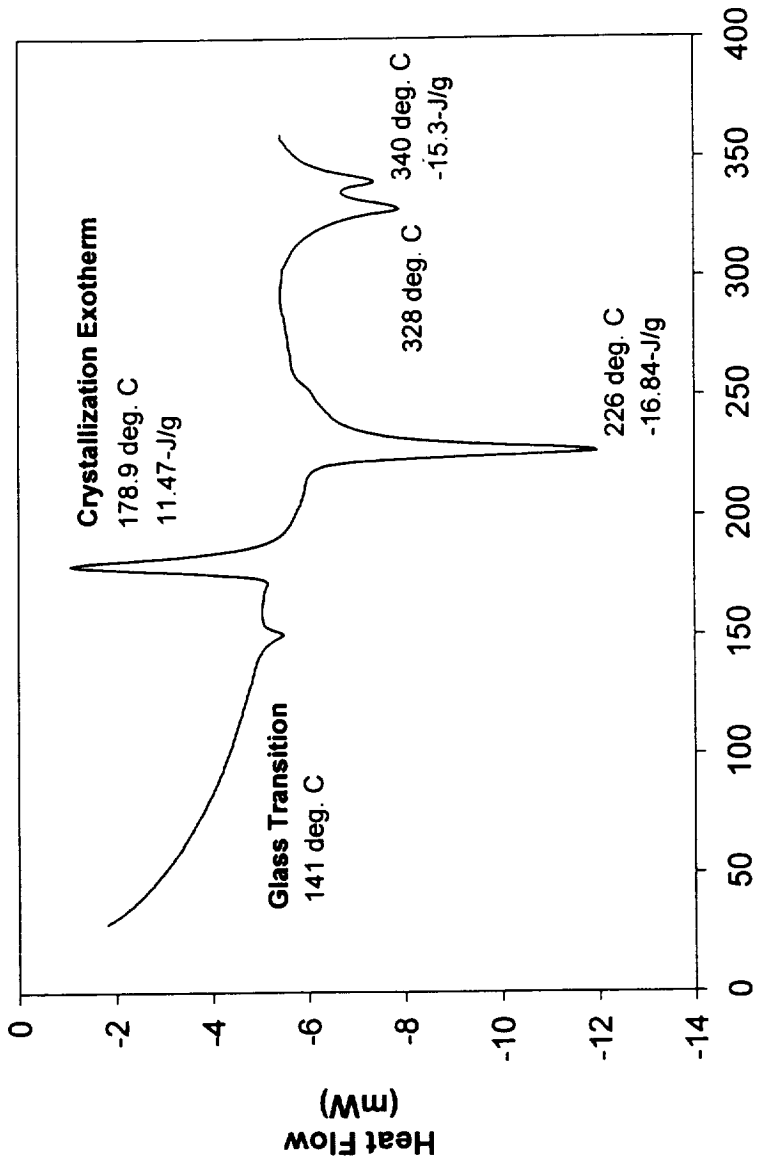

Figure 3.2. *Differential scanning calorimetry thermogram of as-received 0.0076 cm PEEK film.*

A photomicrograph of the as-received composite tape is shown in Figure 3.4. Five specimens of the 0.014-cm thick tape are shown. The micrograph reveals smooth, flat ribbon surfaces on both sides of the tape and low void content.

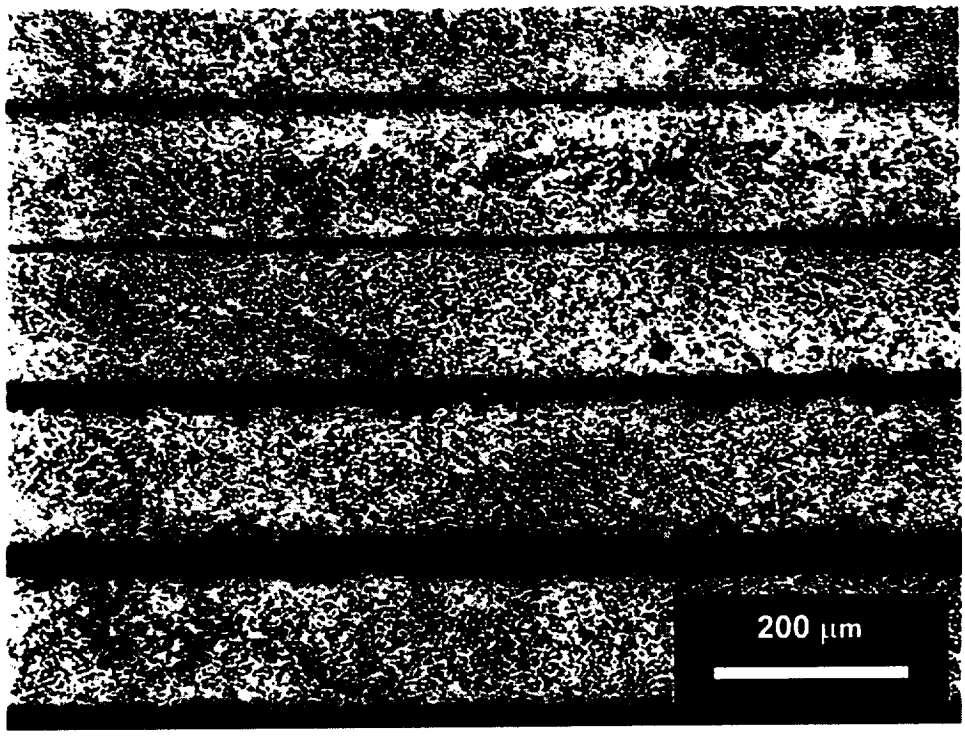

Figure 3.3. *Photomicrograph of as-received PEEK/IM7 composite tape.*

SECTION 4

COMPOSITE PROCESS DEVELOPMENT

4.1 Preliminary Processing Trials

Initial studies were performed to obtain the lower and upper bounds of a processing window for the fiber placement of the composite. This would allow for the narrowing of processing variable ranges during a more in-depth designed-experiment study.

A preliminary study focusing on the interfacial bond strength of the composite was conducted. The strength of the interface was measured by the wedge peel test, which is described in detail in Appendix A. Two-ply peel specimens were placed with the 3.17-cm wide fully consolidated composite tape mentioned previously. The specimens were fabricated on a flat, unheated steel tool. The tool was prepared by applying 7.62-cm wide Kapton tape to the surface. To facilitate the adhesion of the first composite ply to the tool, the surface of the tape was roughened with 400-grit emery paper. The placement processing rate and the IR lamp power were held constant at 2.54-cm/s and 100%, respectively. The hot gas torch temperature was varied from 550°C to 850°C in increments of 100°C. Three peel specimens were fabricated at compaction loads of 0.44-kN, 0.89-kN, and 1.33-kN at each of the torch temperature settings. A Kapton film insert was taped over the end of the first ply prior to the placement of the second ply to serve as a crack starter for peel testing. The as-placed length of the specimens was 45.7 cm. The test specimens were cut in half prior to peel testing to provide additional material for optical microscopy and void content analysis.

The wedge peel tests were performed on a SATEC model T1000 test frame at a cross-head rate of 1.27-cm/s. Except in cases of specimen cohesive failure, data was collected over 15.24-cm of specimen length. The data were then averaged and normalized with respect to specimen width.

The variation in average peel strength with compaction load is presented below in Figure 4.1. Increases in peel strength with compaction load are evident. Specimen placement at torch temperatures of 650°C resulted in the highest average strength values at each of the compaction load settings. Peak peel strength values were also recorded and exhibited similar trends. It should be noted that cohesive failure was not observed in any of the specimens placed at a compaction load of 0.44-kN but was observed in all but two of the specimens fabricated at higher compaction loads.

The effect of compaction load on the increase in tape width is illustrated in Figure 4.2. A direct relationship between the compaction load and the amount of tape width increase is evident over the range of torch temperatures. There also exists a somewhat weaker relationship between the magnitude of width increase and torch temperature. The relationship between peel strength and tape width is graphically presented in Figure 4.3. The general trend exhibited is that as tape width is increased during placement, peel strength also increases. This increase in strength is thought to be a result of the increased melt flow of the matrix resin. The benefit of increased matrix resin flow in terms of peel strength is evident.

The purpose of the initial peel tests was to gain information regarding the approximate range of torch temperatures and compaction forces that should be investigated in a

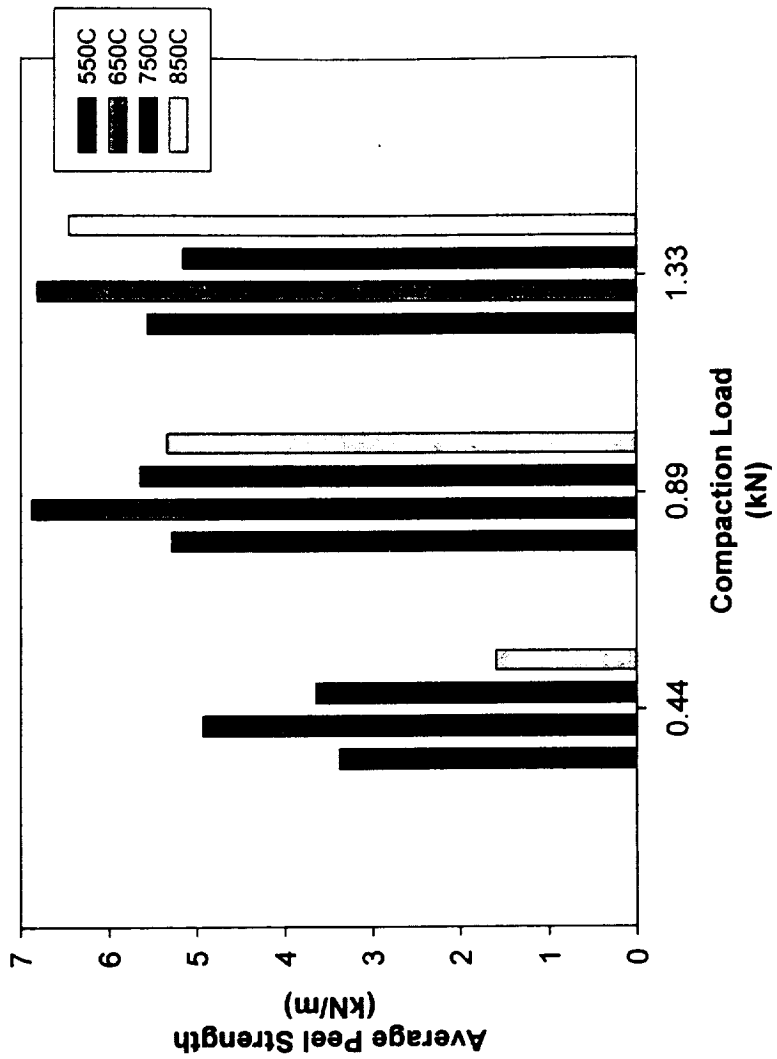

Figure 4.1. *Average peel strength at various compaction loads for the preliminary composite processing trials.*

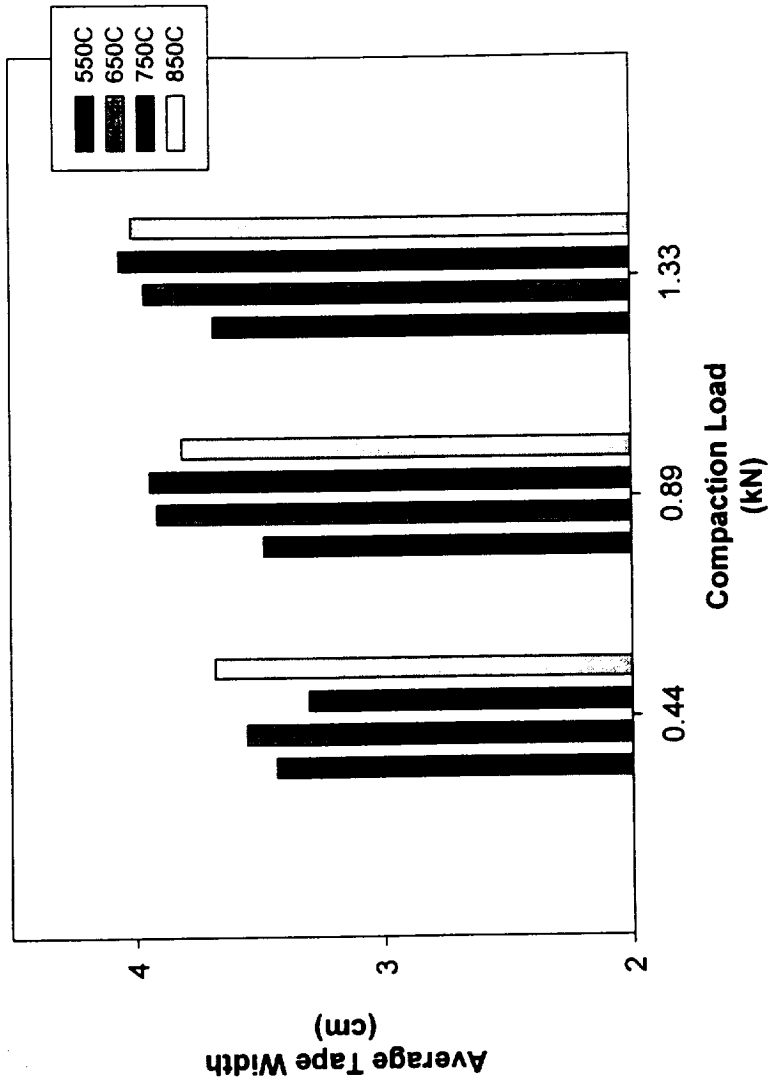

Figure 4.2. *Variation in tape width with compaction load for the preliminary composite processing trials.*

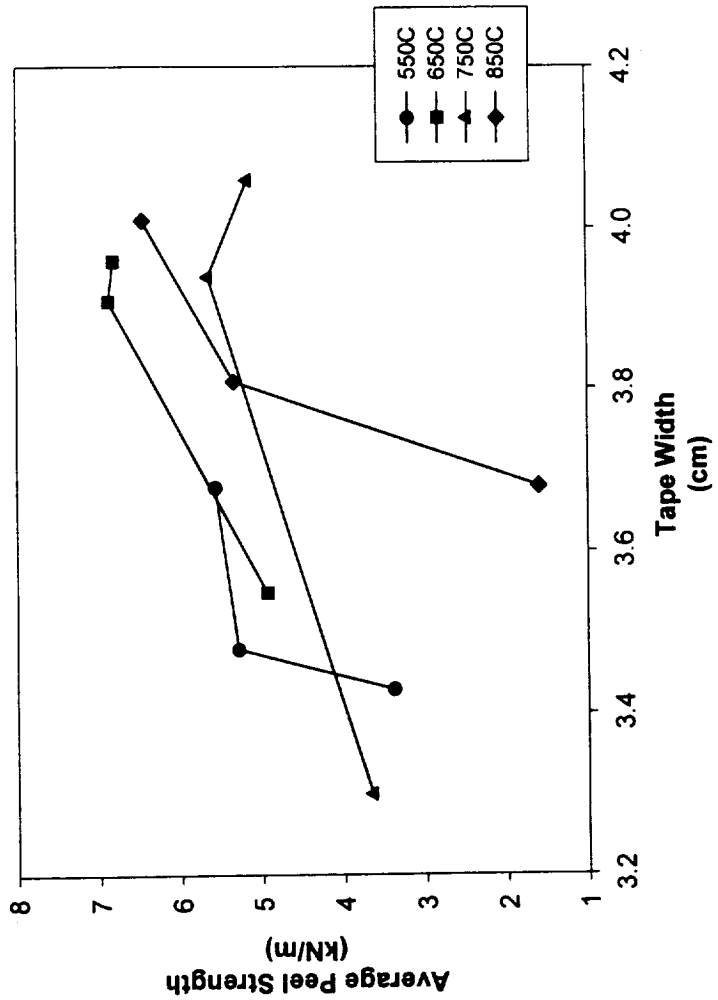

Figure 4.3. *Average peel strength variation with tape width for the preliminary composite process development trials.*

designed-experiment approach. Such an approach would provide more detailed information on the process and lead to a well-defined range of optimal placement variables. The resulting placement conditions that yield the highest peel strength values will then be used for processing the composite during the film inter-ply processing study to follow.

Based on peel strength values, compaction loads in the range of 0.89-kN to 1.33-kN are necessary to provide the force necessary to effect adequate resin flow and intimate contact between the composite plies. This is also evidenced by the increased tape widths, as shown in Figure 4.2. A torch temperature of 650°C was found to give the highest peel strengths for each of the compaction load values.

4.2 Process Optimization by Design of Experiments

A designed experiment approach was used to further investigate the effects of the processing variables on panel quality and to determine optimal settings for gas torch temperature and compaction force. The Box-Wilson method was chosen as the designed experiment approach. This method is a central composite, rotatable design that is of the type generally used for the exploration of quadratic response surfaces.

A torch temperature range of 600°C - 800°C and a compaction load range of 0.67-kN – 1.20-kN were used in the designed experiment. These ranges were selected based on the results from the previous trials and the range limits of the processing variables. Since the Box-Wilson design creates experiments with variables located outside of the given

ranges, these ranges must be chosen so that the values at the star points are within the capabilities of the placement machine.

Held constant for the Box-Wilson experiments were placement speed, roller temperature, and IR lamp output at 2.54-cm/s, 475°C, and 100%, respectively. Experience gained with the wedge peel test indicates that the range of interlaminar bond strengths for which the tests can give meaningful data can be extended by use of four-ply peel specimens. It is because of this that four-ply specimens were fabricated for testing. Further discussion on the use of four-ply peel specimens is presented in Appendix A.

The results of the preliminary trials detailed in Section 4.1 indicate that compaction loads of 0.44-kN result in the lowest peel strengths recorded. At compaction loads of 0.89-kN and 1.33-kN, peel strengths are at the highest values and are relatively constant. Therefore, the designed experiment variable range for the compaction load was 0.667-kN - 1.20-kN and was 600°C - 800°C for the torch temperature. As in the preliminary study, the placement speed was held constant at 2.54-cm/s. Compaction roller temperature and lamp percent output were also held constant at 475°C and 100%, respectively.

4.3 Results and Conclusions

A set of thirteen experiments was generated using XSTAT statistical experiment design software. The schedule of experiments performed and the results of the peel tests are presented in Table 4.1. Trial runs number 2, 4, 6, 7, and 12 are replicated tests and

Table 4.1 Experimental design placement worksheet and results for process development of the composite.

Trial Run Number	Compaction Load (kN)	Torch Temperature (°C)	Peak Peel Strength (kN/m)	Average Peel Strength (kN/m)
1	0.934	558.6	7.14	4.73
2	0.934	700.0	8.84	5.99
3	1.31	700.0	11.06	5.79
4	0.934	700.0	9.63	5.81
5	0.934	841.4	5.10	3.64
6	0.934	700.0	9.93	7.21
7	0.934	700.0	9.82	7.86
8	1.20	600.0	9.33	7.04
9	1.20	800.0	9.79	6.81
10	0.667	800.0	6.52	4.40
11	0.556	700.0	8.18	6.58
12	0.934	700.0	8.26	6.75
13	0.667	600.0	9.12	7.25

are designed to provide a measure of experimental accuracy. Peak and average peel strength data for each test specimen is listed in the table. A quadratic model was specified for regression of the data. A separate quadratic regression equation was generated for both the peak and average peel data and was used to generate a response surface for each as a function of compaction load and torch temperature.

Statistical analyses were then conducted to determine the goodness-of-fit of the regression models to the experimental data. An analysis of the standard deviation about the regression for the average peel data indicated a 70% probability that an additional measurement of this value within the region under investigation would fall within 1.029 units of the predicted response. Analysis of the peak peel data indicated a 70% probability that any additional measurement will be within 0.71 units of the predicted response. The R-squared value, which is the explained variation about the mean, was 0.883 for the peak data, and 0.603 for the average data; the R-squared value for a perfect fit is unity. The sum of the residuals (the observed minus the predicted values of the peel data) for both the peak and the average peel strengths sum very close to zero. This is as expected for a least squares regression model containing a constant term. The analysis of variance results for the peak strength regression model indicated a 99.2% confidence that the regression equation is non-zero and a 50.5% confidence that pure error explained a lack of fit. Similar analysis for the regression model of the average peel strength indicated an 81.9% confidence of a non-zero regression equation and a 25.3% confidence that pure error explained a lack of fit. Based upon these statistical considerations, a higher degree of confidence could be placed in the regression model of the peak strength data. The

resulting quadratic response surfaces for both the average and peak peel strength data are presented below in Figures 4.4 and 4.5, respectively. Similarities in the two plots are evident. Peel strength values in both of the plots are observed to decrease at intermediate values of compaction load at each extreme of torch temperature. Additionally, a broad region of higher strength values is observed for intermediate values of both compaction force and torch temperature. Unexplained regions of high strength are present in the Figure 4.4. Each of the plots exhibit a region of interest at high consolidation load and intermediate torch temperature. In Figure 4.4, it is unclear whether the strength values increase or decrease in this region. The plot of Figure 4.5 would indicate that the ideal placement conditions in terms of peak peel strength are obtained at torch temperatures of 700°C and compaction loads of 1.33-kN. Data obtained during preliminary investigations, as reported in Section 4.1, tend to support these conclusions.

Regions of minimum strength values in both plots at lower torch temperatures may be due to inadequate supply of thermal energy to the material, resulting in incomplete melt flow of the matrix and therefore poor interfacial healing. At higher torch temperatures, low strengths could be contributed to possible thermal degradation of the matrix resin. The improvement in strengths at greater loads and similar torch temperatures may be explained by higher thermal dissipation rates, leading to a decrease in actual peak resin temperature. This dissipation could be due to an increase in resin melt and flow and to more intimate contact between the incoming and substrate plies, both the result of higher consolidation forces.

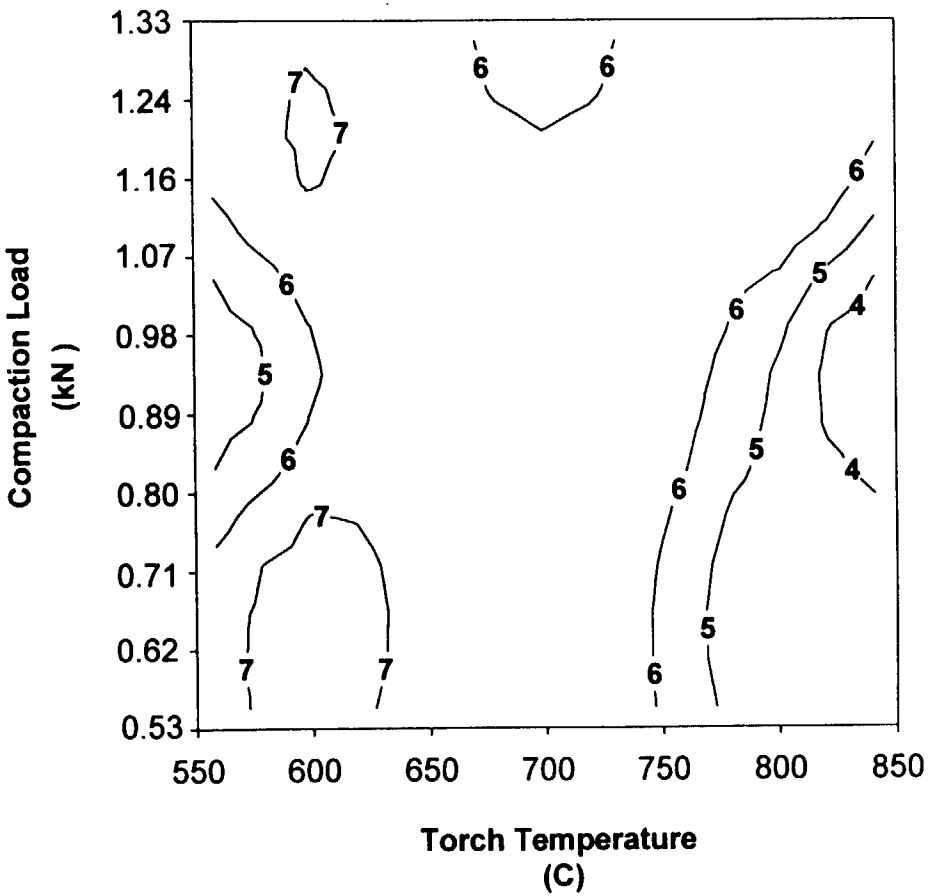

Figure 4.4. Contour plot showing average peel strength in kN/m as a function of torch temperature and compaction load for the experimental range of interest.

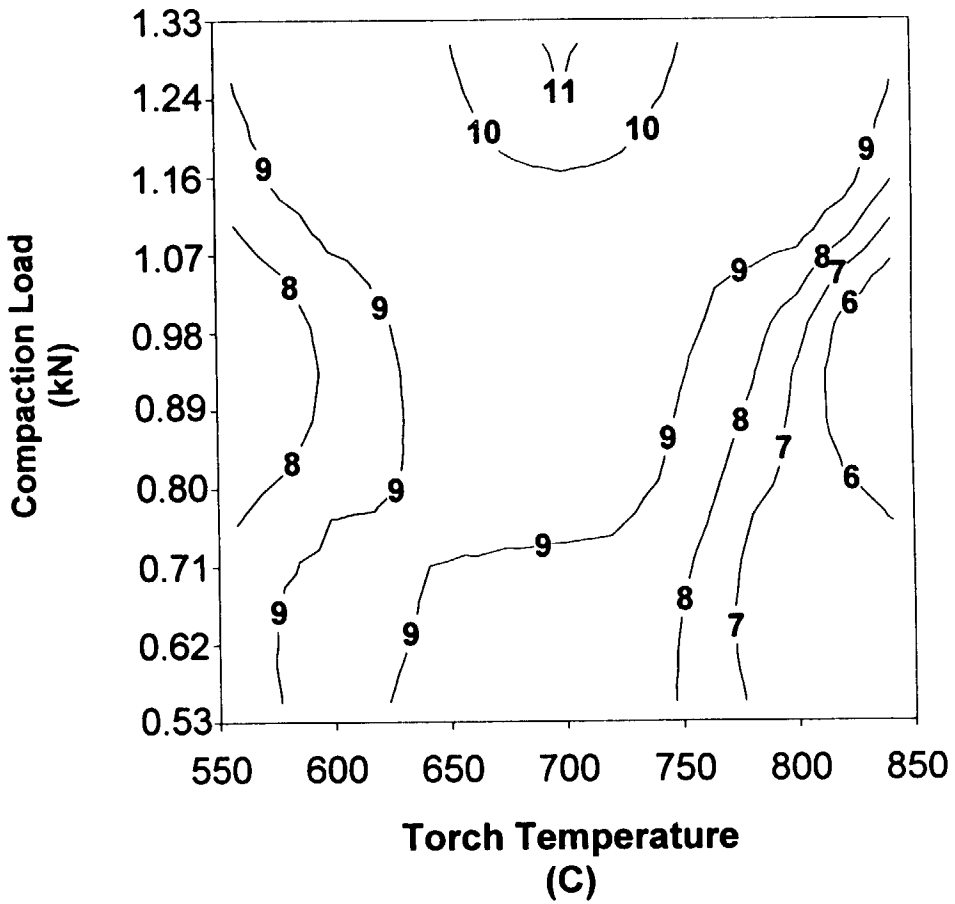

Figure 4.5. *Contour plot showing peak peel strength in kN/m as a function of torch temperature abd compaction load for the experimental range of interest.*

Void content analysis was performed on specimens taken from each of the 13 experimental runs. Specimen samples were potted and polished on a BUEHLER Vanguard Automated Polishing System. Image analysis was performed on an Olympus BH-2 laboratory microscope using an Olympus Cue 2 image acquisition and analysis system. Void content analysis was performed at a magnification of 200X, resulting in an image area of 0.002-cm^2. Thirty screen images per specimen were analyzed for a total area of 0.06-cm^2 per specimen. The average void percent and standard deviation results determined from the image analysis are presented in Table 4.2.

In an attempt to determine if a correlation between peel strength and void content existed, linear regressions were performed on cross-plots of the void percent as functions of both the average and peak peel strength data. Regression analysis was performed on the data to quantify the goodness-of-fit of the regression model. The cross-plots of the void content percent versus average peel strength and peak peel strength, including 95% confidence limits, are presented in Figures 4.6 and 4.7, respectively.

Statistical analysis of the linear regression resulted in an R-value of 0.521 for the average peel data and an R-value for the peak data of 0.517. These values indicate a weak relation between peel strength and void content. Additionally, the power of the fit, which is the probability that the model correctly describes the relationship of the dependent to independent variables, was 0.45 for the average peel strength and 0.44 for the peak strengths. The minimum value required to establish a positive relation between variables is 0.80. This indicates that a poor relationship exists between the data and the fit, and thus a lack of predictive capability of the regression models.

Table 4.2 Void content percent and standard deviation as determined by optical image analysis for composite process development.

Specimen Trial Number	Void Content (%)	Standard Deviation
1	3.72	1.73
2	1.47	1.05
3	1.43	0.72
4	2.59	1.40
5	3.29	1.89
6	0.64	0.42
7	1.80	1.34
8	0.18	0.21
9	2.57	0.83
10	1.58	0.68
11	1.86	0.96
12	3.00	2.03
13	1.39	0.82

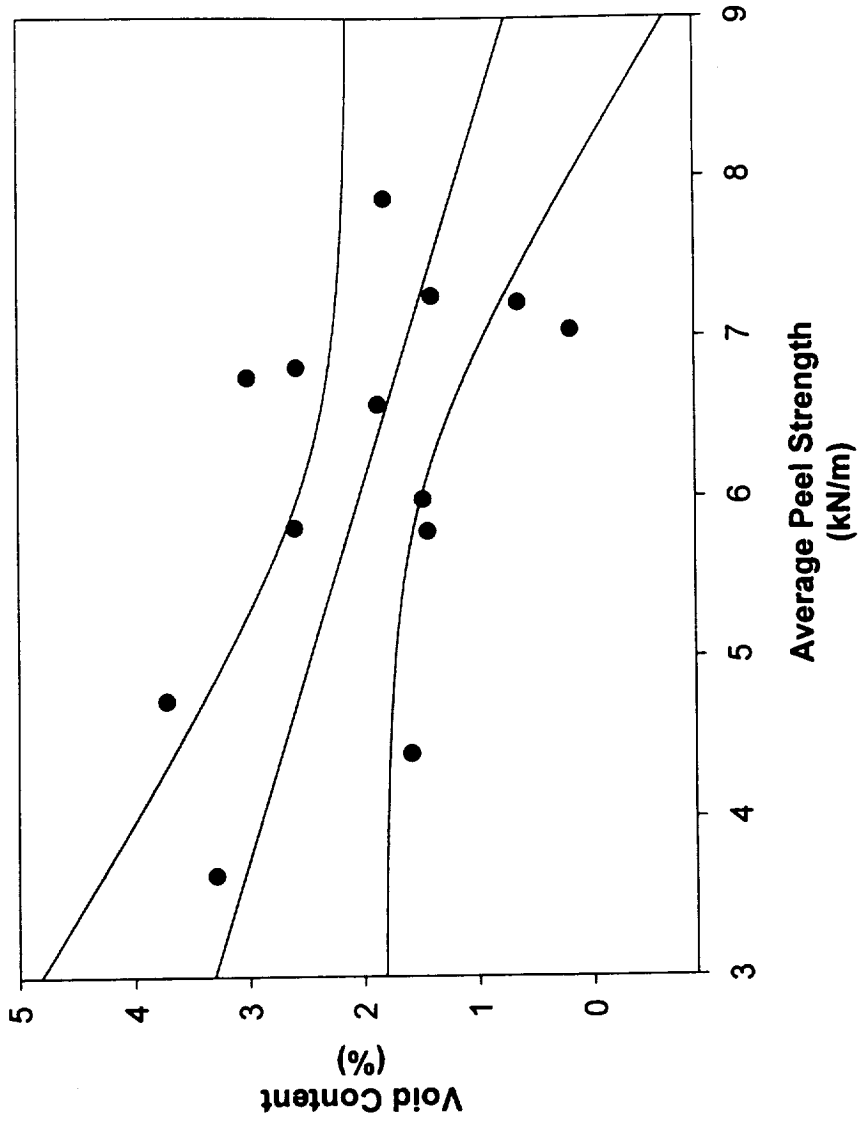

Figure 4.6. *Relationship between void content and average peel strength for the data of the Box-Wilson experiment design with 95% confidence limits.*

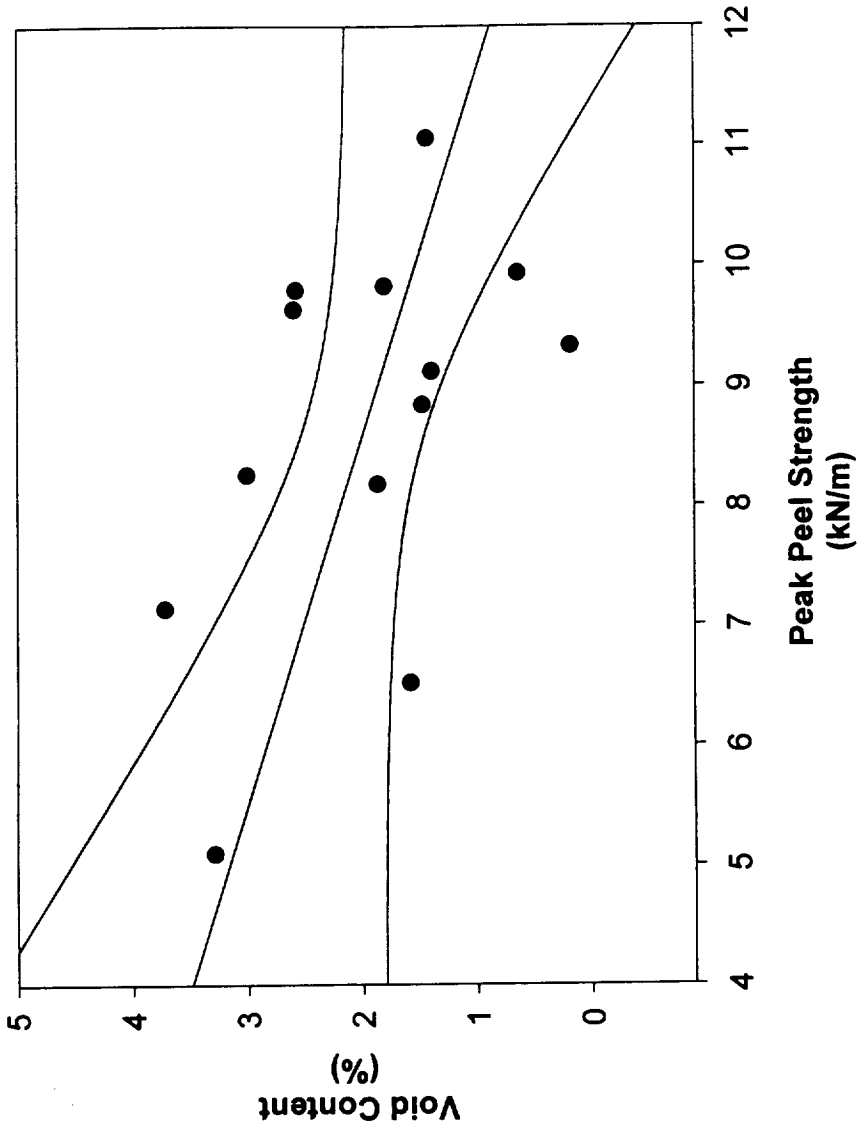

Figure 4.7. *Relationship between void content and peak peel strength for the data of the Box-Wilson experiment design with 95% confidence limits.*

The poor fit between the two data may be explained by the high consolidation quality at the ply interfaces. Inspection of the peel specimen interfaces by optical microscopy indicates the virtual absence of voids at the ply interfaces, as shown in Figure 4.8. In short, the peel test is not influenced by voids within the constituent plies. Another possible explanation may be that the wedge peel test is not sensitive to void content percent below some minimum value.

The question arises as to whether peak peel strength or average peel strength data is most meaningful in terms of describing an optimal process. The presence of a resin-rich region at the end of the crack starter has been reported as source of scatter in the DCB Mode I interlaminar fracture toughness test; a similar resin-rich region exists in the peel specimen[26]. It has been observed that the majority of peak peel strength values typically occur in this region of the specimen. Additionally, only one data point per specimen is reported as the peak value; average peel data are acquired over the length of the specimen. For the typical peel lengths of 15.0-cm as performed in this study, a total of 600 data points, or 236 data points per centimeter, is obtained. These factors would indicate that the average peel data give more meaningful results.

A cross-plot of peak peel strength and average peel strength was performed to determine if a correlation between the two existed. The resulting plot is presented in Figure 4.9. Statistical analysis of the linear regression was performed on the fit. The power of the regression was found to be 0.876 and the R-value was 0.755. Based on these values, the model may therefore be used with confidence to state that a significant

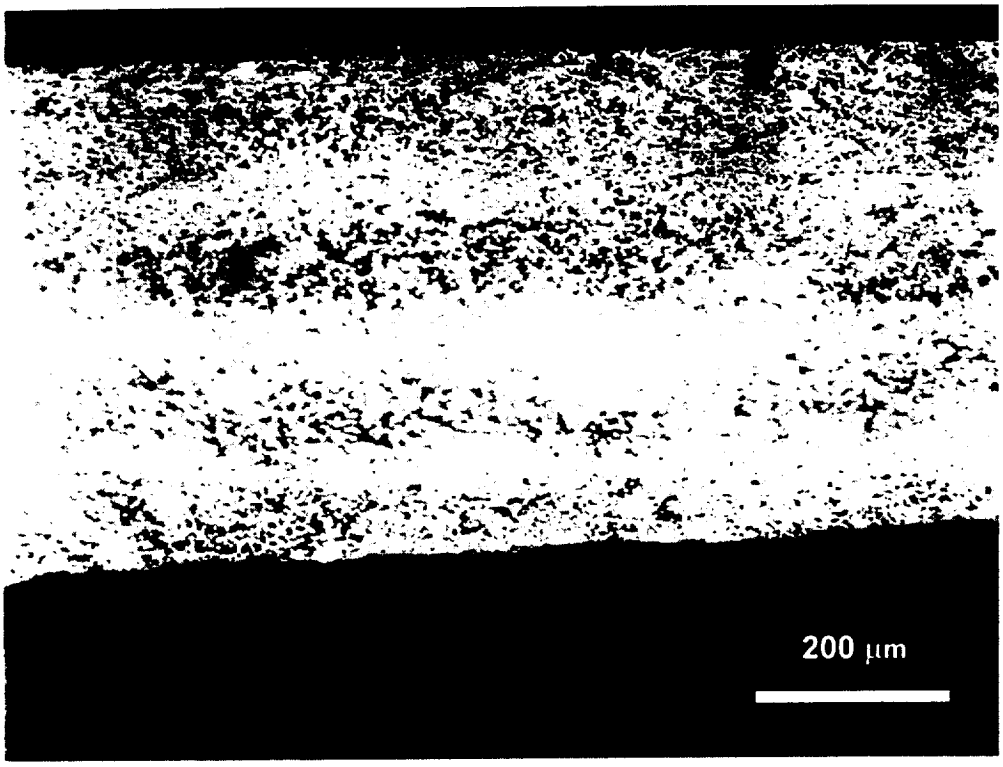

Figure 4.8. *Photomicrograph of cross-section of 4-ply composite peel specimen. Void content of specimen as measured by image analysis is 0.18%.*

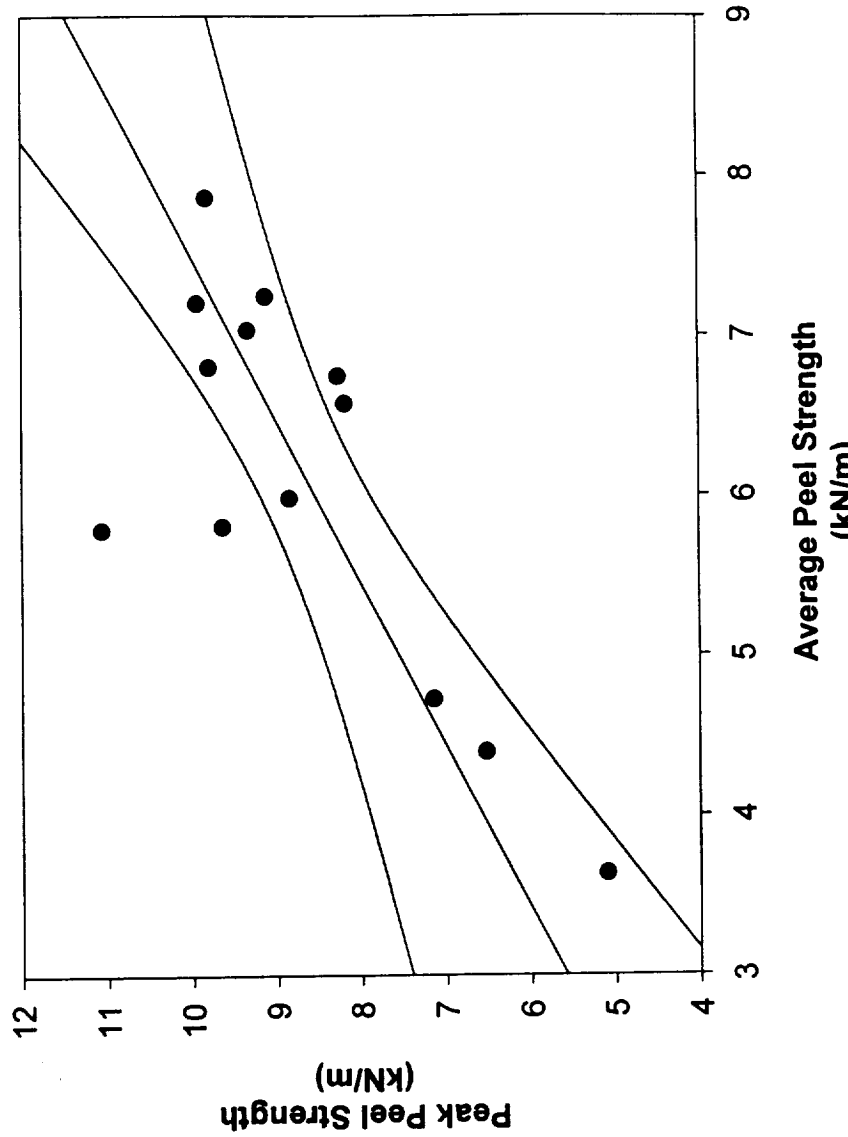

Figure 4.9. *Cross-plot of peak peel strength versus average peel strength with 95% confidence limits.*

relation exists between the two variables and that both data may be used to make predictions of behavior outside of the test region.

Several observations may be made in the final determination of the optimal placement parameters to be used in processing the composite. First, from Table 4.1, the highest peak strength occurs at a compaction load of 1.31-kN and a torch temperature of 700°C. Also from Table 4.1, the highest average peel strength value occurs at a compaction load of 0.95-kN and a torch temperature of 700°C. Additionally, from the contour plot of peak peel strength given in Figure 4.6, peak strength is seen to increase with compaction load to 1.33-kN. Finally, the statistics on the fit of the regression for the cross-plot of peak and average peel strength indicate that a definite correlation exists between the data, justifying the use of both sets of results in the determination of optimal parameters. Based on these observations, the processing set points for the compaction load and torch temperature for all subsequent composite processing will be 1.33-kN and 700°C, respectively.

SECTION 5

FILM INTERLEAF LAMINATE PROCESS DEVELOPMENT

5.1 Preliminary Processing Trials

Initial placement trials were conducted with 0.076-cm PEEK film. Single strips of composite tape, 45.7-cm long and 3.17-cm wide, were placed onto the tool surface at the conditions described at the end of the previous section. Strips of film were taped to the composite ply at the beginning end of each strip and draped along the length of the composite. These strips were manually constrained and placed slightly in tension at the free end. This served to prevent the film from buckling upward from the composite ply surface and thus from contacting the heated roller prior to the moment of adhesion.

Difficulties in effecting adhesion of the film to the composite at the beginning end of the strip were encountered due to the short contact dwell time at the start of placement motion that resulted in film melt and adhesion to the roller surface. A solution to this problem was found by taping a 7.62-cm length of composite over the film at the beginning end of the strip as shown in Figure 5.1. This method resulted in good adhesion at the start of each film processing trial and was used for all subsequent film processing experiments.

A first set of experiments was conducted using the heated compaction roller as the sole heat source. The roller compaction force and placement processing rate were held constant at 0.44-kN and 2.54-cm/s, respectively. The roller temperature was varied from 270°C to 520°C. This range was used such that actual film temperatures from above the

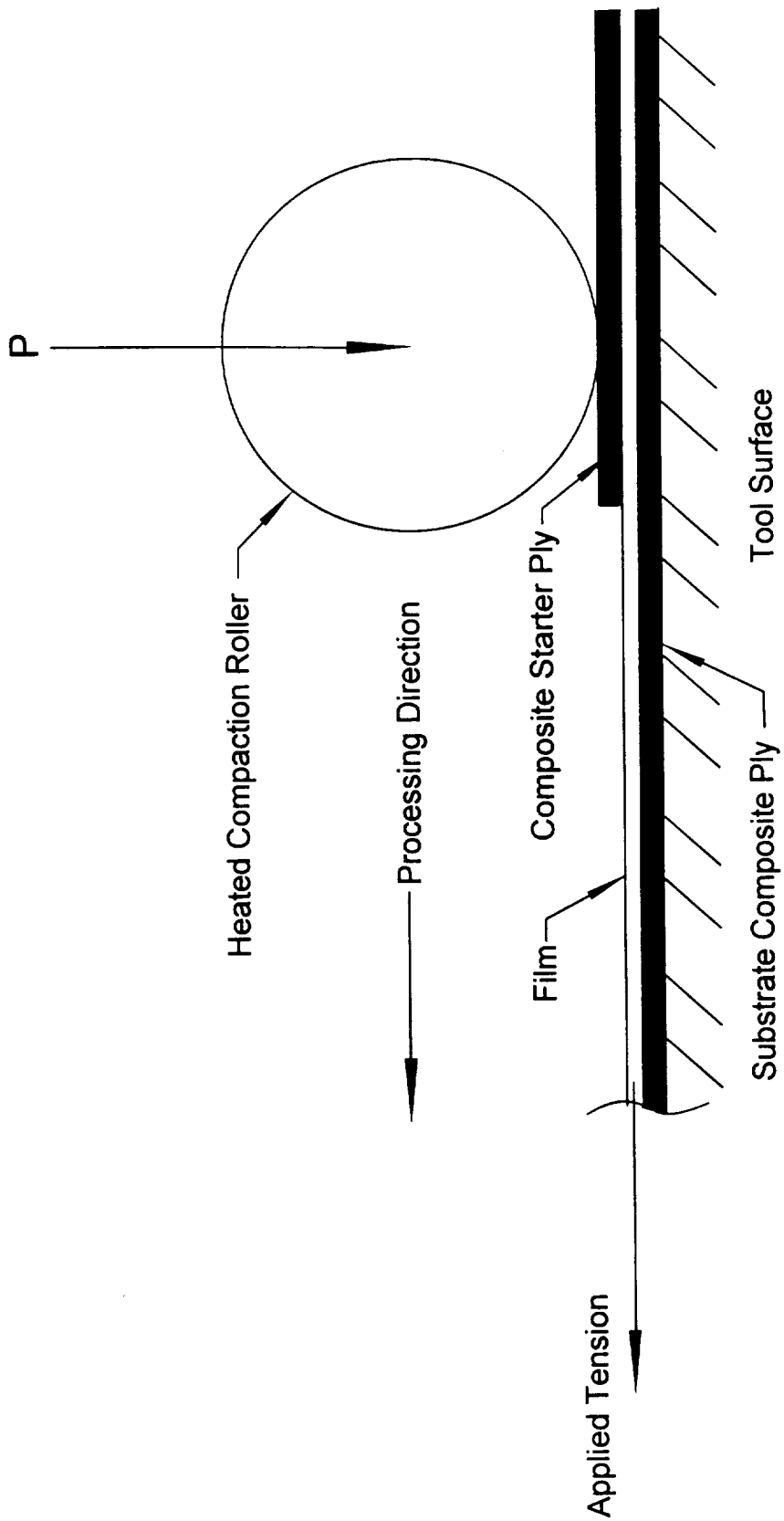

Figure 5.1. *Film processing set-up for start of strip.*

glass transition temperature to above the melt temperature could be attained at the fixed placement speed of 2.54-cm/s. The results for roller temperatures of up to 410°C - 420°C indicate that the films could be made to adhere lightly or be 'tacked' to the composite ply surface. The best results for light adhesion as indicated from visual inspection of the film were obtained with roller temperatures of between 320°C and 400°C. These films were observed to be of high integrity and uniformity along the specimen length and could be readily removed from the ply surface by peeling. This would indicate that the film and composite matrix resin had not yet fully melted and thus interfacial healing had not been achieved. Measurement of the film thickness and width indicate no change of dimension and hence no resin melt flow, supporting this conclusion. After tack staging, film surfaces appeared rough and mottled. This was thought to be due to the adhesion of the upper film surface to the compaction roller. The greater adhesion of the film to the substrate caused the film to pull off of the roller, resulting in the rough film surface as witnessed in the trials.

A series of 4-ply peel specimens were fabricated to determine the peel strengths at the film layer interface using only a film tack processing stage. A drawing of the as-tested peel specimens is given in Figure 5.2. Roller temperatures for the tack stage were varied between 300°C and 390°C. Compaction force during film processing was held constant at 0.56-kN. The composite plies were again processed at the conditions deemed optimal in the composite processing experiments of Section 4. The results of the preliminary study are presented in Table 5.1.

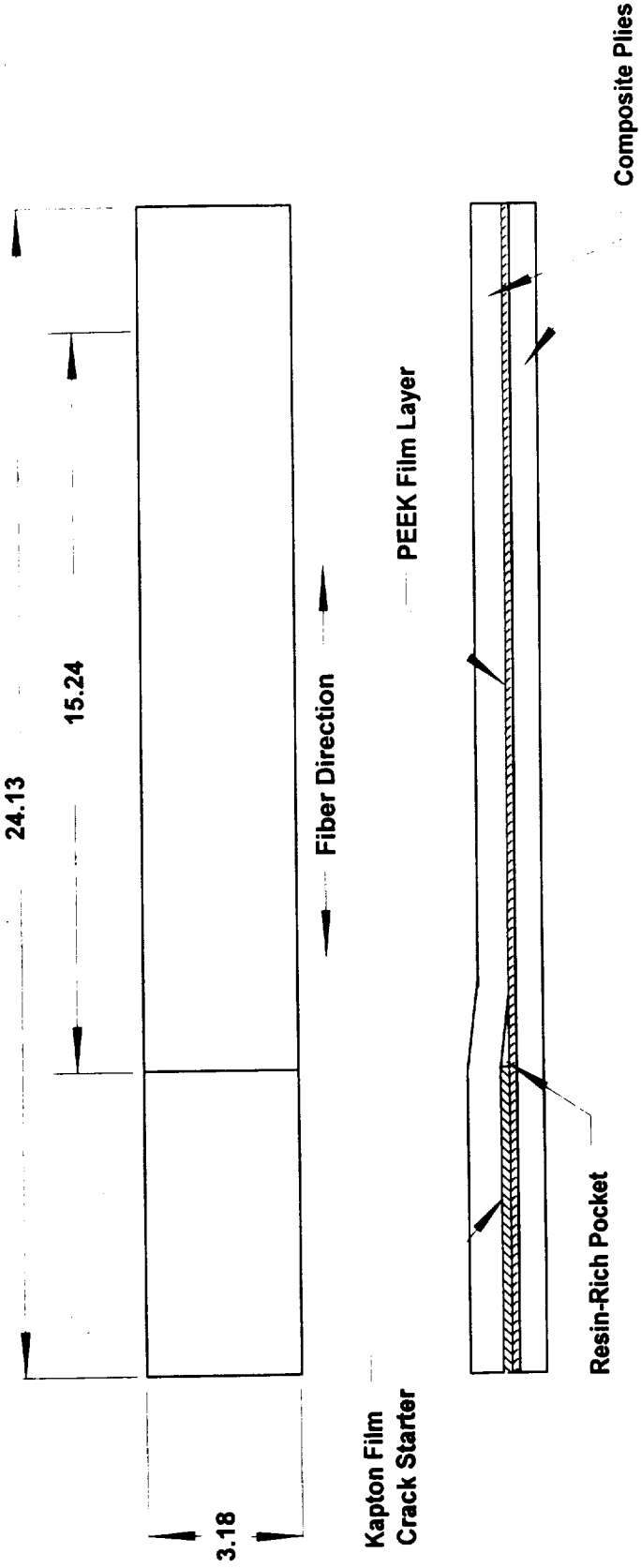

Figure 5.2 *Wedge peel specimen geometry. Scale in lower view is exaggerated for clarity. Note the presence of the resin-rich region just ahead of the crack starter film. Dimensions are in centimeters.*

Table 5.1 Results of 4-ply peel tests of film trials processed with film tack stage only. Composite processing conditions: 480°C roller, 700°C torches, 1.33-kN compaction force and 2.54-cm/s processing rate. Film processing constants: 0.56-kN compaction force and 2.54-cm/s processing rate.

Specimen No.	Roller Temp. (°C)	Peak Strength (kN/m)	Ave. Strength (kN/m)
020900-5	300	12.64	2.83
020900-4	330	6.63	3.22
020900-3	340	12.11	5.08
020900-2	360	9.72	4.26
020900-1	390	5.63	2.72

No general trend is exhibited in the strength data with increases in roller temperature, indicating that film tack temperatures in this region do not significantly influence the quality of the interfacial bond. Although several of the peak strength values are high, the average strength values are well below those found for the composite alone. Visual inspection of the fracture surfaces after testing revealed resin-rich regions on the upper ply surfaces and bare composite surfaces on the lower plies. This would indicate significant adhesive failure of the film at the lower composite ply surface. Composite cohesive failure was observed as evidenced by fiber pullout, however this failure was considered to be minimal for this specimen group.

The above results led to the conclusion that a second processing pass would have to be executed in order to more fully melt and bond the film to the lower ply surface. A second set of peel specimens was fabricated in an attempt to increase film adhesion to the composite substrate ply. Films were lightly tacked to the substrate as previously accomplished and a second, or film 'melt', processing pass was performed. These melt staging trials were conducted at higher compaction roller temperatures and with additional thermal energy supplied by the IR radiant heat source. The results of this study are presented in Table 5.2.

Preliminary melt stage trials using a rotating compaction roller resulted in severe film de-bonding from the lower composite ply as the result of adhesion to the roller surface. This difficulty was effectively eliminated by restraining the rotation of the roller during the melt stage processing pass. The use of a sliding roller was continued throughout the remainder of the study during film melt processing.

Table 5.2 Results of 4-ply peel tests of film trials processed with film tack and melt staging. Composite processing constants: 1.33-kN compaction force, 700°C torch temperature. Film processing constants: 340°C roller at tack stage, 0.56-kN compaction force for tack and melt stage processing.

Specimen ID	Roller Temp. @ Melt (°C)	Lamp @ Melt (Y/N)	Speed Melt / Composite (cm/s)	Peak Strength (kN/m)	Ave. Strength (kN/m)
021000-1	450	N	1.27 / 2.54	6.11	3.63
021000-4	450	Y	1.90 / 2.54	8.83	3.72
021000-5	480	Y	1.27 / 2.54	12.05	5.59
021000-6	480	Y	1.27 / 1.90	12.41	3.58
021000-7	480	N	1.27 / 2.54	8.81	4.73

The data show only a marginal improvement in the peel strengths over the previous results. The average of both the peak and the average strengths from the specimens having no melt stage were 9.34-kN/m and 3.62-kN/m, respectively. The averages for the results of melt stage processing for the same data were 9.64-kN/m and 4.25-kN/m, respectively. The fracture surfaces were visually inspected and adhesive failure of the film at the upper surface of the substrate composite ply was again observed, though to a lesser extent than for the previous experiment set. These results indicate that the use of a second processing pass is beneficial in terms of increasing film adhesion to the substrate ply. The average peel data, however, were still lower than the data for the composite alone.

A final set of preliminary experiments using the gas torches was conducted in an attempt to achieve complete film adhesion and higher peel strengths. The first, second and fourth composite plies were all fabricated at the same processing conditions determined to be optimal in Section 4. Due to the possible influence of the processing parameters of the ply immediately preceding the film layer on specimen quality, the compaction load and torch temperatures for this ply were varied in the experiment. Held constant for the film processing passes were the film tack stage roller temperature at 340°C, the film melt stage roller temperature at 480°C, compaction load of 0.56-kN during both film tack and melt stage processing, and the lamp percent output during the melt stage at 100%. Processing parameters that were varied for the experiments were the film melt stage processing rate, the 'upper' composite ply compaction load and torch

temperature, and the torch temperature during the film melt stage. The results of the study are presented in Table 5.3.

The data indicate a significant increase in peel strength as compared to the previous two experiment sets. The data represent a 43% increase in average peel strength and an 18% increase in peak peel strength as compared to the previous experiment set. In contrast to the previous studies, examination of the peel surfaces revealed the absence of a distinct film layer on the upper ply fracture surfaces, which would be indicative of good adhesion of the film to the lower composite ply. Additionally, inspection of both lower and upper specimen fracture surfaces revealed fiber pullout and thus cohesive failure within the composite tape.

Several observations regarding the result of these trials may be made. Specimens 1 and 3 of Table 5.3 were placed at the same conditions with the exception of the upper-ply composite compaction load. This force was 1.33-kN for specimen 1 and 1.11-kN for specimen 3. The average peel strength for specimen 1 was 38% higher than for specimen 3. The mean value of the average strength data of the specimens fabricated with a 700°C torch during upper composite ply processing was found to be 20% lower than the mean of those fabricated with a torch temperature of 850°C. Each of these findings would indicate that the processing parameters used during placement of the third composite ply are a significant factor in the process. The specimens having the highest average peel strengths overall, specimens 4 and 6, were processed without the gas torches during the melt stage. The only difference in the processing of these two specimens was the

Table 5.3 Results of 4-ply peel testing of film trials processed at increased melt stage and upper composite ply processing temperature and compaction force. All composite plies placed at 2.54-cm/s. Film processing constants: 340°C film tack roller temperature, 480°C film melt roller temperature, 0.56-kN compaction force, 100% lamp power at melt stage.

Specimen Number	Load Composite (kN)	Torch Temp. Melt/Composite (°C)	Speed @ Melt (cm/s)	Peak Strength (kN/m)	Ave. Strength (kN/m)
1	1.33	- / 700	1.27	10.73	7.84
2	1.33	700 / 700	1.27	12.18	8.19
3	1.11	- / 700	1.27	11.94	4.89
4	1.11	- / 850	1.27	12.34	9.92
5	1.11	700 / 850	2.54	10.93	7.79
6	1.11	- / 850	2.54	11.42	8.33

processing rate during the film melt stage. Specimen 4 was placed at half the rate of specimen 6, and shows an increase in both peak, and average peel strength. This would be expected from placement at lower rates; the amount of thermal energy available is a function of both placement rate and thermal energy source temperatures. Also noted was that three out of the top four specimens in terms of average peel strength were fabricated without gas torches during the film melt stage. An explanation for this could be that due to stagnation flow of the hot gas in the nip-point region, only small increases in actual material pre-heat temperatures result from relatively large changes in torch temperature [25].

5.2 Screening Experiments

A relatively large number of process variables could possibly influence the adhesion quality and the resultant peel strengths of the film specimens. In an attempt to determine which, if any, of these variables have little or no measurable impact on the quality of the film-composite bond, a set of screening experiments was performed. A Plackett-Burman design was chosen for the screening experiment set. This design is specifically intended to screen a large number of potentially important factors that may affect the desired characteristic. The disadvantage with this design is that, while the main effects of a large number of factors may be determined, knowledge of any non-linear effects is forfeited.

The screening test matrix used is shown in Table 5.4 in coded format. The process parameters for the first, second, and fourth composite plies were held constant as follows: placement rate, 2.54-cm/s; compaction load, 1.33-kN; compaction roller temperature,

480°C; torch temperature, 700°C; IR lamp output, 100%. Film tack stage processing parameters held constant were processing speed, 2.54-cm/s; compaction load, 0.56-kN; compaction roller temperature, 360°C. Specimens were peel tested and values for both the peak and average peel strengths were recorded and are presented in Table 5.5.

The average peel data were fitted using a linear regression model. The relative importance of each factor in affecting the outcome of the peel tests is given by the confidence coefficients. The factors may be ranked in the order of relative importance by the magnitude of these coefficients. The results of this ranking are given, in order from most to least important, in Table 5.6.

Clearly the most significant factors influencing the peel strengths are the melt roller temperature, the compaction force at the film melt stage, and the use of the IR lamp. It is assumed that the majority of thermal energy available to melt and bond the film to the lower composite ply is transferred via conduction by the heated compaction roller. The relatively minor influence of the torch temperature during the melt stage is thought to be due to gas flow stagnation in the nip point region, as mentioned previously. The IR lamp was originally added to the placement machine to serve as a supplemental preheat source due to the inability to elevate the nip point temperatures sufficiently with heated gas alone. The high ranking and relative importance of the IR heat source is therefore confirmation of the benefit of this additional heat source for material preheating. The importance of the compaction load during the film melt stage is thought to be due to the

Table 5.4 Screening experiment worksheet in coded format. Film melt compaction load range: 0.56-kN – 1.33-kN; film melt torch temperature range: 0℃ - 700℃, lamp at film melt stage: 0% - 100%; upper ply composite torch temperature range: 700℃ - 850℃ and film melt processing rate range: 1.27-cm/s – 2.54-cm/s.

Run No.	Film Melt Compaction Load	Film Melt Torch Temperature	Lamp at Film Melt	Upper Ply Composite Torch Temperature	Film Melt Placement Speed
1	+1	-1	1	-1	+1
2	-1	-1	1	+1	+1
3	-1	+1	-1	-1	-1
4	+1	-1	-1	-1	+1
5	+1	+1	-1	+1	-1
6	-1	-1	1	-1	-1
7	-1	+1	1	+1	+1
8	-1	-1	-1	+1	+1
9	+1	+1	-1	-1	+1
10	+1	-1	1	+1	-1
11	-1	-1	-1	-1	-1
12	-1	+1	-1	+1	+1
13	+1	+1	1	-1	+1
14	+1	+1	1	+1	-1
15	+1	-1	-1	+1	-1
16	-1	+1	1	-1	-1

Table 5.5 Plackett-Burman Screening Experiment table and average peel strength results.

Melt Compaction Load (kN)	Melt Torch Temperature (°C)	Lamp at Melt (%)	Upper Composite Ply Torch Temperature (°C)	Film Melt Speed (cm/s)	Average Peel Strength (kN/m)
0.56	700.0	100	700.0	1.27	6.51
0.56	0.0	100	700.0	1.27	5.94
0.56	700.0	100	850.0	2.54	5.31
1.33	0.0	0	700.0	2.54	3.80
1.33	700.0	0	850.0	1.27	4.67
1.33	700.0	100	700.0	2.54	3.15
0.56	0.0	0	700.0	1.27	5.17
1.33	700.0	0	700.0	2.54	2.34
0.56	700.0	0	850.0	2.54	3.16
1.33	0.0	100	700.0	2.54	5.18
1.33	0.0	0	850.0	1.27	4.82
1.33	700.0	100	850.0	1.27	5.53
0.56	0.0	100	850.0	2.54	5.12
0.56	0.0	0	850.0	2.54	5.58
1.33	0.0	100	850.0	1.27	3.84
0.56	700.0	0	700.0	1.27	4.13

Table 5.6 Confidence coefficients obtained from process variable screening experiment on average peel strength data.

Process Variable	Confidence Coefficient
Melt Roller Temperature	0.89
Compaction Load at Melt	0.85
Lamp on at Melt	0.80
Melt Processing Speed	0.70
Torch Temperature for Upper Composite Ply	0.61
Torch Temperature at Melt	0.38
Compaction Load for Upper Composite Ply	0.22

increase in melt flow and interfacial healing at higher consolidation pressures. A similar benefit was noted in the composite studies of Section 4.

The processing variables for placement of the upper composite ply were investigated in the study to determine if the presence of the film layer on the substrate would significantly alter the optimal conditions of the composite found in Section 4. The torch temperature and compaction force were varied for placement of this ply. The torch temperature was found to be more significant during placement of the upper composite ply than during the film melt processing stage. The compaction load for placement of the upper ply was found to be the least important of the screened parameters. This may be explained by the presence of the film layer; this layer provides a smooth resin-rich surface for the upper composite ply to adhere to. The contrast in film tack and film melt stages on the quality of the film surface is readily apparent in Figures 5.3 and 5.4.

The processing speed during the film melt stage was found to be of borderline importance in the screening experiment. Due to the uncertainty in the significance of this parameter in the process and to the relatively low values of peel strength obtained in the screening experiments, further experiments designed to optimize the process will be carried out at lower placement speeds.

5.3 Process Optimization by Design of Experiments and Response Surface Methodology

The results of the Plackett-Burman screening experiments of the previous section suggest that the three most significant parameters for processing film interleaves, in terms

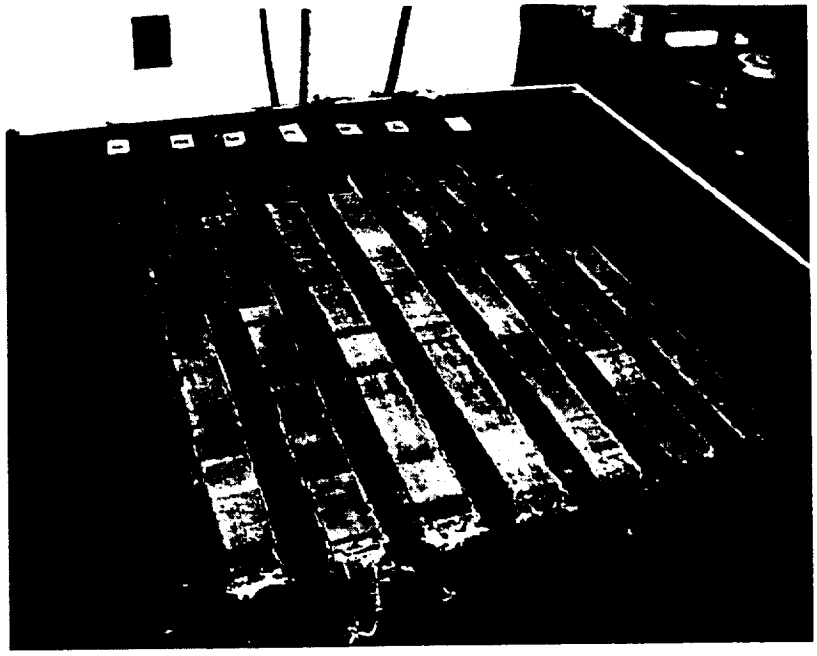

Figure 5.3. *Film placement specimens after film tack stage.*

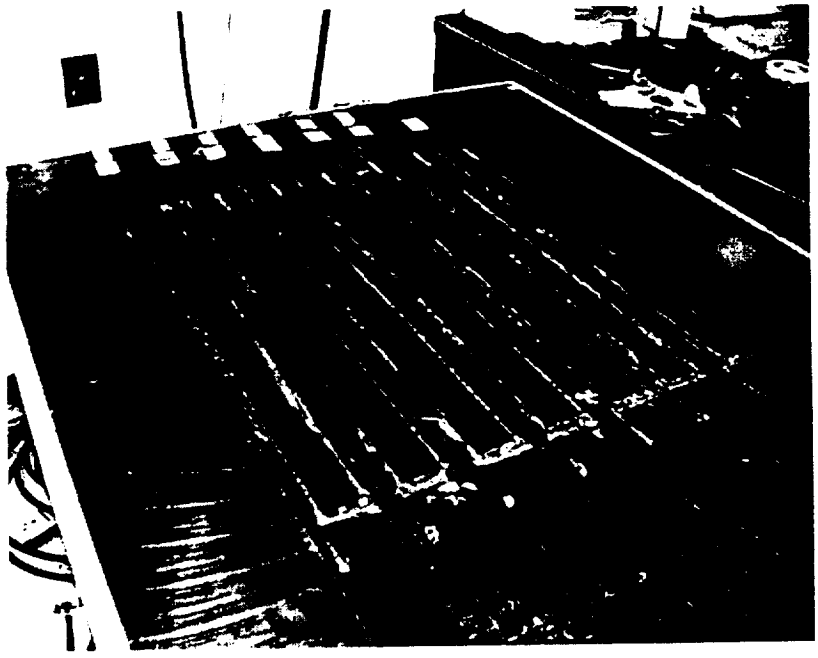

Figure 5.4. *Film placement specimens after film melt stage.*

of average peel strength, are the melt stage roller temperature, the melt compaction load, and the IR heat source. The most insignificant parameters were determined to be the torch temperatures and the compaction load during upper composite ply placement and the torch temperatures during the melt stage. As previously stated, the processing rate during the film melt stage was of borderline importance.

Further investigations to determine the bounds of an optimal process were conducted. A series of experiments, utilizing a Box-Behnken design, were conducted at film melt rates of 1.27-cm/s , 0.95-cm/s, and 0.64-cm/s. Torch temperature values for placement of the upper composite ply and for the melt stage were held constant at 700°C. The compaction load for placement of the upper composite ply was also held constant at 1.33 -kN. The processing rate for all of the composite plies was held constant at 2.54-cm/s. The compaction roller temperature, the compaction load, and the lamp percent output during the film melt stage were varied during the experiments.

A schedule of permuted experiments is given in coded form in Table 5.7 and was performed at each of the three film melt rates. The melt stage roller temperature range investigated was 400 to 480°C, the compaction load range was 0.56-kN to 1.22-kN, and the lamp output power range was set from 0% to 100%.

5.4 Results and Conclusions

The results of the experiments are given in Table 5.8. The data were fitted using a quadratic regression model and the resultant response surfaces were generated using JMP statistical software. An analysis of the results was undertaken to determine the goodness-

Table 5.7 Box-Behnken permutated placement schedule for optimization of film processing parameters in coded format.

Melt Stage Roller Temp.	Melt Stage Compaction Load	Melt Stage Lamp Power
0	-1	+1
+1	+1	0
+1	0	-1
0	0	0
0	+1	+1
+1	-1	0
0	+1	-1
0	0	0
-1	+1	0
-1	0	-1
-1	0	+1
0	0	0
-1	-1	0
0	-1	-1
+1	0	+1

Table 5.8. Results of Box-Behnken designed experiment for optimization of film processing parameters at film melt processing rates of 0.64-cm/s, 0.95-cm/s and 1.27-cm/s.

Specimen Number	Melt Roller Temperature (°C)	Melt Compaction Load (kN)	Lamp Output (%)	Average Peel Strength @ 0.64cm/s, (kN/m)	Average Peel Strength @ 0.95 cm/s, (kN/m)	Average Peel Strength @ 1.27 cm/s, (kN/m)
1	440	0.56	100	3.11	8.00	4.08
2	480	1.22	50	6.56	4.94	3.89
3	480	0.89	0	7.89	6.14	2.68
4	440	0.89	50	5.54	6.86	3.76
5	440	1.22	100	7.80	5.95	8.03
6	480	0.56	50	5.52	4.99	4.33
7	440	1.22	0	4.50	5.67	8.30
8	440	0.89	50	5.88	1.86	2.84
9	400	1.22	50	2.37	2.08	4.33
10	400	0.89	0	2.62	1.75	4.13
11	400	0.89	100	2.70	3.60	3.37
12	440	0.89	50	3.52	2.73	7.37
13	400	0.56	50	1.86	1.53	7.26
14	440	0.56	0	2.10	1.63	4.26
15	480	0.89	100	8.60	7.26	7.65

of-fit for the response surface models at each of the three film melt processing rates. The response surfaces are presented for the 1.27-cm/s, 0.95-cm/s, and 0.64-cm/s film melt rates in Figures 5.5, 5.6 and 5.7, respectively.

The indicators used to determine the quality of fit of the quadratic model to the data were the R-value, the sum-of-squares of the model (SS_m), and the sum-of-squares of the error (SS_e). An R-value of 1 signifies a perfect fit and complete confidence in the predictive capability of the model. Conversely, low R-values signify a poor fit, and hence an inability of the model to make predictions regarding the dependent variable. Additionally, the goodness-of-fit may be determined from the sum of the squares of the model and the error. Good correlations have SS_e values much less than the SS_m .

The quality of fit of the model for the experiments performed at a melt speed of 0.64 cm/s was found to be the best of the three experiment groups. The R-value for the fit of the experiments performed at a melt processing speed of 0.64 cm/s was found to be 0.929. The SS_m and the SS_e were found to be 63.75 and 10.02, respectively. It is concluded that a high degree of confidence may be attributed to the model for this data set. The R-value for the model for the experiments performed at 0.95-cm/s melt processing speed was found to be 0.879 and the SS_m and SS_e were found to be 56.38 and 16.62, respectively, indicating justification in the confidence of this model as well.

Analysis of the fit of the model for the experiments performed at 1.27-cm/s give an R-value of 0.612 and an SS_m and SS_e of 21.1 and 35.1, respectively. These values would indicate that little or no confidence can be attributed to the fit of the model for this data set.

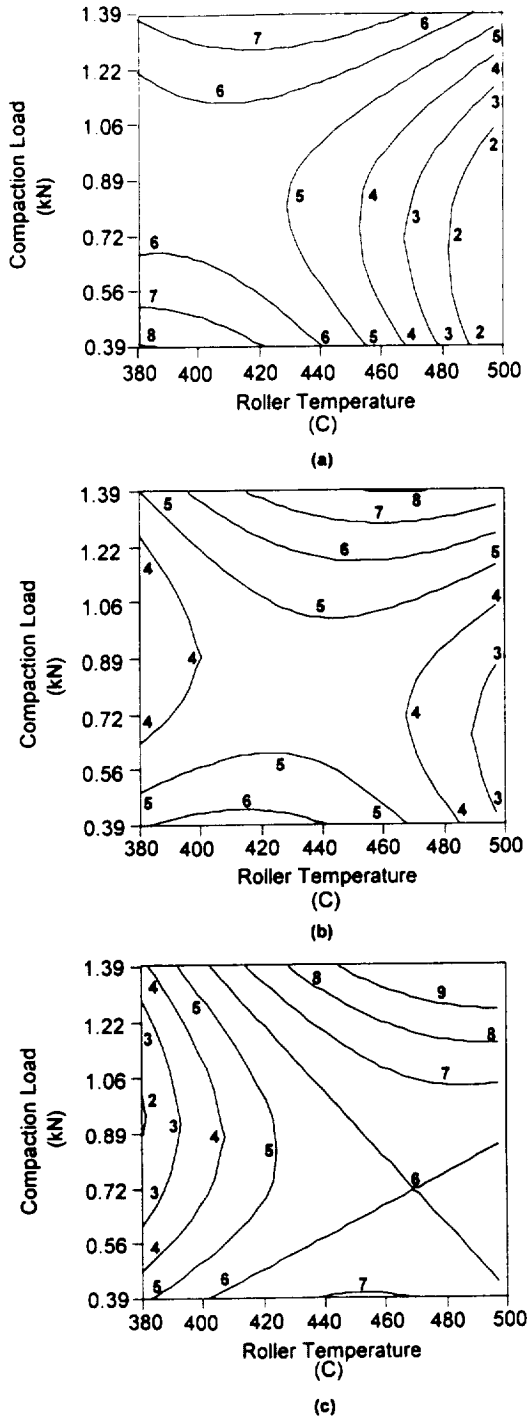

Figure 5.5. *Response surface plots of peel strength as a function of compaction load and roller temperature at a film melt processing rate of 1.27-cm/s. IR lamp output: (a) 0%, (b) 50%, (c) 100%.*

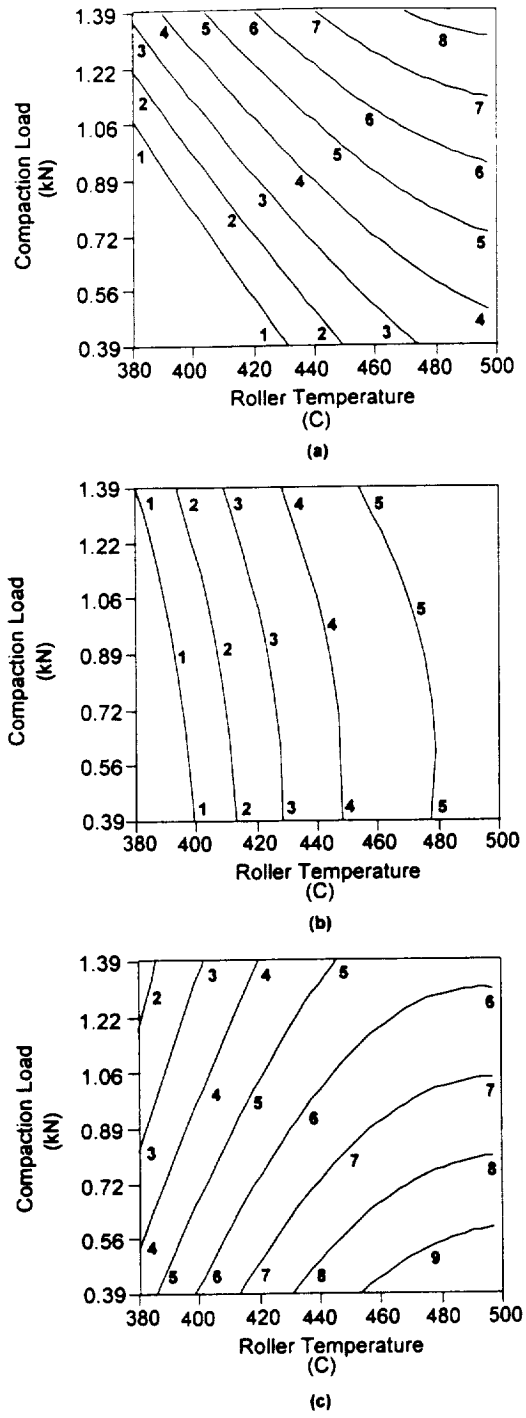

Figure 5.6. *Response surface plots of peel strength as a function of compaction load and roller temperature at a film melt processing rate of 0.95-cm/s. IR lamp output: (a) 0%, (b) 50%, (c) 100%.*

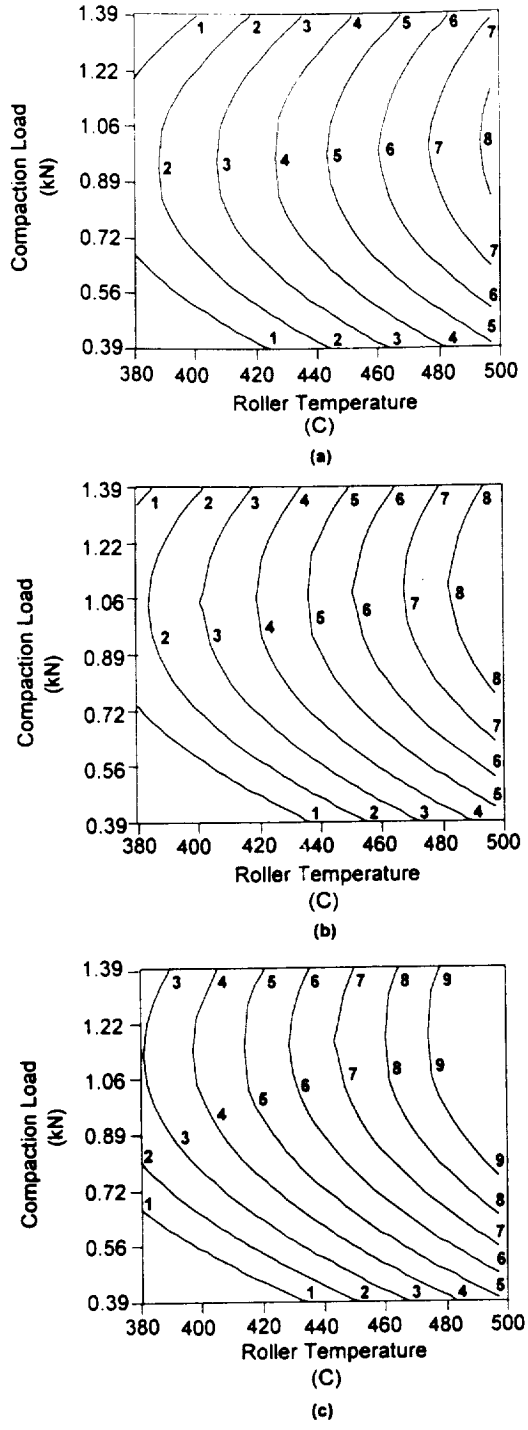

Figure 5.7. *Response surface plots of peel strength as a function of compaction load and roller temperature at a film melt processing rate of 0.64-cm/s. IR lamp output: (a) 0%, (b) 50%, (c) 100%.*

Inspection of the plots reveals a general upward trend in peel strength with increases in compaction roller temperature and load at each lamp output setting. Clearly evident is the upward trend in strength values with increases in IR lamp output power. Also noted is the increase in the maximum peel strength as placement rates decrease from 1.27-cm/s to 0.64-cm/s. An unexplained decrease in peel strength with compaction load is shown in Figure 5.5(c). It may be concluded that wedge peel strengths are maximized at the conditions represented in Figure 5.6(c). This plot represents both 100% lamp output and 0.64-cm/s placement rate, conditions that provide maximum thermal energy flux into the material.

Photomicrographs of the peel specimen having the highest peel strengths at each of the film processing rates are presented in Figures 5.8, 5.9, and 5.10. All three specimens exhibit well-consolidated, void-free interfaces at both the upper and lower film interleaf surfaces. A general decrease in film thickness, however, was observed with decreasing film melt processing rates. Measurements of the resultant film thickness of each of the specimens was performed using an optical microscope fitted with a Boeckeler Instruments, MicroCode II digital position readout. The microscope magnification power used was 500X. Forty film thickness measurements were recorded for each of the three specimens. The original measurements were taken in units of inches and converted to centimeters by use of a spreadsheet software program. This program was also used to calculate the mean and standard deviations of the film thickness measurements for each of the specimens. The results are presented in Table 5.9.

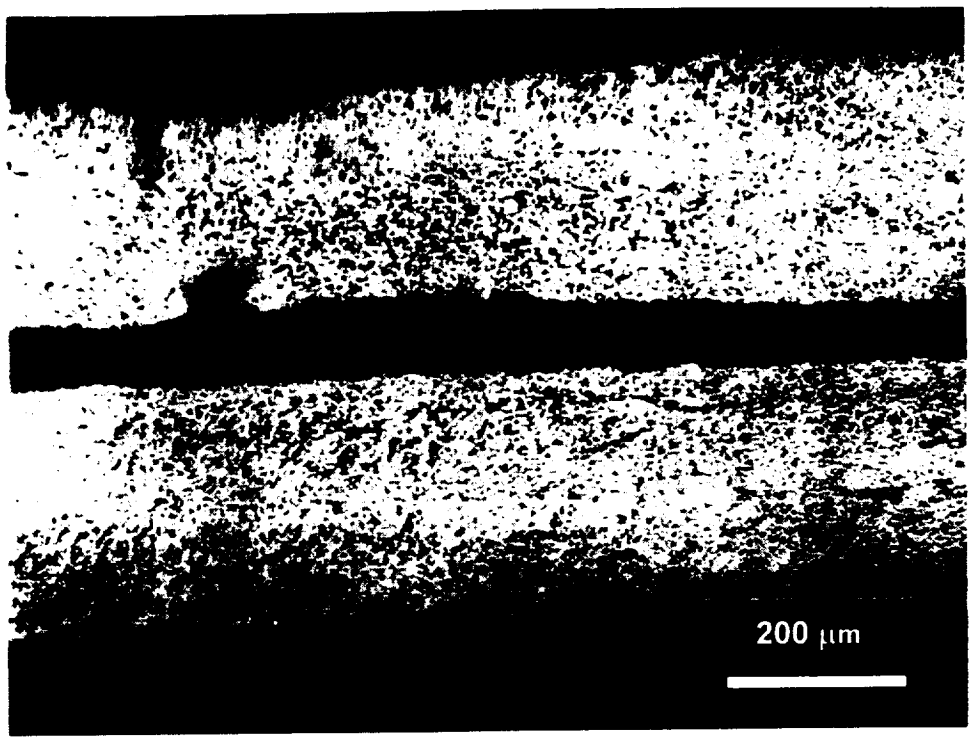

Figure 5.8. *Photomicrograph of 4-ply peel specimen placed at melt stage conditions of 440°C roller temperature, 1.22-kN compaction load and without supplemental IR lamp energy. Shown is cross-section of specimen having the highest peel strength (8.30-kN/m) of those fabricated at 1.27-cm/s. Average film thickness after processing is 0.0069-cm.*

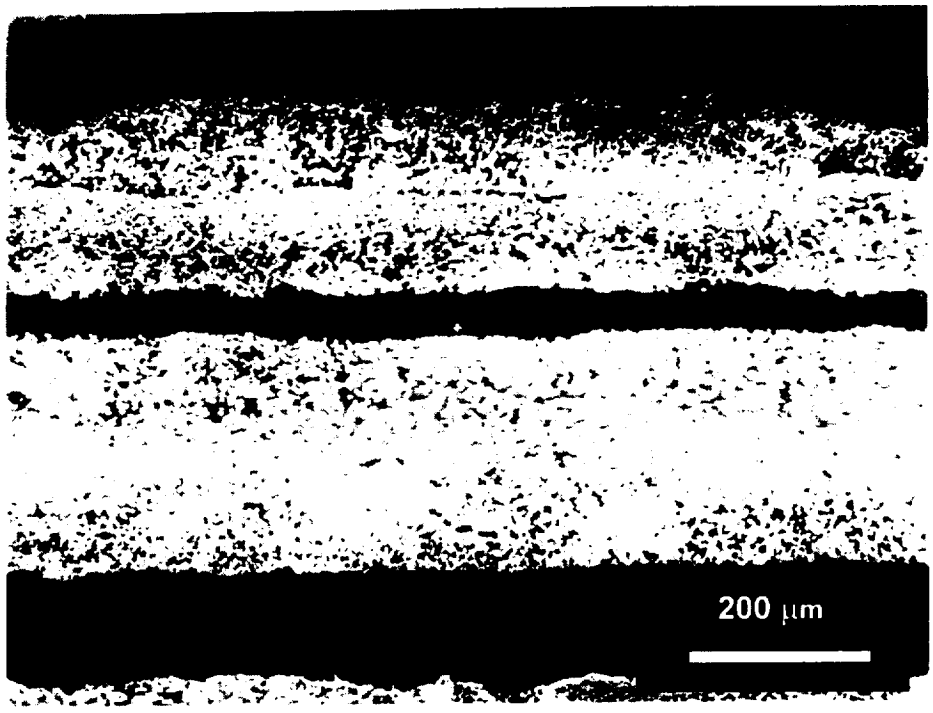

Figure 5.9. *Photomicrograph of 4-ply peel specimen placed at melt stage conditions of 440°C roller temperature, 0.56-kN compaction load, and at 100% lamp power. Shown is cross-section of specimen having the highest peel strength (8.00-kN/m) of those fabricated at 0.95-cm/s. Average film thickness after processing is 0.0049-cm.*

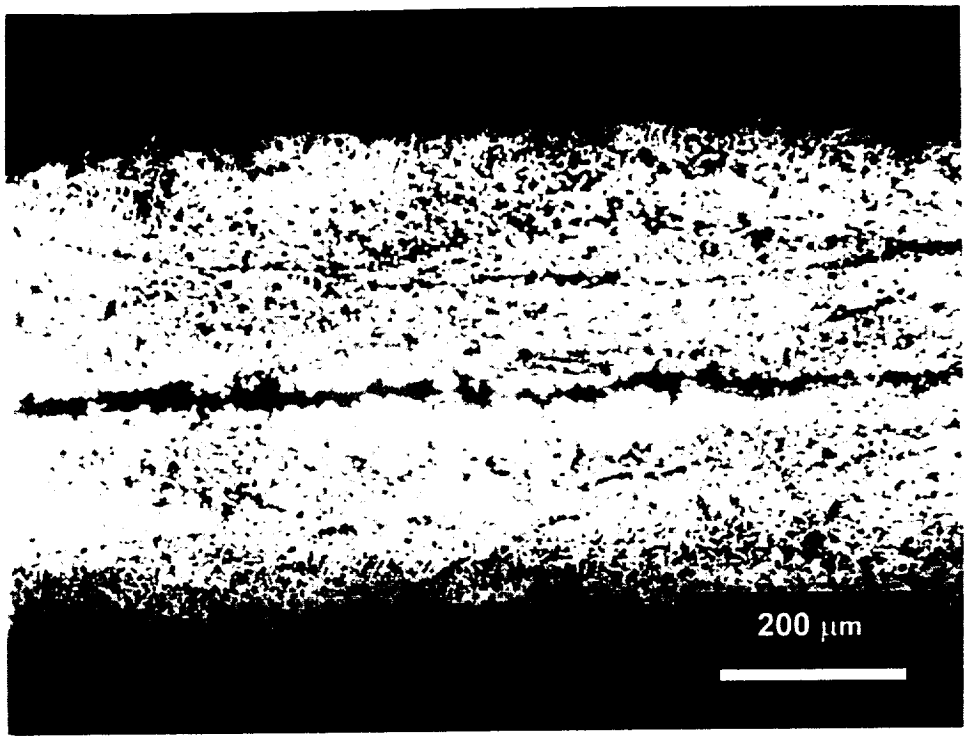

Figure 5.10. *Photomicrograph of 4-ply peel specimen placed at melt stage conditions of 480°C roller temperature, 0.89-kN compaction load and 100% lamp power. Shown is a cross-section of specimen having the highest peel strength (8.60-kN/m) of those fabricated at 0.64-cm/s. Average film thickness after processing is 0.0024-cm.*

Table 5.9 Film thickness measurements and standard deviations for the specimens having the highest average peel strengths at each of the melt processing rates.

Film Melt Processing Speed (cm/s)	**0.64**	**0.95**	**1.27**
Average Peel Strength (kN/m)	8.60	8.00	8.30
Mean Thickness (cm)	0.0024	0.0049	0.0069
Standard Deviation (cm)	0.0011	0.0018	0.0011
Standard Dev. / Mean Thickness (%)	15.9	36.7	45.8

Film thickness was observed to decrease by 8%, 35.5%, and 68.4% for the specimens placed at 1.27-cm/s, 0.95-cm/s, and 0.64-cm/s, respectively. Additionally, a decrease in standard deviation relative to film thickness was observed as film melt processing rates decreased. The decrease in film thickness may be primarily attributed to the increased melt flow of the film due to the higher thermal energy fluxes attained at lower placement rates. As a result of the increase in melt flow, the amount of resin that adheres of the resin onto the roller surface also increases. This leads to a 'skimming' of the resin from the specimen during the melt processing stage, and hence the observed decrease in film thicknesses.

A final set of experiments was performed in an attempt to confirm the results of the Box-Behnken experiments and to gage the accuracy of the response surface predictions for higher peel strengths. Four-ply peel specimens were fabricated at 100% lamp output power at each of the film melt processing rates. Maximum values of peel strength occurred at high values of torch temperature at each of the three film processing rates. Specimens were therefore fabricated at both 480°C and 500°C melt roller temperatures. Similarly, high values of compaction load were found to produce specimens of higher peel strength. These higher placement settings were used to fabricate the additional specimens for each melt processing rate. The response surface for the film melt processing rate of 0.95-cm/s, however, predicted high peel strength values at low compaction force settings. Due to the relatively good fit attributed to this response surface, four specimens were fabricated and tested in this lower compaction force region. The region of high peel strength for the processing rate of 0.64-cm/s was the largest in

size of the three; therefore, two additional specimens were fabricated for this experimental set. The results of these experiments are presented graphically in Figure 5.11. The average peel strength data recorded for each of the test specimens is superimposed onto its respective contour plot.

The results for the melt processing rate of 1.27-cm/s show a relatively high degree of variability, which may be attributed to the poor fit of the model to the data determined for this processing rate. It should be noted however, that the two specimens fabricated at a roller temperature of 500°C are both significantly higher in peel strength as compared to those placed at 480°C. This would tend to confirm earlier conclusions regarding the importance of conduction heat transfer in the film melt processing stage.

The results for the film processing rate of 0.95-cm/s would indicate that peel strength is relatively unaffected by compaction force in the range of roller temperatures investigated. The average of the specimens fabricated at high compaction loads was 7.04 -kN/m, and the average for those placed at lower compaction loads was 6.81-kN/m. The specimens fabricated at 0.64-cm/s had the highest average peel strength of the three test groups in addition to the smallest variation. The average for this set was 8.74-kN/m. This would appear to be a strong confirmation of both the prediction and the goodness-of-fit of the response surface model for this test set. However minor thermal degradation of the resin was seen to occur during the film melt stage at 0.64-cm/s in some of the specimens. The roller temperature would therefore seem to be very close to an upper bound for the film melt stage processing pass.

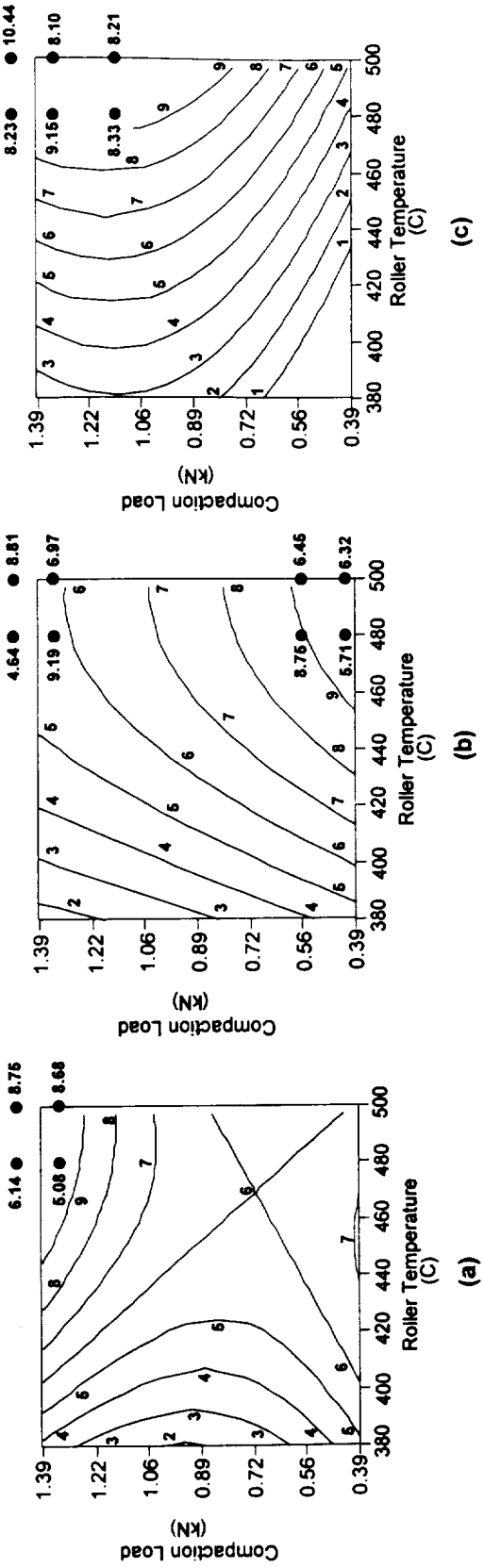

Figure 5.11. *Confirmation experiment results, (●), superimposed onto response surface plots. Lamp output constant at 100%. Melt processing rates shown are (a) 1.27-cm/s, (b) 0.95-cm/s, and (c) 0.64-cm/s.*

SECTION 6

SUMMARY AND CONCLUSIONS

6.1 Summary of Placement Efforts

6.1.1 Summary of Process Development

A series of experiments were conducted to determine the optimal placement processing parameters for the fabrication of composite laminates having polymer film interleaf layers by fiber placement. Initial investigations centered on determination of the optimal conditions necessary for processing the composite material without films. The resulting set of placement variables was then used for the composite for the film processing portion of the study. Preliminary trials with the PEEK film indicated that for best results, film placement should consist of a two-stage process. First, a film 'tack' stage was implemented to achieve light adhesion of the film to the substrate composite ply. A second film 'melt' processing stage was found to be necessary to intimately bond the film to the substrate ply. A Plackett-Burman screening experiment was then conducted to determine the relative influence of the process variables on the quality of the composite/interlayer specimen as determined by the wedge peel test method. This allowed for the elimination of process variables having little effect on the peel strength in subsequent optimization studies. Processing studies were then focused on determination of the optimal settings for the process variables that were found to be of greater significance in terms of panel peel strengths in the screening study. The factors having the

greatest influence on specimen peel strength were found to be the compaction roller temperature and the compaction force at each of the three placement rates investigated. A summary of the optimal processing conditions for the composite with and without the film interleaf layer are given in Tables 6.1 and 6.2, respectively.

6.1.2 Specimen Fracture Morphology

As seen previously in optical micrographs of the specimen cross-sections, both upper and lower film interfaces of the peel specimens appeared to be well consolidated. Additional SEM images of specimen fracture surfaces were obtained to investigate the damage morphology of the film interleaf layer. Wedge peel fracture surfaces are shown in the micrographs of Figures 6.1 and 6.2. Shown in Figure 6.3 is a cross-sectional end-view of a fractured four-ply specimen. All SEM photomicrographs were taken of the peel specimen having an average peel strength of 10.44-kN/m. This the highest value of those tested in the study.

Extensive fiber pullout and surface roughness is evident in Figure 6.1, indicating cohesive failure of the composite ply. Interleaf film resin is visible in the figure (white areas), and is indicative of both adhesive failure of the resin from the adjacent peel surface and cohesive failure, or fracture, within the resin layer. Evidence of such cohesive failure is seen in Figure 6.2. From top to bottom in the central portion of the figure is the interleaf resin material. In the upper third of the resin area, the surface of the

Table 6.1 Optimal processing parameters for PEEK/IM7 composite based on peel strength results.

Parameter	Value
Lamp Power	100%
Placement Rate	2.54-cm/s
Compaction Force	1.33-kN
Torch Temperature	700°C
Roller Temperature	480°C

Table 6.2 Optimal processing parameters for PEEK/IM7 composite with PEEK film layer based on peel strength results.

Process Variable	Composite	Film Tack	Film Melt
Torch Temperature (°C)	700	-	700
Roller Temperature (°C)	480	400	480-500
Compaction Load (kN)	1.33	0.22	1.47
Processing Rate (cm/s)	2.54	2.54	0.64

Figure 6.1. *Scanning electron micrograph of the peel fracture surface of a film interleaved specimen. Specimen average peel strength: 10.44-kN/m.*

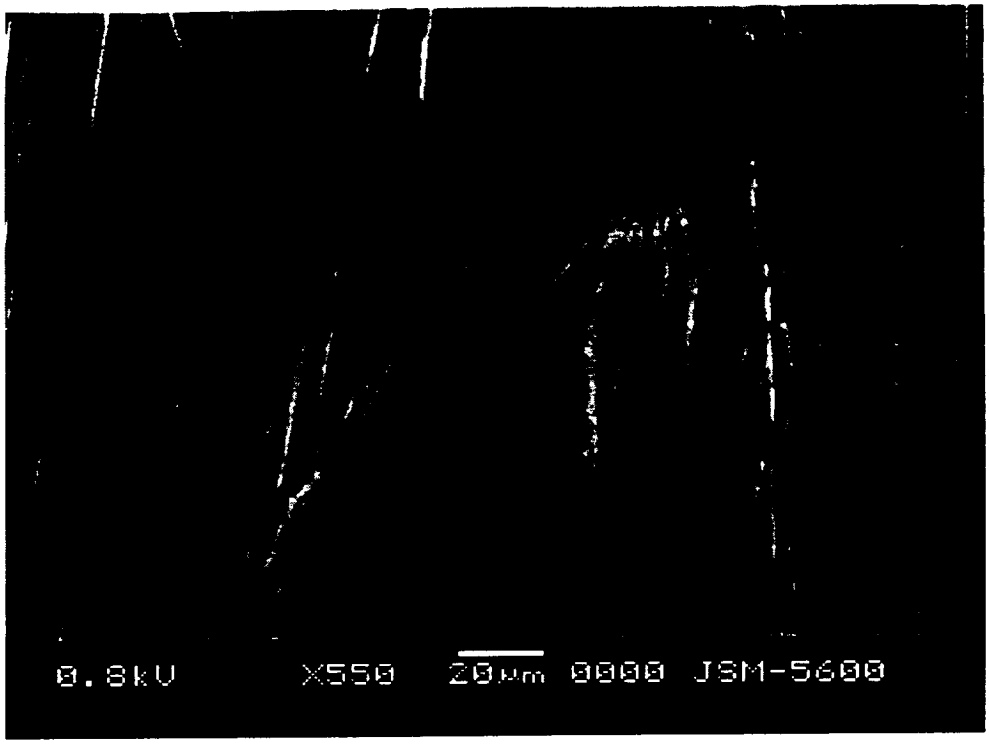

Figure 6.2. *Scanning electron micrograph of peel specimen showing film interleaf cohesive failure.*

resin is smooth, possibly indicating de-bonding of the resin from the adjacent ply. However, resin fracture is clearly apparent in the remaining portion of the figure, as would be evident with cohesive failure within the interleaf resin layer.

Figure 6.3 shows an end-view of a fractured four-ply peel specimen perpendicular to the fibers. The fracture was produced by folding the specimen in the transverse fiber direction until complete breakage across the width occurred. In the upper portion of the figure, fiber pullout is seen and is evidence of tensile failure in the specimen. The compressive half of the specimen is seen in the lower portion of the figure is quite different in appearance. Although some minor de-bonding of the resin layer from the lower fibers is seen in the center of the figure, the matrix resin and the interleaf layer appear to be continuous, indicative of intimate melt and bonding of the two constituents. A similar situation is seen at the upper film interface. No distinct delamination of the film layer from either composite ply was observed by scanning electron microscopy.

6.1.3 Discussion on the Validity of the Wedge Peel Test Method

The wedge peel test initiates and propagates fracture of the specimen at the peel interface in what is essentially opening or Mode I failure. The ASTM standard test for this failure mode in laminated composite materials is the DCB test. Several differences between the peel test as performed in this work, and the DCB test should be noted. In the DCB test the specimen arms are extended by the load frame, initiating and propagating fracture at the laminae interface. During testing, the crack length, load, and specimen arm deflection are recorded for the crack initiation point and for five additional propagation

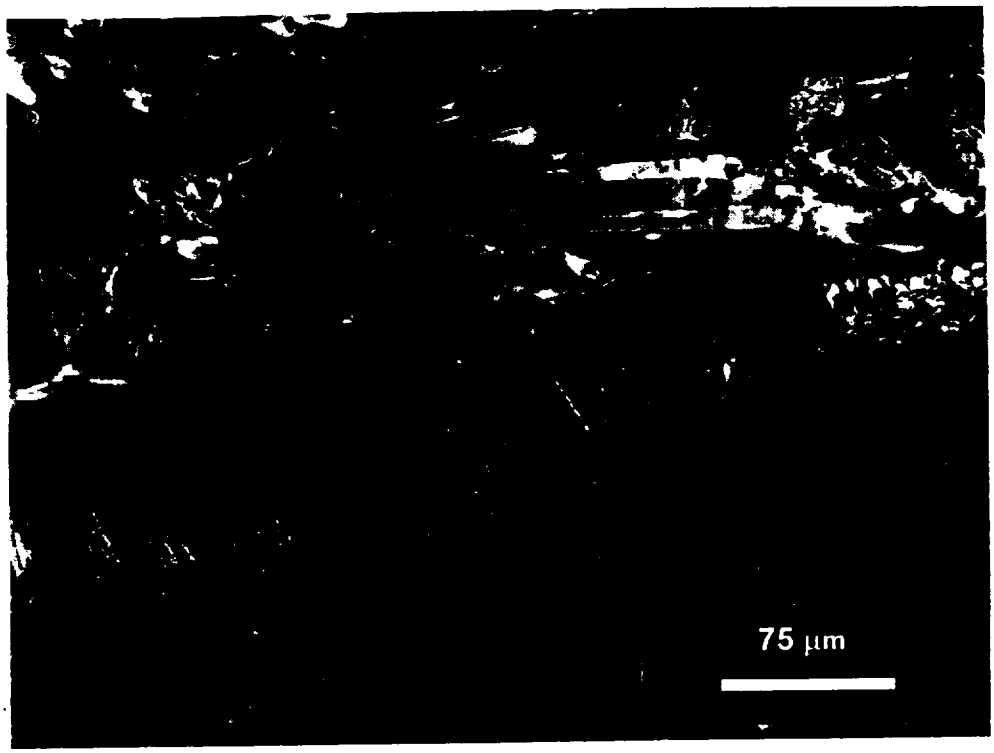

Figure 6.3. *Scanning electron micrograph of fractured cross-section of 4-ply peel specimen. Film interleaf layer is present from left to right just above center in the figure.*

points along the specimen length. Calculations using this data describe the behavior in terms of the amount of energy required to fracture the specimen. In contrast, the wedge peel test is a constant-displacement test; specimen arm displacement is held constant and is determined by the wedge thickness. The distance between the specimen crack front and the wedge is related to the specimen peel strength, with the crack front of weaker specimens appearing further ahead of the wedge than for stronger specimens. Since crack displacement is not measured in the peel test, a true fracture energy value is not obtained and therefore a direct one-to-one correspondence to the DCB data cannot be made.

An earlier study was performed to determine if a correlation exists between the wedge peel test and the DCB test [35]. The primary conclusion of this work was that both high and low fracture toughness and peel strength data were found at similar processing conditions. The motivations for use of the peel test for process development are the simplicity of the specimen geometry, the small amounts of material needed per specimen, and the speed at which testing and data reduction can be performed. The disadvantage of the peel test as performed in the present study is that the influence of the tool/substrate thermal boundary condition is neglected. This boundary condition changes with number of plies placed. A more thorough study in the use of fiber placement for film interleaf processing should make attempts to account for this changing parameter [32].

As mentioned previously in Section 1.2, studies by other researchers have indicated that increases in interlaminar fracture toughness of from 20% to 45% are possible with polymer film interleaf composite systems. A similar comparison was performed on the results of the current study. The five highest values of average peel strength for both the

interleaved and non-interleaved peel specimens, regardless of processing conditions, were averaged and compared. The peel strength averages of the non-interleaved and interleaved systems were found to be 7.234-kN/m and 9.268-kN/m, respectively. This represents an increase of 21.9% for the interleaved materials. This increase in is good agreement with those as previously reported in the literature [9,13]. Additionally, this would further indicate that the wedge peel test and the DCB test are likely measuring the same phenomenon.

6.2 Suggestions for Future Work

The results of the study indicate that the fabrication of composite structures having film interleaves layers by automated fiber placement is possible. The current study brings to light both processing issues and machine and equipment issues that may be addressed in future similar processing studies.

6.2.1 Processing Issues

Initially, plans were in place to investigate the processing of laminates having both 0.0025-cm and 0.0076-cm thick films. After several trials, work with 0.0025-cm films was abandoned, as difficulties in achieving complete, high integrity film coverage on the specimen surface were encountered. The ability to have a robust process, one capable of processing very thin films, would be advantageous in that a decrease in laminate properties such as specific strength generally accompany the addition of resin film interleaf regions within a composite. The results of the present study indicate that a

decrease in film thickness is made possible by the process itself. Additional studies might be directed towards controlling the film thickness during processing. This would likely require close control of such processing variables as compaction roller force and temperature.

Another important processing issue that may be addressed in future work is film gaps and overlaps. Early trials were conducted with film sheets several times the width of the heated compaction roller and composite substrate. It was immediately apparent that, due to local film melting and severe buckling and distortion of the film sheet, these materials would have to be processed in strip form. Other trials were conducted with films much narrower than the composite substrate. This was done in an attempt to determine how straight these films could be tacked to the substrate ply. Measurements indicated that film strips could be tacked to within 0.051-cm straightness deviation over a length of 46- cm. Accurate preliminary bonding, or tack staging, of the film is critical in terms of integrity of the film layer in the case of gaps, and in uniformity of the film thickness in the case of overlap regions. A substantial increase in film width is seen to occur during the melt stage processing pass and might conceivably eliminate any gaps in a completed film layer. Perhaps a more conservative approach might be to study the effect of the overlapping of films during the tack stage; relying on the melt stage process to eliminate any gaps would require a high level of confidence in the predictability of the extent of film melt flow.

6.2.2 Machine-Related Issues

Several machine-related issues regarding the processing of film interleaves became apparent during the course of the study. The primary issue concerns the heated

compaction device. It was determined that a rolling compaction device could not be used during the film melt stage processing pass due to film adhesion to the roller surface and to subsequent de-bonding of the film from the substrate ply. During placement trials, manual intervention was necessary to constrain roller rotation during this processing stage. A specially designed heated skid device would be advantageous for this process. Additionally, during the film melt stage pass, and to a much lesser degree, during the film tack stage, resin was found to accumulate onto the roller surface. The possibility exists that this material could de-bond from the compaction device and fall onto the laminate damaging or fouling the part surface. A method must be employed for the removal of this material from the device during placement processing operations to avoid such an occurrence.

The supply of the film to the placement head could be achieved in similar fashion as the composite tape by the addition of a film spool creel to the placement machine. However, due to the increase in film length during the tack stage as reported in Section 5.1, the spool would have to be actively controlled to keep the necessary minimum tension in the film during processing.

In order to increase throughput and thus realize a more economical process, future studies might be directed towards the elimination of either the film tack or film melt stages as presented herein. If it is subsequently found that both stages are necessary, modification to the placement machine hardware may allow both the tack and the melt stages to be performed concurrently. Presented in Figure 6.1 is a schematic drawing detailing a possible machine configuration to accomplish both film tack and film melt

processing stages with a single pass. In the fabrication of large positive-curvature parts such as fuel tanks, where the envelope of the placement head is not critical, this configuration may be placed in front of the standard composite tape feed system and compaction roller. This would allow for the processing of the film layer and the next composite layer simultaneously. One obvious disadvantage of this method, however, is that visual inspection of the film layer would not be possible; a high degree of confidence in the process would be required.

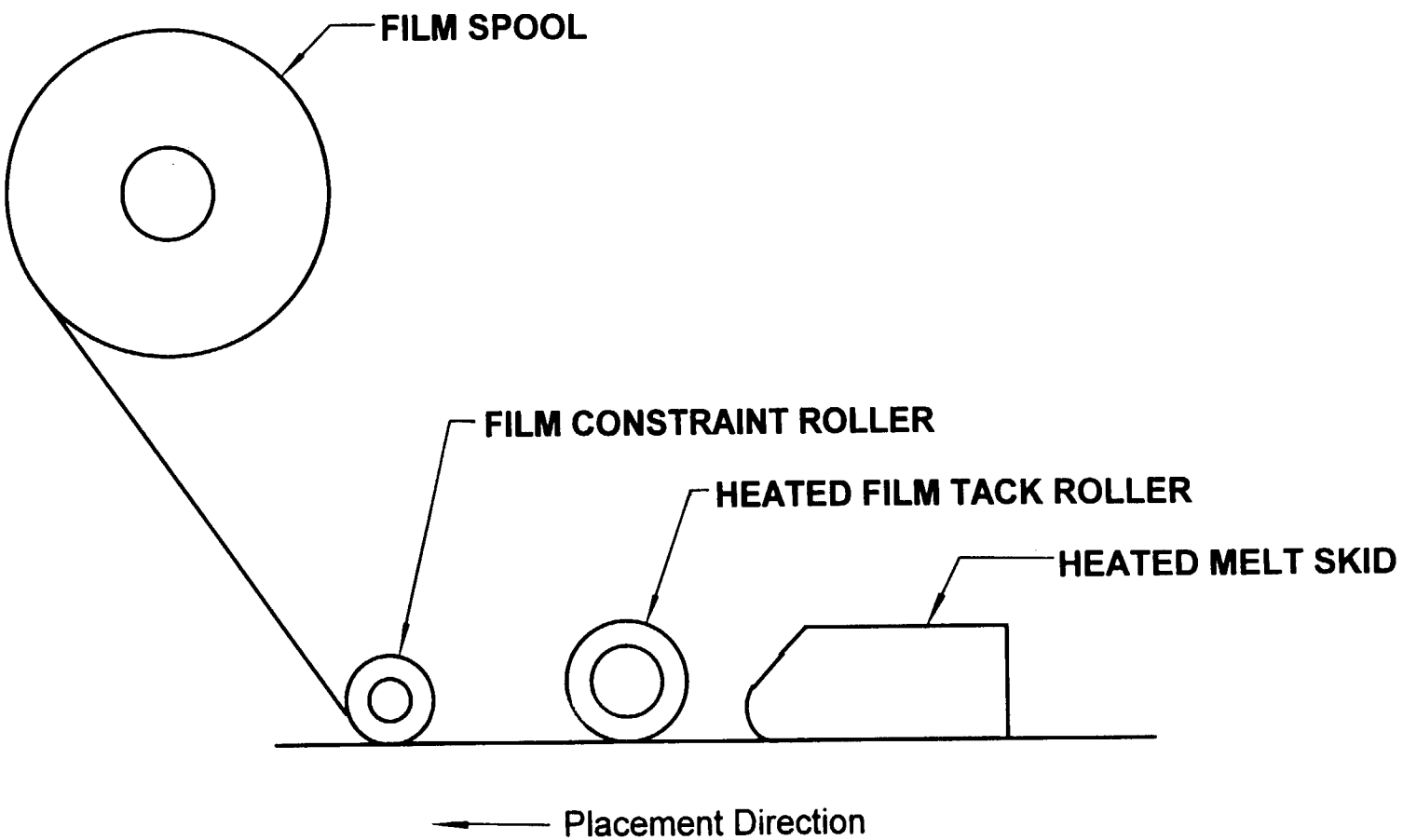

Figure 6.4. *Schematic of possible machine configuration for simultaneous processing of both film tack and film melt stages.*

REFERENCES

1. Williams, L.A., 1987. Engineered Materials Handbook, ASM International, Metals Park Ohio. 1:631-635.
2. Measom, R. and Sewell, K., 1996. Annual Forum Proceedings of the American Helicopter Society, 52(1):611-622.
3. Martin, J.P., Langone, R.P., Pasenen, M.J. and Mondo, J.A., 1997. Science of Advanced Materials and Process Engineering Series, 42: 48-55.
4. Smith, A. and Anthony, D. 1992. International SAMPE Technical Conference Series, 24:T399-T407.
5. Evans, D.O., 1993. Science of Advanced Materials and Process Engineering Series, 38:170-181.
6. Enders, M.L. and Hopkins, P.C., 1991. Science of Advanced Materials and Process Engineering Series, 36:778-790.
7. Munjal, A.K., 1987. Advanced Composites III: Expanding the Technology, ASM, Metals Park, Ohio, pp. 53-56.
8. Sela, N. and Ishai,O., 1989. Composites, 20(5):423 - 435.
9. Dolan, G.L. and Masters, J.E., 1998. International SAMPE Technical Conference Series, 20:34-45.
10. Kaw, A.K. and Goree, J.G., 1987. International Conference on Composite Materials Series, 3:3.146-3.145.

11. Lagace, P.A., Weems, D.B. and Brewer, J.C., 1986. Composites '86 - Japan Society for Composite Materials, pp. 323-330.

12. Partridge, I.K., Jaussaud, J.M. and Neyrat, T., 1990. ECF 8, Fracture Behaviour and Design of Materials and Structures, 1:231-236.

13. Hirschbuehler, K.R., 1985. Toughened Composites, ASTM, pp. 61-73.

14. Masters, J.E., 1987. Sixth International Conference on Composite Materials and Second European Conference on Composite Materials, 3:3.96-3.107.

15. Munjal, A.K., 1988. AHS Annual Forum, 44th. pp. 931-988.

16. Evans, R.E.and Masters, J.E., 1985. Toughened Composites, ASTM, pp. 413-436.

17. Wang, C.Z., Jang, B.Z., Liu, C.W., Shih, W.K. and Valiare, B.T. 1989. Proceedings of the 7th International Conference on Composite Materials, 1:325-330.

18. Frazier, J.L. and Clemons, A., 1990. Science of Advanced Materials and Process Engineering Series, 1990. 35:1620-1627.

19. Krieger, R.B., 1987. SAMPE Quarterly, 23:30-32, 83.

20. Chan, W.S., 1991. Journal of Composites Technology and Research, 13:91-96.

21. Chen, S.F.and Jang, B.Z., 1991. Composites Science and Technology, 41(1):77-97.

22. Messersmith, P.B. and Gianellis, E.P., 1995. Journal of Polymer Science, 33:1047-1057.

23. Robinson, M. J., 1994. Proceedings of the 35th AIAA/ASME/ASCE/AHS/ASC Structures, Structural Dynamics, and Materials Conference, pp.544-551.

24. Towell, T. W., Johnston, N. J., Grenoble, R. W., Marchello, J. M. and Cox, W. R., 1996. Science of Advanced Materials and Process Engineering Series, 41:1701-1711.

25. Grenoble, R.W., M.S. Thesis, Old Dominion University, Norfolk, VA., 1998.

26. Talbott, M. F., Springer and G. S., Berglund, L. A., 1987. Journal of Composite Materials, 21:1056-1081.

27. Barton, J. M., Lloyd, J. R., Goodwin, A. A. and Hay, J. N., 1990 British Polymer Journal, 23:101-109.

28. Curtis, P.T., Davies, P., Partridge and I. K., Sainty, J. P., 1987. Proceedings of the 6th International Conference on Composite Materials, and 2nd European Conference on Composite Materials, 4:4.401- 4.412.

29. Cebe, P., Chung, S.Y. and Hong, S-D., 1987. Journal of Applied Polymer Science, 33:487-503.

30. Kelly, W.E., 1988. Engineered Materials Handbook, ASM International, Metals Park, Ohio. 2:142-144.

31. Hatekeyama, T., Quinn, F.X., 1994. Thermal Analysis: Fundamentals and Applications to Polymer Science, John Wiley and Sons, West Sussex, England.

32. Pitchumani, R., Gillespie, J.W. and Lamontia, M.A., 1997. Journal of Composite Materials, 31(3): 244-275.

33. ASTM D 5528. 1994. Standard Test Method for Mode I Interlaminar Fracture Toughness of Unidirectional Fiber-Reinforced Polymer Matrix Composites, 14.02:272-281.

34. O'Brien, T.K. and Martin, R.H., 1993. Journal of Composites Technology and Research, 15(4):269-281.

35. Humer, K., Tschegg, E.K., Platschka, R. and Weber, H.W., 1995. Cryogenics, 35(11):697-699.

36. Newaz, G.M. and Ahmad, J., 1989. Engineering Fracture Mechanics, 33(4):541-5520.

37. Glessner, A.L., Takemori, M.T., Vallance, M.A. and Gifford, S.K., 1989. Composite Materials: Fatigue and Fracture, 2nd Vol. ASTM STP 1012, pp.181-200.

38. Barlow, C.Y. and Windle, A.H., 1988. Composites Science and Technology, 33:135-150.

39. Gutkowski, W.S. and Pankevicius, E.R., 1994. Fatigue and Fracture of Engineering Materials and Structures, 17(3):351-360.

40. Hinkley, J.A., Grenoble, R.W. and Marchello, J.M., 1995. Science of Advanced Materials and Process Engineering Series, 40:1560-1571.

41. ASTM D 3167. 1993. Standard Test Method for Floating Roller Peel Resistance of Adhesives, 14.8:212-215.

42. Hulcher, B., Marchello, J.M. and Hinkley, J.A., 1999. Journal of Advanced Materials, 31(3):37-43.

APPENDIX A

THE WEDGE PEEL TEST METHOD

A.1 Wedge and Peel Testing Literature Review

The primary failure mode in laminated composite materials tends to cause failure by delamination of the component. Extensive research has been conducted on the interlaminar fracture toughness of fiber-reinforced composite materials, a property that plays a significant role in delamination failures. One of the most common mechanical tests performed to determine the interlaminar fracture toughness of composites is the double cantilever beam (DCB) test method. This method has been in use for several years and is an ASTM recognized test for Mode I fracture toughness. There also exists a relatively large body of data on the DCB fracture toughness of various composite materials [33,34].

Other test methods have been used to determine fracture toughness. These tests frequently employ a wedge driven into the material both to initiate and to propagate the fracture. The majority of these tests are simply variations on the standard DCB test method. These test methods are typically offered as alternatives to the DCB, which has several disadvantages such as lengthy and detailed specimen preparation and testing.

Humer et al. report on the use of a wedge splitting test for use in their work on the characterization of the interlaminar fracture behavior of an epoxy composite (Isoval 10) at room temperature and at 77 K. In their method, the specimen is prepared with a starter notch and is placed vertically in the test machine. A wider region above the crack starter

notch is present in the sample and is used for the location of load transmission hardware. Between the wedge and the load transmission hardware are located two steel pins on each side of the wedge. A razor blade is forced into the starter notch to sharpen it prior to testing. A wedge having a 16° included angle is placed into the specimen and is forced downward by the test frame. Cross-head speed is held constant during testing at 0.5-mm/s. High standard deviations are reported and are believed to be the result of differences in starter notch location and to non-uniform crack sharpening with the razor blade [35].

Newaz and Ahmad have employed an alternative technique to determine the Mode I delamination energy release rate of polymeric composites. Their method employs the insertion of a small cylindrical rod into the test specimen. Testing is performed under constant displacement control. The advantage of their method is the relative simplicity and ease of preparation of the specimen as compared to the DCB test configuration. An additional purported advantage is the ability to test specimens in adverse environments due to lack of need for standard DCB loading hardware [36].

Glessner, Takemori, et al. take a somewhat similar alternative approach to interlaminar fracture toughness testing. The opening load is introduced by means of an apparatus that is forced into the opening of the specimen. The loading device consists of double counter-rotating bearings, each set of which make contact with opposing sides of the specimen arms. During testing, the sample is forced over the loading device, which is held fixed with respect to the test frame. The main purpose of this design is to reduce the friction component that is present in the wedge-type test methods. The authors report that

the advantages of the use of this technique is that it provides direct crack velocity control and a stationary crack tip front relative to the laboratory test frame [37].

Barlow and Windle use a razor-blade technique in the investigation of fracture toughness. In this test, a thin section of specimen is split off from the sample, and measurements are made of the crack length, section thickness, and wedge thickness. This information, in addition to the material elastic modulus, allows for the determination of the interlaminar fracture toughness of the material. The authors report that the use of this test requires no need for the measurement of loading during testing. Another benefit reported is that no special specimen geometry is necessary [38].

Gutkowski and Pankevicius utilized both the DCB test and a peel test method to assess the use of a new surface preparation process on the adhesion properties of ultra-high-molecular-weight polyethylene (UHMPE) fibers to an epoxy matrix. The peel test specimens were prepared by bonding two composite strips to a rigid substrate. A crack starter was introduced at the ply interface by use of a thin Teflon film. The upper specimen ply was attached to the test frame cross-head so that the angle between the upper and lower specimen arms approached 90° during testing. Specimens were tested at three peel rates ranging from 0.5 to 5.0-mm/min. Again, as with many of the alternative test methods, the results are reported to compare favorably with DCB results and that the peel method is the simpler of the two [39].

Hinkley, Grenoble, and Marchello make use of the ASTM D 3167 floating roller peel resistance test method in their investigation of the time-dependent behavior of thermoplastic welding during the fiber placement process. The use of the test is to obtain

relative bond strength data in investigation of the use of a ribbon-welding device to simulate the placement process. The test was designed primarily to determine the peel resistance of adhesively bonded metallic joints. The test specimen consists of both a rigid and a flexible adherend. A relatively complicated apparatus is used in the test. This test method does not purport to give data indicating a relative fracture toughness value; the method is employed to determine relative peel resistance values [40,41].

A.2 Introduction to the Wedge Peel Test

The optimization of fiber placement processes for a particular material requires the investigation of the effects of many process variables on part quality. The relatively large number of processing variables inherent in fiber placement processing typically requires the performance of numerous placement trials to assess the relative importance of the variables on part quality. The need for a quick, simple test method to determine the relative interfacial strengths during process development led to the use of the wedge peel test method in the present study. An earlier study was conducted to determine if a correlation existed between the data obtained for Mode I interlaminar fracture toughness as obtained by the DCB test method and peel strength as determined by the wedge peel test method. The results of the study indicated that a general correlation did indeed exist between the data from the two test methods [42]. The primary benefit of the alternative wedge peel test is the speed at which specimens can be fabricated and tested. Additionally, a high number of data points are acquired and averaged for each peel

specimen as compared to one crack initiation data point and five propagation data points for the DCB test.

A.3 Test Hardware and Procedure

The wedge peel fixture as currently used consists of a stainless steel wedge held in an aluminum frame. Incorporated into the upper end of the fixture is a threaded mount block for attachment of the peel fixture to the load cell of the test frame. A set of two simply-pinned joints connects the frame to the threaded mount, providing rotational freedom of the fixture about axes both parallel and normal to the specimen interfacial plane. This reduces or eliminates the introduction of forces due to specimen or test hardware misalignment from affecting the results of the test. Adequate length between the upper portion of the fixture and the wedge has been added to enable the testing of longer specimens without the need to curl or bend the specimen to fit the fixture.

A scale drawing of the wedge peel test fixture is presented in Figure A.1. The drawing is presented only to illustrate the basic design and size of the fixture, hence the omission of many of the dimensions. The right frame member of the fixture in the left view of the figure has been removed for clarity. The wedge is fabricated from 0.16 cm stainless steel and has an included angle at the nose of approximately 45°. Small radii are present at the nose and on both sides of the wedge to remove sharp edges and to reduce the frictional component during testing. The as-designed test fixture is capable of peeling specimens up to 6.35-cm wide. A photograph of the test hardware is presented in Figure A.2. Note that the specimen arms straddle the wedge and are held in the grips in the lower portion of the

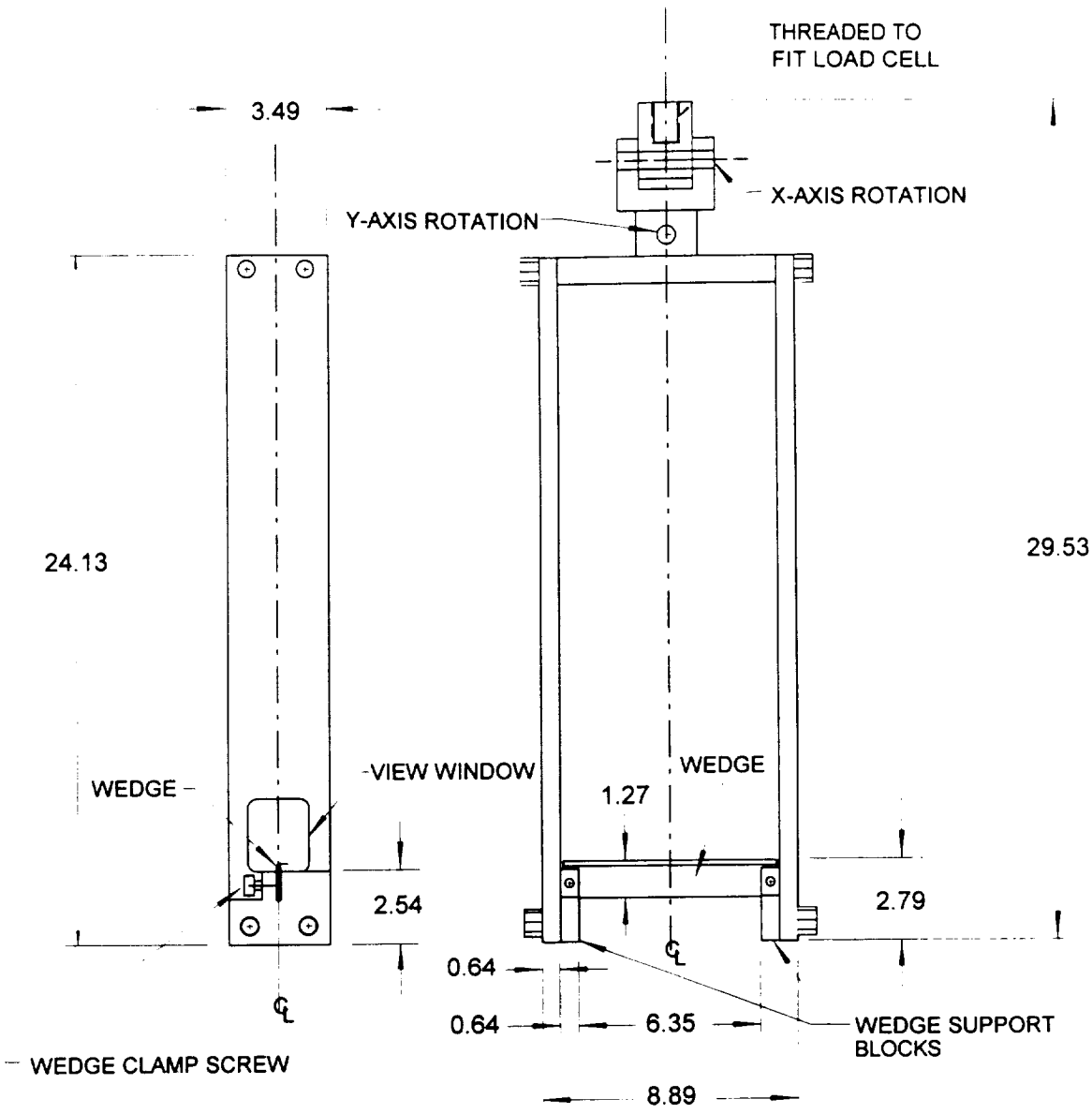

Figure A.1. *Wedge peel test fixture. Part of frame is removed in left view for clarity. Dimensions are in centimeters.*

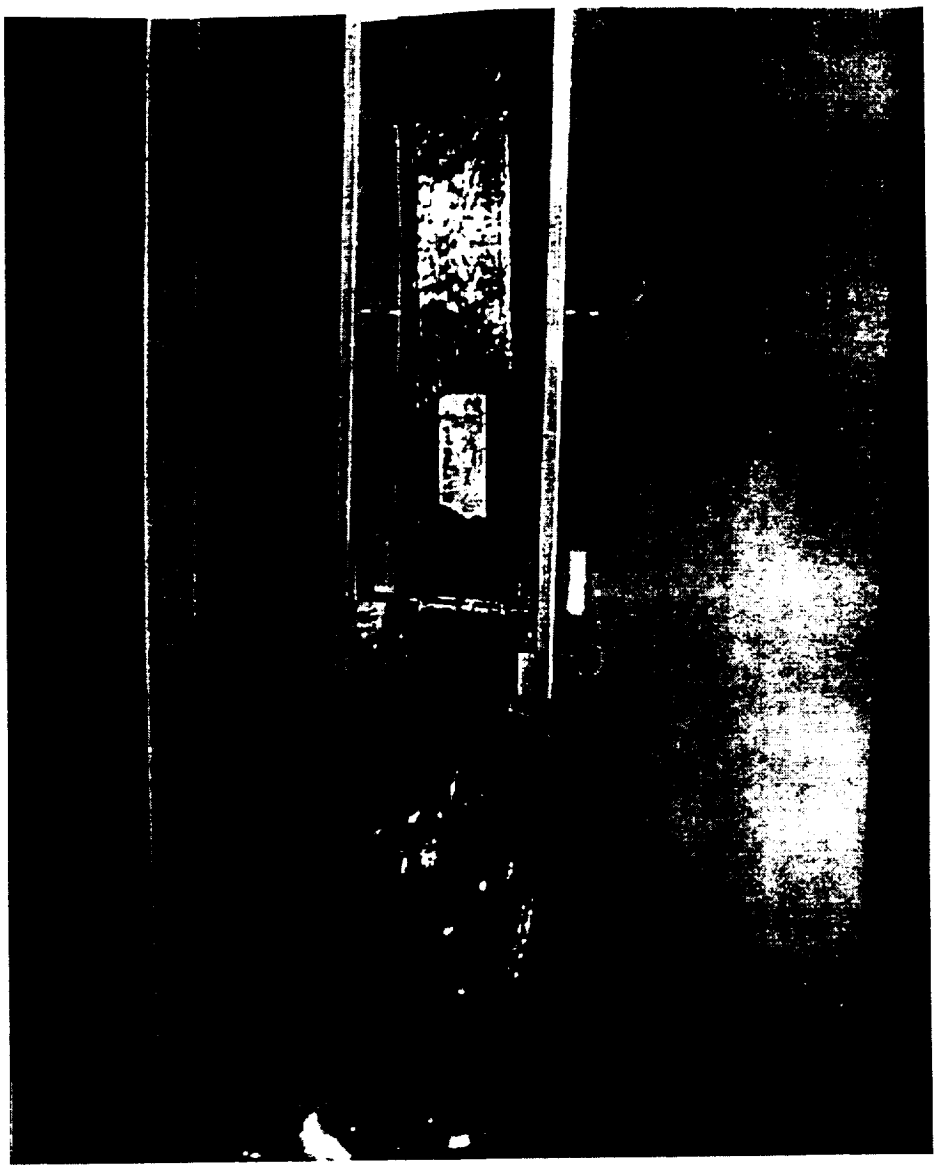

Figure A.2. *Photograph of wedge peel test fixture in use on SATEC test frame.*

figure. The test frame cross-head, together with the wedge test fixture, is actuated upward, while the test specimen is held fixed. In this manner, the wedge is driven upward through the interface between the specimen plies. Data is acquired on the cross-head position and load, and the results are stored in a computer file by the system software. A 2.22-kN load cell is used during testing. Cross-head speed is held constant during testing at 1.27-cm/s. Typically, peel specimens are 24.13-cm in length, with 6.45-cm of un-bonded length available to straddle the wedge and be held in the machine grips. An additional 2.54-cm of the specimen remains bonded after testing so that the specimen halves remain together for future reference, including possible fracture surface inspection. This provides a total as-tested length of 15.24-cm. Section 4.1 contains additional information on specimen fabrication and geometry.

A.4 Data Reduction and Observations

During testing, the peel data are displayed in real time on the test system computer monitor. At the conclusion of each test, a worksheet containing a plot of the data and the value of the peak load is printed for documentation and reference purposes. The average peel strength for each specimen was found by using a data area transform in the SigmaPlot graphing and data analysis software. The transform performs the area integration by use of the trapezoidal rule numerical integration technique. The data, which are acquired in units of pounds and inches, are then normalized with respect to both specimen width and length and converted to the SI units of kN/m.

In order to initiate fracture at the specimen interface, and to have an un-bonded length of material to straddle the wedge and be gripped in the test frame, specimens must be fabricated with a thin film in place at the interface to serve as a crack starter. The presence of this film during placement of the upper composite ply introduces a resin-rich region at the end of the film. In composites having tough resin matrices such as PEEK, the values of the peel strength are typically quite large in this region and are evidenced as peak values at the start of the peel tests. In specimens of low peel strength, these crack-initiation values tend to be the highest recorded for the specimen. In higher strength specimens, these values are quite often eclipsed by data acquired further along the specimen length.

Specimens of low peel strength tend to fail adhesively at the peel interface. Such specimens exhibit a high degree of stick-slip behavior. Test data of such a specimen is shown in Figure A.3. Specimens of higher peel strength tend to fail cohesively at the interface and have a reduced tendency to exhibit such stick-slip behavior. An example of data from such a specimen is presented in Figure A.4.

Earlier wedge peel testing was conducted using 2-ply peel specimens. Cohesive failure through the specimen plies was frequently observed for specimens of higher peel strength. Observations revealed that the specimen plies were simply not stiff enough to resist bending and fracture as the crack front distance ahead of the wedge became increasingly short. The use of 4-ply peel specimens has extended the range of strengths that may be tested by increasing the specimen arm thickness.

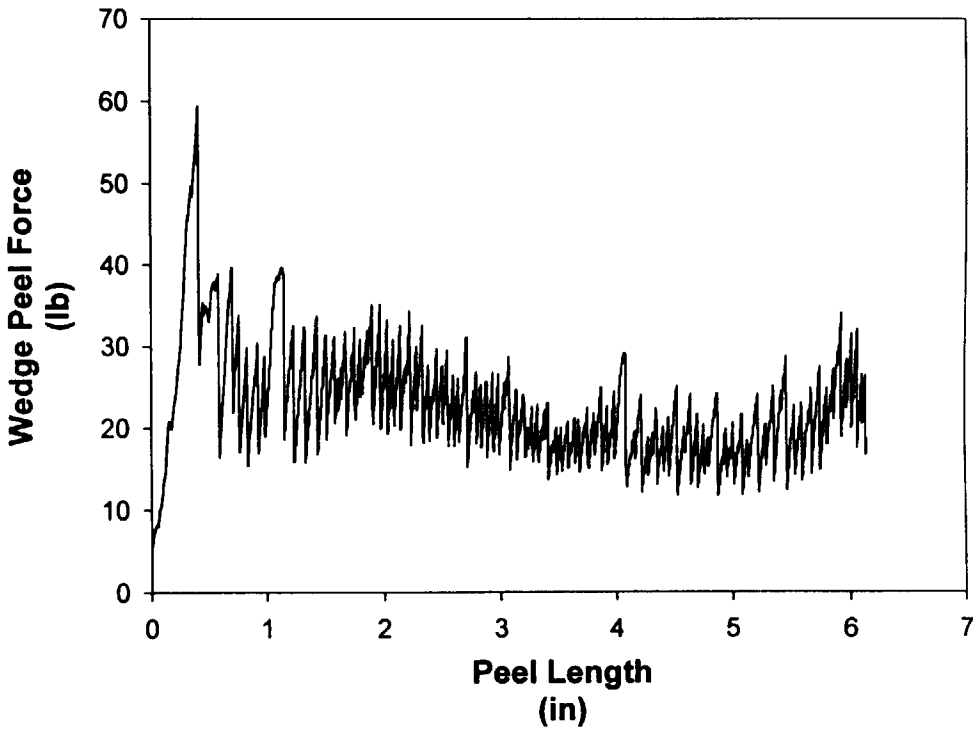

Figure A.3. *Wedge peel test data of low peel strength specimen as recorded by test software. Note initial peak in peel force. Sawtooth profile shown is common in cases of adhesive failure at the peel interface. Average peel strength of this specimen was 3.10-kN/m.*

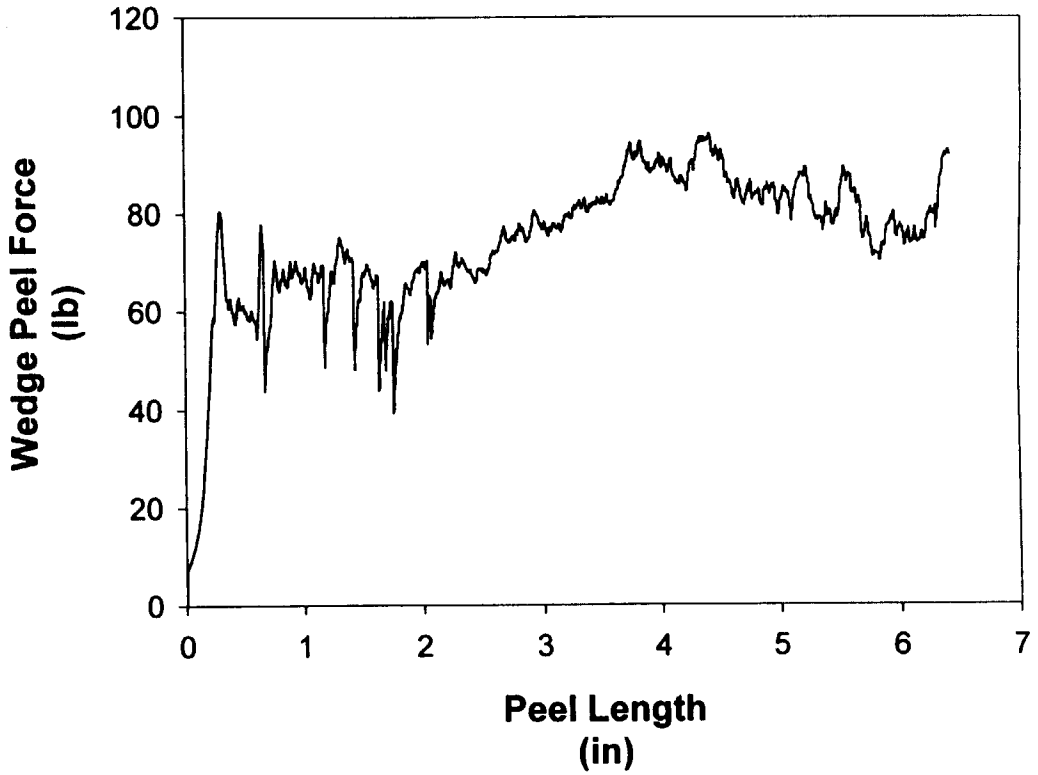

Figure A.4. *Wedge peel test data from a specimen of high peel strength as eworded by test software. Note the reduction in stick-slip behavior as compared to Figure A.3, and the absence of such behavior at higher peel force values. The average peel strength for the specimen shown was 10.44-kN/m.*

APPENDIX B

PLACEMENT TRAILING SHOE DESIGN*

B.1 Introduction

The processing of fiber-reinforced polymer-matrix composite materials by fiber placement requires the use of material preheating sources, as well as a heated compaction roller. The purpose of the heated compaction roller is to apply the pressure required for the adequate bonding between the incoming composite tape and substrate plies. The compaction roller must be heated so as to avoid being a heat sink, drawing heat away from the material interface being processed. This would result in inadequate melt flow and adhesion during processing. The need to maintain the roller at relatively high temperatures may, however, result in polymer/fiber adhesion to the roller surface. This adhesion results in damage to the upper composite ply surface. Additionally, this material must be removed from the roller surface prior to the continuation of the processing effort.

One way in which this problem may be solved is to have a device follow directly behind the heated compaction roller to keep the material from adhering to the roller surface. During placement of flat composite panels, a simple flat-surfaced trailing shoe is used. For placement of cylindrical parts, the shoe must have a contoured surface that fits the placement tool being used.

---

* This design has been submitted for United States Patent protection, NASA LaRC Patent Disclosure No. LAR 16097-1-CU.

Most composite articles consist of several plies with each ply having a pre-specified fiber direction or angle. A trailing shoe must therefore be designed and fabricated for use with each ply angle. Additionally, separate shoe systems must be designed and produced for use with specific cylinder diameters due to the non-compliant nature of the shoe hardware.

The challenges in the design of a trailing shoe system for composite cylindrical shell fabrication are in the need for the shoe to fit the placement surface accurately and that it approach the rear of the compaction roller as closely as possible, which is necessary to achieve maximum effectiveness. Additionally, design difficulties are increased if it is desired that the shoe system be actuated independently of the compaction roller, as might be the case if different contact forces on each are desired. The shoe must be accurately located and mate precisely to the placement surface after each retract and extend cycle of the shoe system.

B.2 Design Methodology

In the operation of robotic systems, specific spatial points are used to establish cartesian coordinate system reference origins for each of the robotic axes as well as for the end-effector, or tool, which is used to accomplish the specific task. Information supplied to the robotic machine to effect coordination of each joint axis, simultaneously, and in real-time utilizes the known locations and distances of each of these reference points to calculate joint rotation and to thus accomplish the desired trajectory of the end-effector. The reference origin for the NASA Langley Research Center placement machine

end-effector coordinate system resides at the center of mass of the of the fiber placement compaction roller. In the design, layout, and installation of the placement facility, care must be taken to accurately position and secure the cylindrical placement tooling with respect to the placement robot to insure that, when using contoured compaction rollers, there is proper alignment for mating of the tool and roller surfaces. Once this has been accomplished, the end-effector coordinate reference system may be used with confidence in the design of other hardware (e.g., the trailing shoe system) that must in operation maintain a very accurate and physically close relationship to both the roller and placement tool surfaces.

The innovation of the trailing shoe system is in the manner in which the system has been designed to allow for the accurate location of the system with respect to the end-effector coordinate system reference origin. This allows for the ultimate goal of obtaining the accurate and full mating of the shoe lower surface and the placement tool surface. Additionally, the design allows for accurate and repeatable positioning of the shoe by having the shoe pivot about the roller, and hence a coordinate system axis.

B.3 System Description

Figures B.1 and B.2 are presented to identify the components used in the design, and to describe the functioning of the device. Shown in Figure B.1 is a side view of the device as it appears in operation on the placement machine. For simplicity, the figure shows the flat-surfaced Trailing Shoe (1) in placement position on a flat tool surface. Figure B.2 shows an exploded view, from above, of the most important components of the trailing

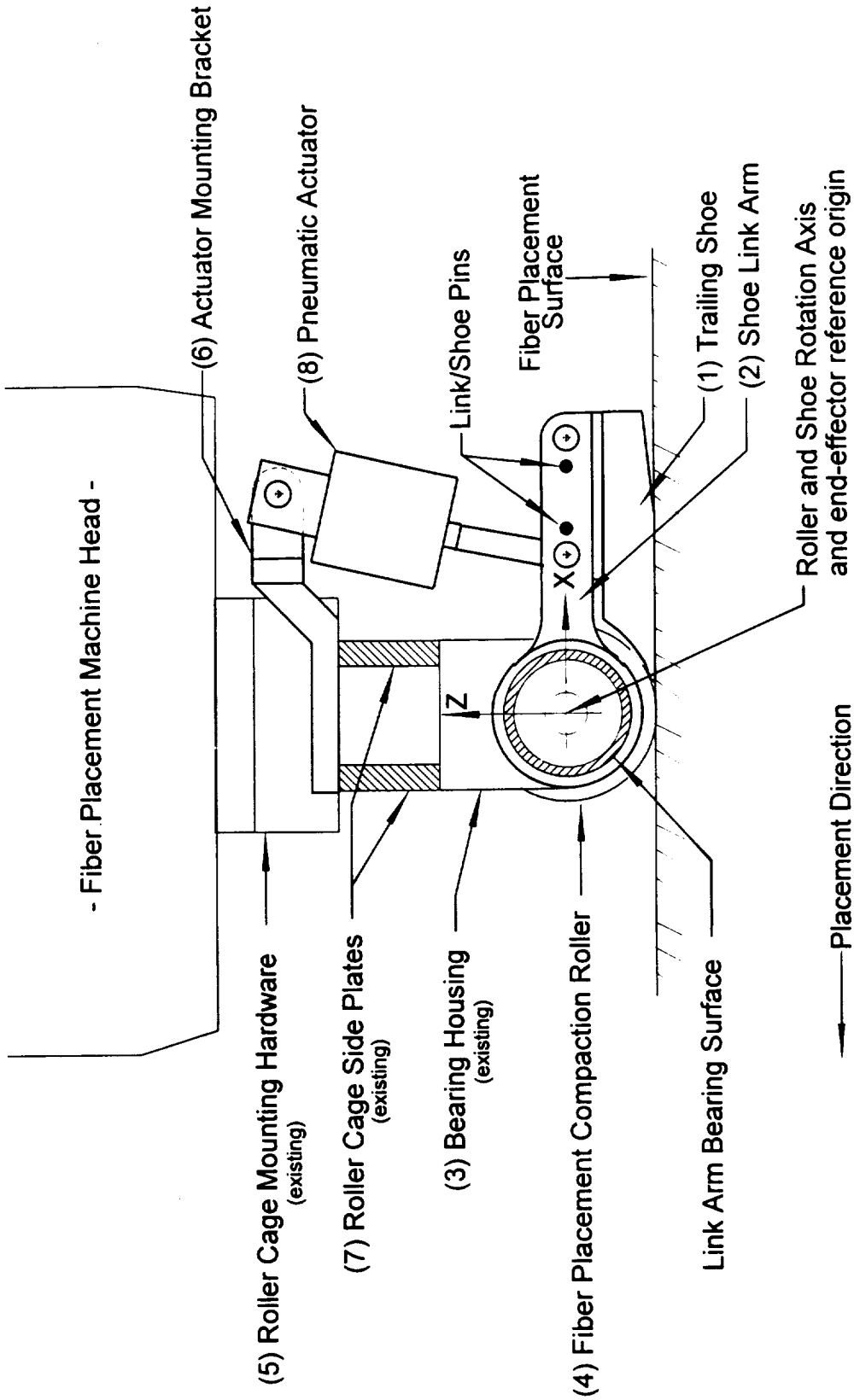

Figure B.1. *Side view of roller cage/trailing shoe assembly with shoe in full extend mode on flat placement tool surface.*

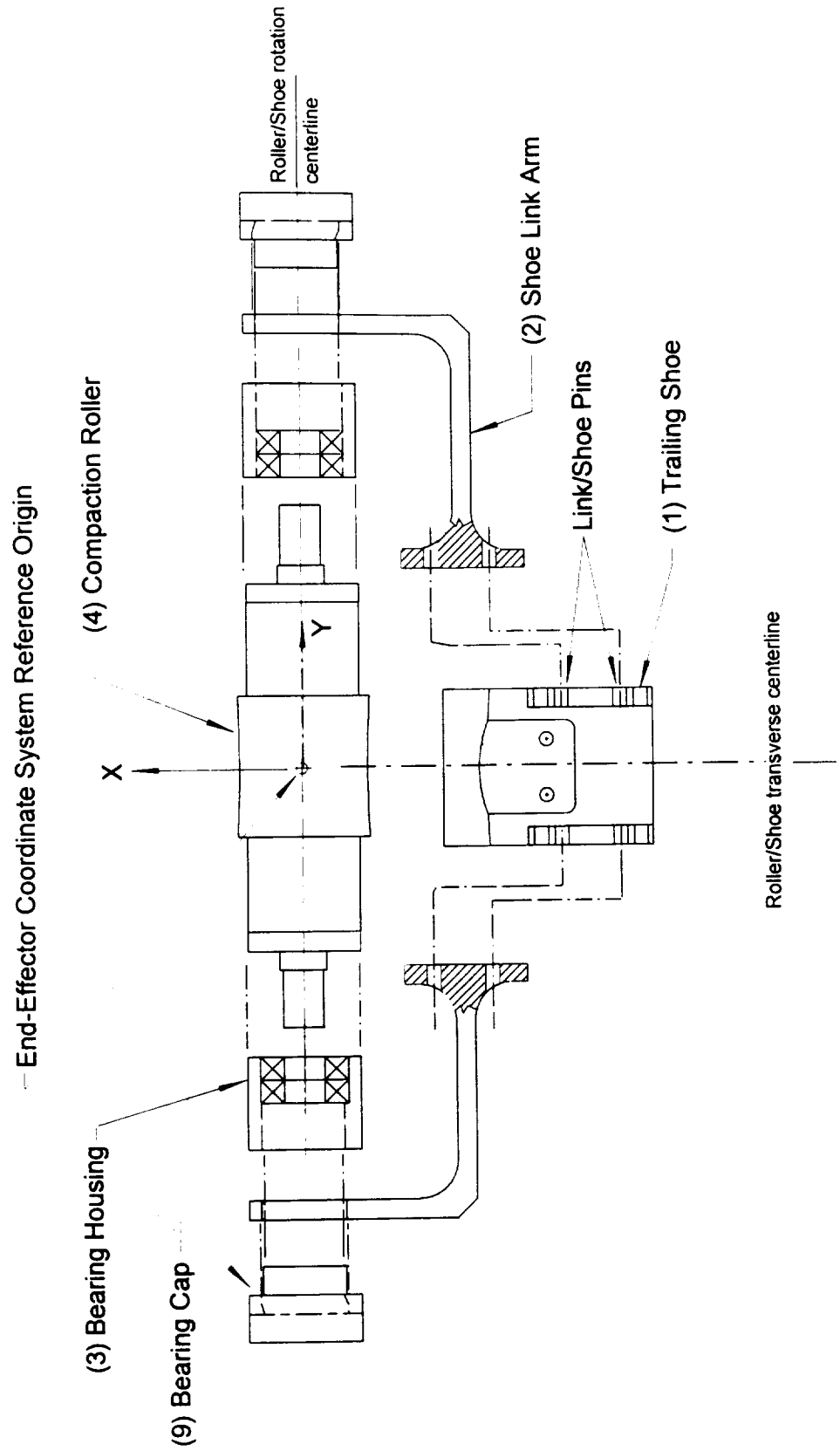

Figure B.2. *Exploded view of roller cage/trailing shoe assembly. Roller shown is contoured for placement of +/- 45 degree plies. Assembly is symmetrical about roller transverse centerline.*

shoe system. Figure B.3 is presented to illustrate and describe the dimensioning method used in the specification of the trailing shoe hardware. The following paragraph describes in detail the components of the shoe system. References should be made to Figures B.1 and B.2 for this discussion.

The Shoe Link Arms (2) are located with respect to the Trailing Shoe (1) by use of precisely located dowel pins, and are secured to the shoe by use of machine screws (Figures B.1 and B.2). The existing Bearing Housing (3) is bored to accept the circular boss detail of the Bearing Cap (9) (Figure B.2). The bore location for the Bearing Cap is machined concentric to the bore that houses the roller bearings. This is crucial for location of the entire shoe system with respect to the roller coordinate reference system. A hole in the Link Arm, which is machined to close tolerance both in diameter, and in location with respect to the shoe pins, is present to accept, and mate to, the larger diameter bearing surface detail of the Bearing Cap (Figure B.1). The clearance between the Link Arms and the bearing surface is kept to a minimum to insure accuracy of location of the shoe system. The Bearing Caps are bolted to the bearing housings, which are then positioned over the roller shaft ends. The Pneumatic Actuator (8) (Fig. B.1) is connected to the Roller Cage Side Plates (7) by means of the Actuator Mounting Bracket (6). Simple extend/retract operation of the actuator effects the limited rotation of the shoe about the roller axis (extend and retract), and thus the ability to provide shoe contact forces independently of the compaction roller load.

The key to the successful implementation of the trailing shoe system, as presented herein, in terms of accuracy and repeatability of position with respect to the placement

X1: determined from roller diameter and any clearances required
X2: determined by desired shoe contact surface area

L1, L2: arbitrarily chosen based on X2
(link arms must have same dimensions)

R1: compaction roller radius

R2: placement tool radius

Location for Y1, Y2 determined by R1, R2, X1, X2 by the following:

$Y1 = (R2 + R1) - (R2^2 - X1^2)^{0.5}$

$Y2 = (R2 + R1) - (R2^2 - X2^2)^{0.5}$

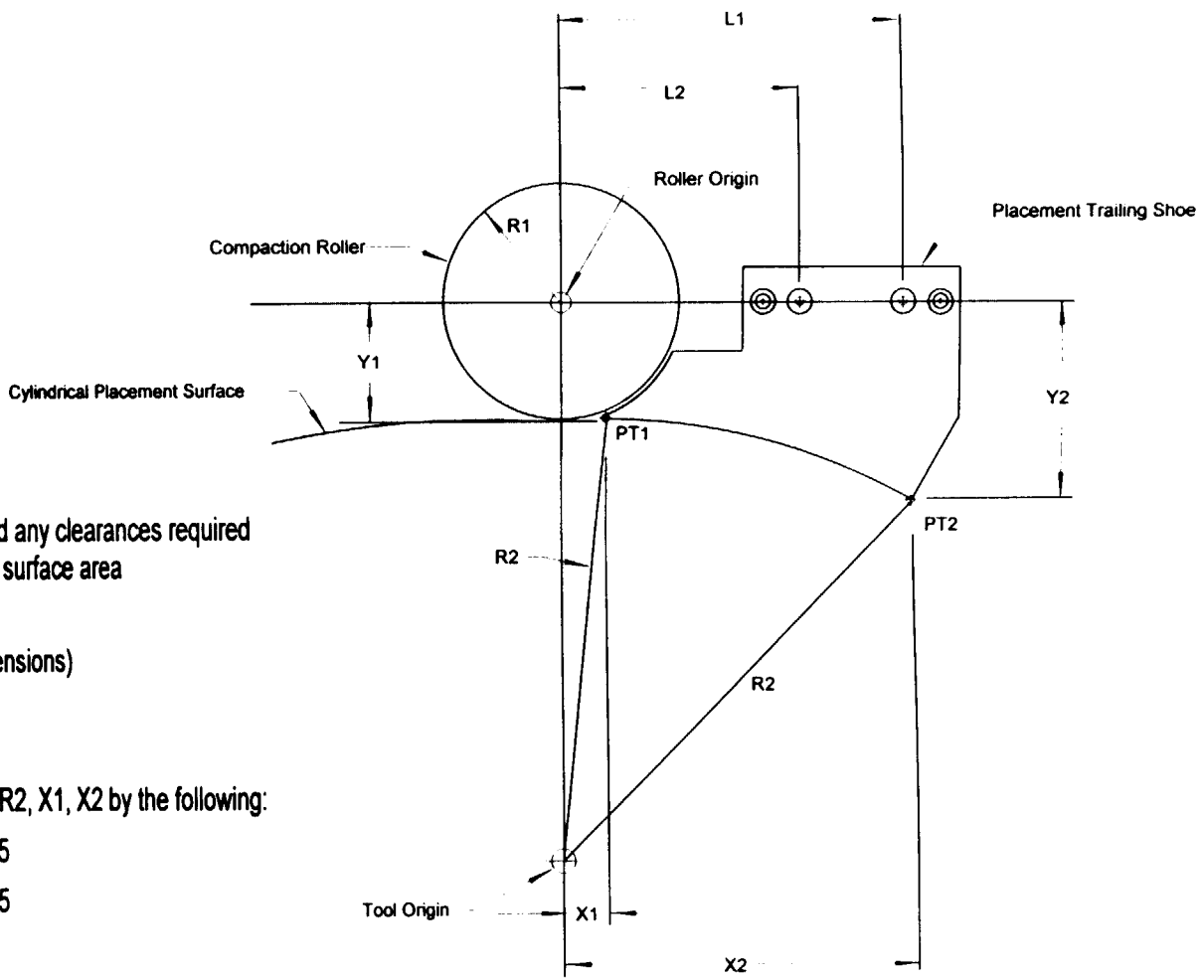

Figure B.3. *Dimensioning methodology employed in the trailing shoe system design. Shown in the figure is the circumferential, or 90 degree, placement shoe. The L1 and L2 dimensions are the same for all shoes, allowing for interchange during placement processing.*

surface, is the maintaining of close geometric and dimensional tolerances during component machining and fabrication.

During fiber placement fabrication operations, the shoe temperature will increase due to convection heat transfer from the roller and conduction from the composite. To prevent polymer or composite material sticking problems, each shoe insert has passages for water-cooling. Figures B.4 through B.9 and the machine drawings of Figure B.9 are provided to further clarify the trailing shoe system design and operation. In each of the photos, the fittings for the shoe cooling water can be seen at the rear of the shoe. The machine drawing entitled '+/-45 DEG. SHOE PLUMBING' is provided in the following machine drawing set to illustrate the cooling water plumbing path and is representative of this feature for all of the shoe inserts.

B.4 System Actuation and Control

The trailing shoe system is designed to be actuated independently of the compaction roller. This allows for the adjustment of shoe contact force values independent of the placement compaction roller as was previously mentioned. A pneumatic piston is used to actuate the shoe and is attached to the shoe at the piston rod end, and to the roller cage by means of the actuator mounting bracket. Connections to both the shoe and the mounting bracket are simple pin and clevis connections. Air pressure is used for both extend and retract functions. Standard shop air pressure of 552-kPa is supplied to the system. Air flow to the cylinder is controlled by an electronic solenoid-activated spool valve. An in-

line air pressure regulator is used to control air pressure to the actuator to adjust shoe contact forces.

The shoe system is slave-controlled by a signal from the roller force actuator solenoid valve. The extend-shoe function signal is keyed from the compaction roller extend function. The retract-shoe function is keyed from a signal which activates the compaction roller retract. Adjustable timer pots are incorporated into the control system to allow for any necessary timing adjustments such as may be required for material placement rate changes. Figure B.4 shows the simple extend and retract function of the shoe system.

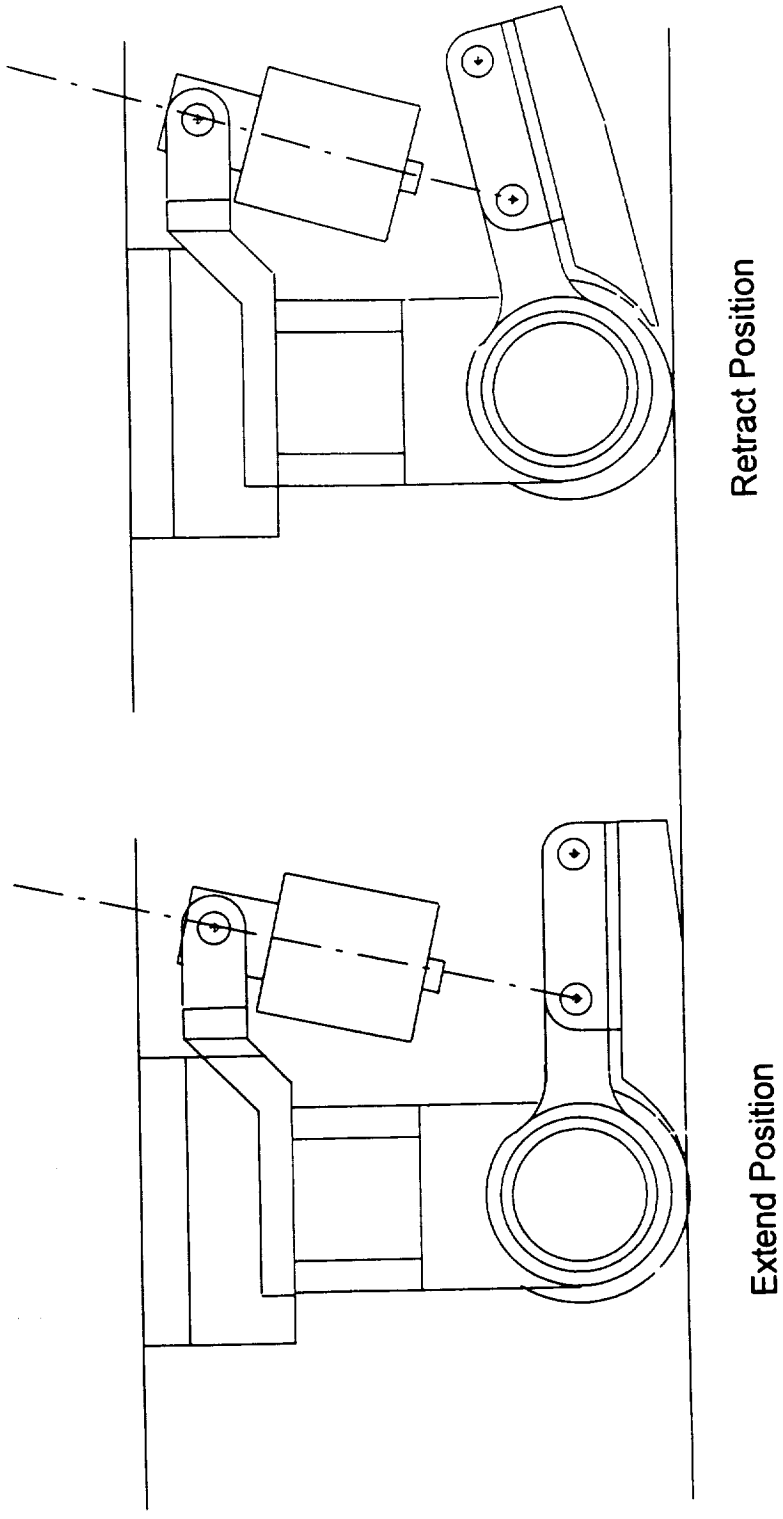

Figure B.4. *Extend and retract actuation of trailing shoe system.*

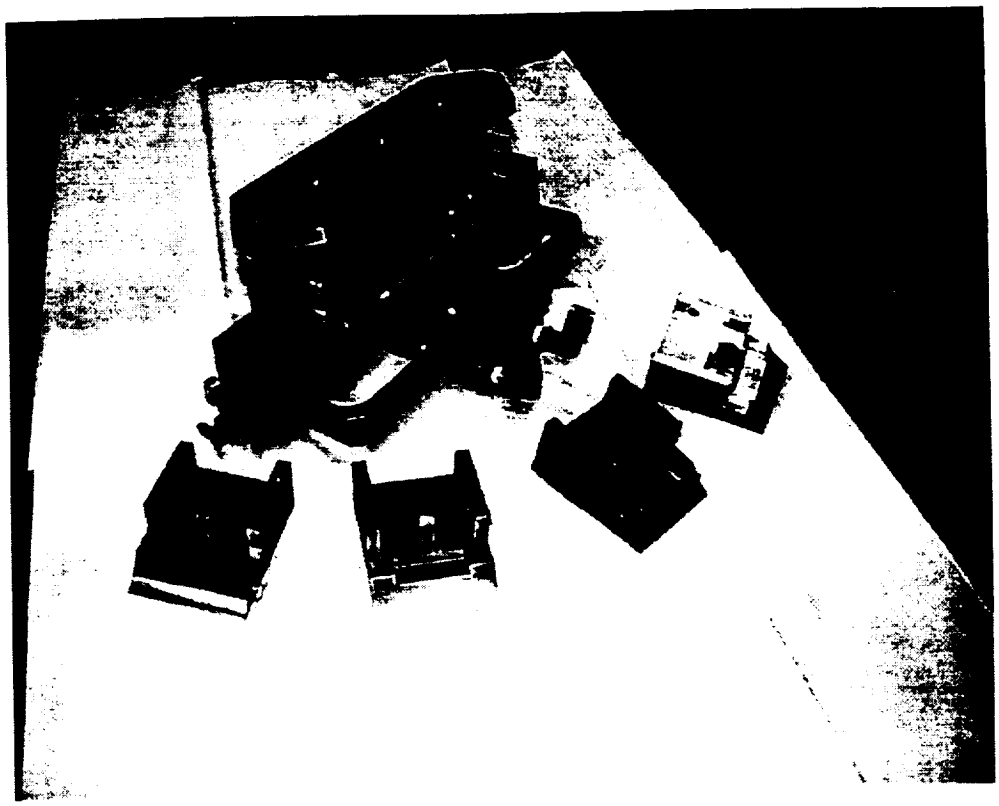

Figure B.5. *Trailing shoe system hardware with +45° shoe insert assembled to roller cage. Visible in foreground from left to right are the 0° (axial), flat, 90° (hoop) and -45° placement shoe inserts.*

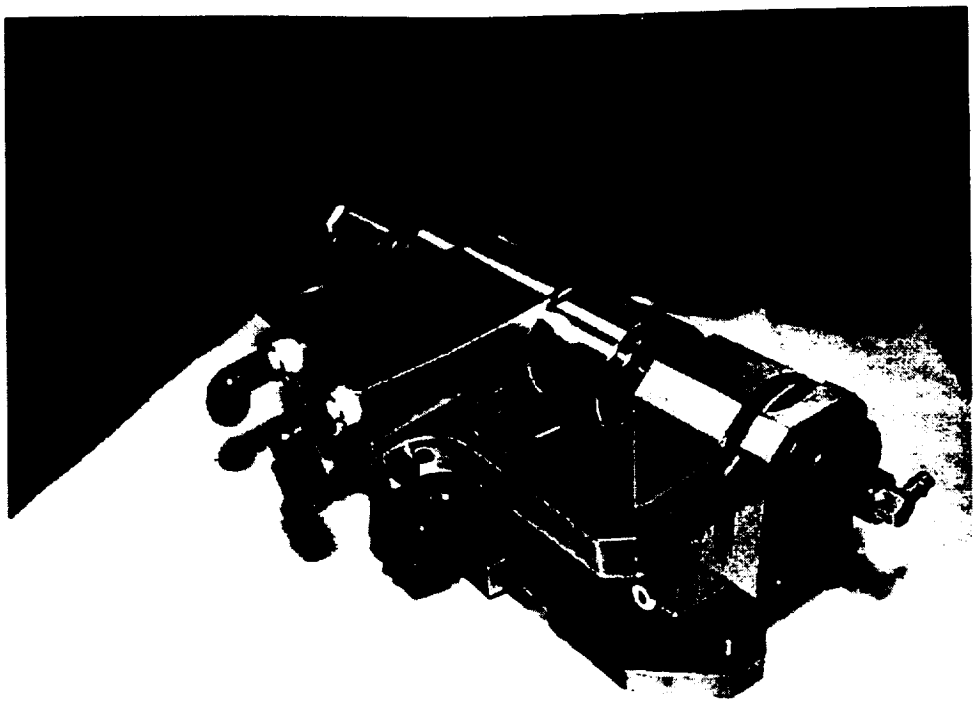

Figure B.6. *Bottom view of roller cage/trailing shoe assembly. Black connectors at left center are fittings for water cooling of shoe.*

Figure B.7. *Trailing shoe in extend position on cylindrical placement tool surface. Note fit of shoe to tool surface.*

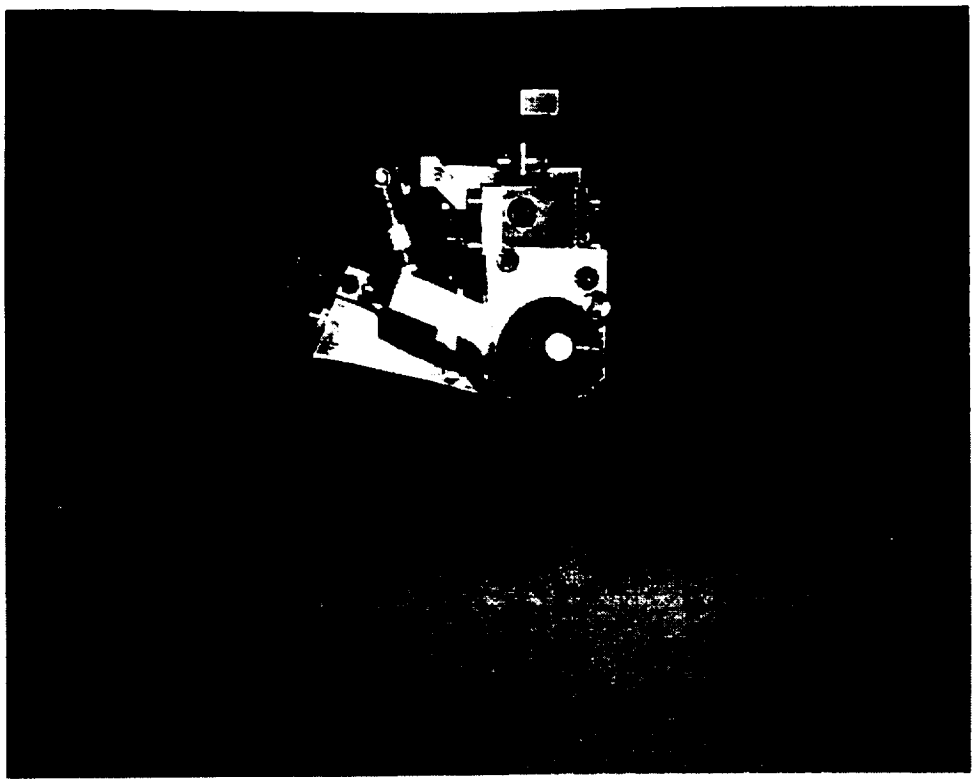

Figure B.8. *Trailing shoe in retract position on cylindrical placement tool surface.*

Figure B.9 *Machine drawings of selected trailing shoe components. All dimensions are in inches.*

This set of machine drawings is provided for further clarification of the function and design of the trailing shoe system. This design has been submitted for United States Patent protection, NASA LaRC Patent Disclosure No. LAR 16097-1-CU.

18 INCH ± 45 DEG. SHOE

QUANTITY REQUIRED: 2 - ONE AS SHOWN, ONE OPPOSITE HAND
MATERIAL: 17-4 STAINLESS
SURFACE FINISH: 32 RMS MIN ALL SURFACES
BREAK ALL CORNERS AND SHARP EDGES .030 MAX. UOS
TOLERANCES: +/-.005 UOS

[redacted]

B. Hulcher - ext 44288

NOTE: ALL VIEWS AND DIMENSIONS
SHOWN WITHOUT .020 RADII
ON SHOE LOWER SURFACE

TABLE OF REFERENCE POINT
DISTANCES FROM DATUM -A -
TO THEORETICAL SHARP CORNERS

POINT	DISTANCE
A	0.868
B	0.893
C	0.952
D	1.310
AC	0.856
BD	1.045
M	0.849
R	1.097

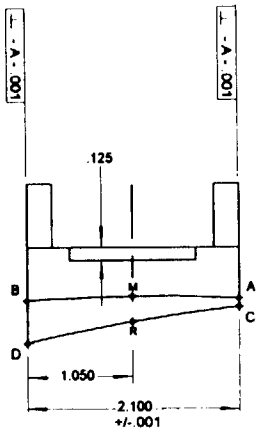

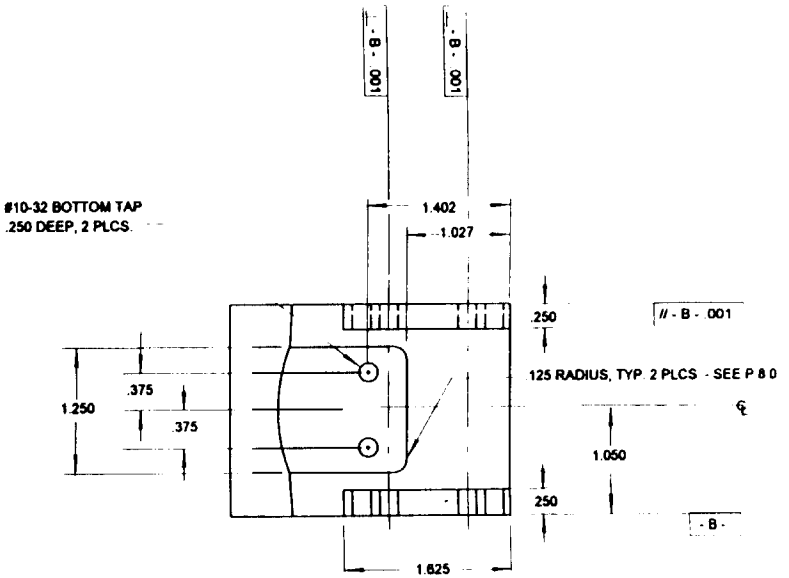

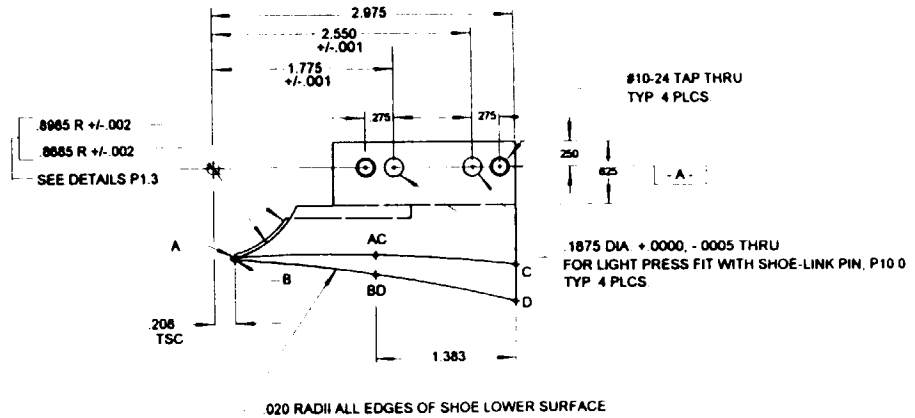

+ 45 DEGREE SHOE SHOWN

18 INCH ± 45 DEG. SHOE
LOWER SURFACE RADIUS DETAIL
+ 45 DEG. SHOE SHOWN

SURFACE FINISH: 32 RMS MIN. ALL SURFACES
TOLERANCES: +/-.005 UOS
ANGULAR: +/-.1 DEG.

filename: 1845shu1.dw2

B. Hulcher - ext 44289

BREAK ALL CORNERS AND SHARP EDGES .030 MAX. UOS

NOTE: ALL VIEWS AND DIMENSIONS
SHOWN WITHOUT .020 RADII
ON SHOE LOWER SURFACE

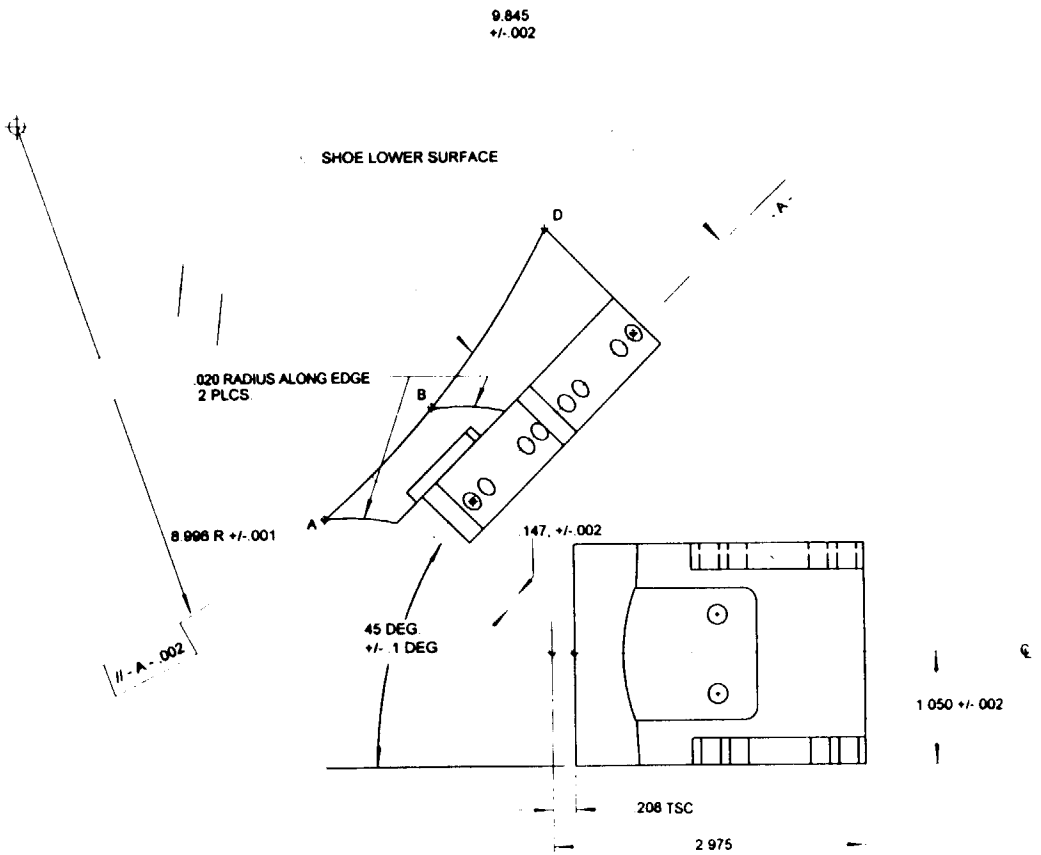

18 INCH ±45 DEG. SHOE

NOSE CONTOUR DETAILS

+45 DEG. SHOE SHOWN

SURFACE FINISH: 32 RMS MIN. ALL SURFACES

TOLERANCES: +/-.002

filename: 1845shu1.dw2

B HULCHER EXT 44289

REFERENCE SECTIONS

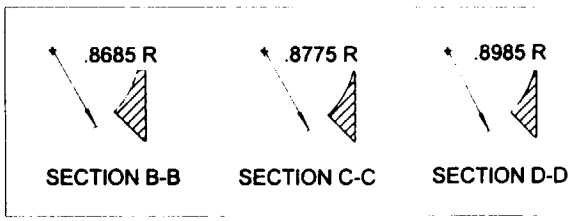

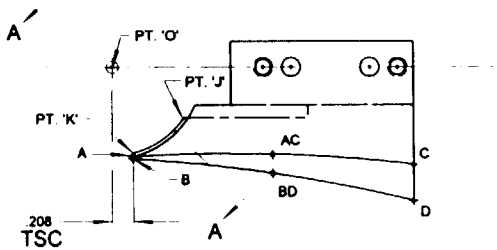

NOTE: ALL SECTIONS TAKEN RADIALLY THRU POINT 'O' AS IN SECT. A-A WILL BE IDENTICAL TO SECT. A-A FROM POINT 'J' TO POINT 'K'

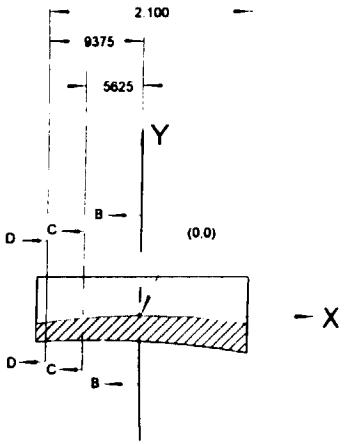

SECTION A-A

TABLE OF POINTS FOR ELLIPTICAL NOSE CONTOUR

X	Y
0.00	0.00
.09735	0.00
.1875	-.001
.2812	-.002
.375	-.004
.4687	-.0055
.5625	-.009
.6562	-.012
.750	-.015
.8737	-.0195
.9375	-.024
1.050	-.030

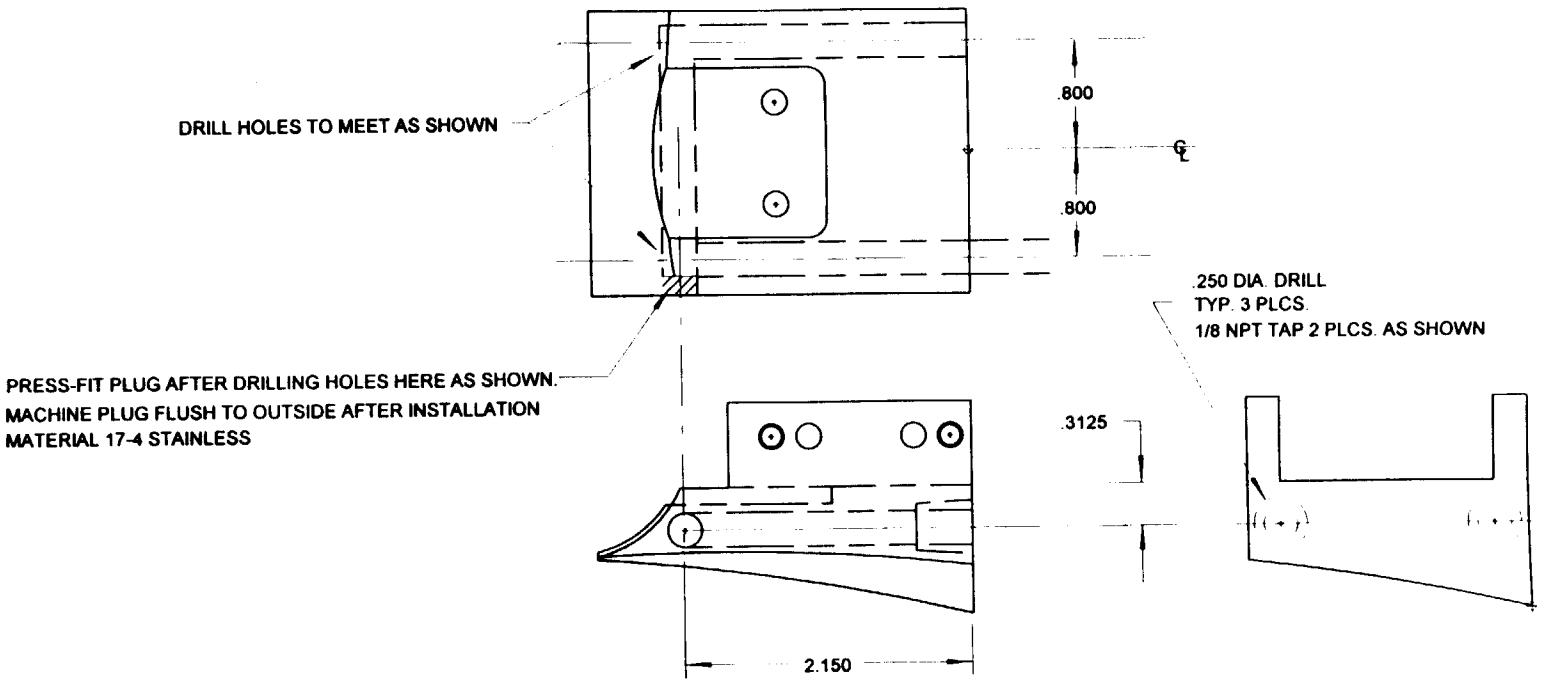

+/-45 DEG. SHOE PLUMBING

TOLERANCES: +/-.005

filename: 1845plmb.dw2

B. HULCHER EXT. 44289

18 INCH AXIAL SHOE

QUANTITY: 1

MATERIAL: 17-4 STAINLESS

SURFACE FINISH: 32 RMS MIN. ALL SURFACES

TOLERANCES: +/-.005 UOS

FILENAME: 18AXIAL.DW2

B. HULCHER EXT. 44289

BREAK ALL CORNERS AND SHARP EDGES .030 MAX. UOS

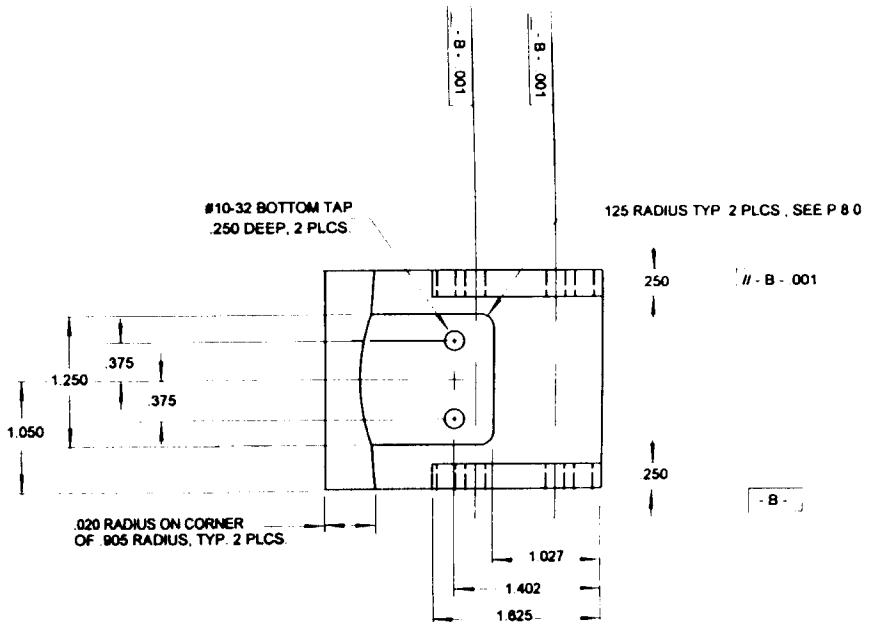

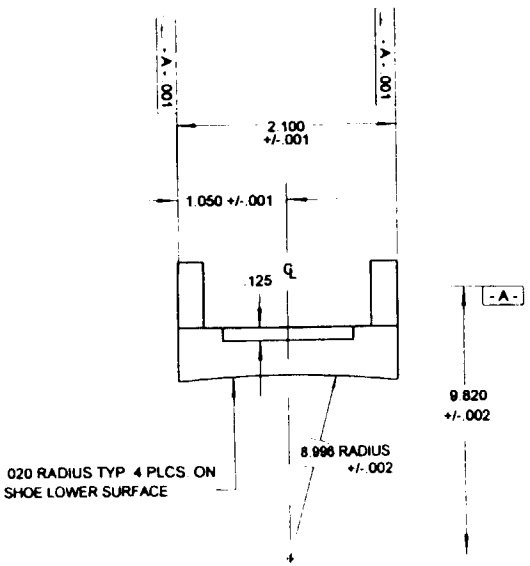

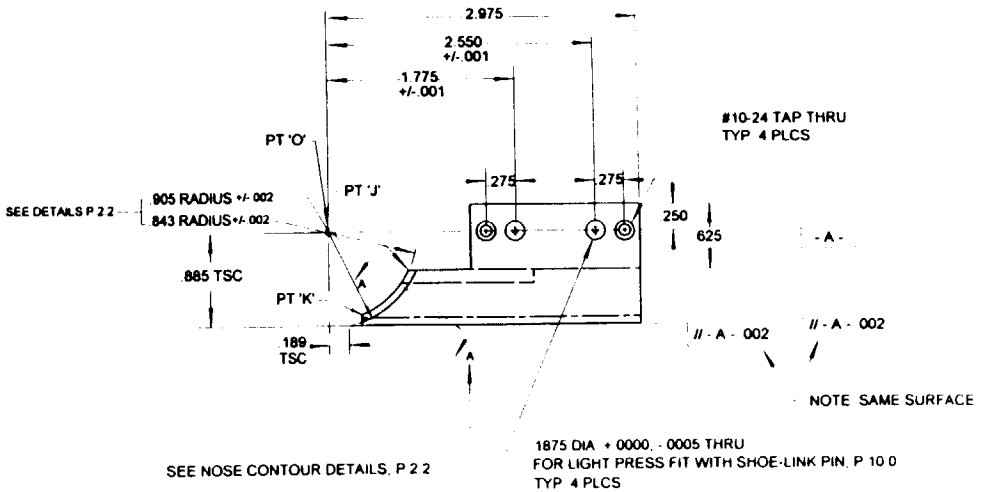

18 INCH AXIAL SHOE
NOSE CONTOUR DETAILS

CONTOUR TOLERANCES: +/-.002

SURFACE FINISH: 32 RMS MIN. ALL SURFACES

FILENAME: 18AXIAL.DW2

B. HULCHER EXT 44289

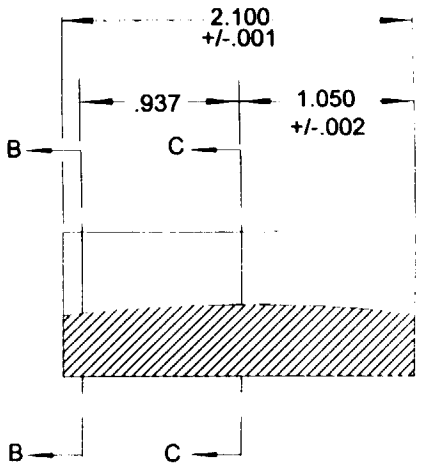

SECTION A-A

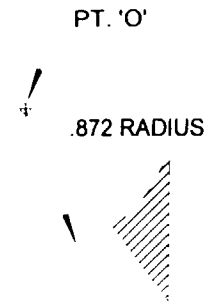

SECTION B-B

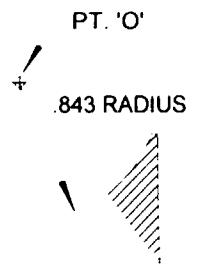

SECTION C-C

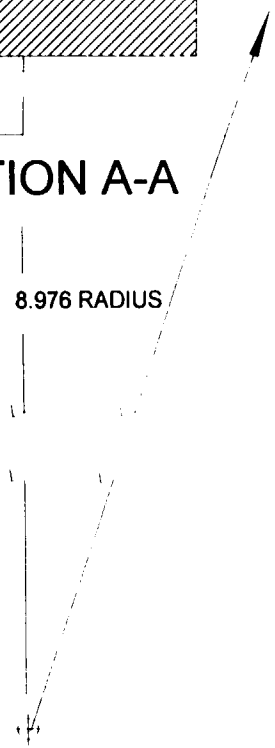

NOTE: ALL SECTIONS TAKEN RADIALLY THRU PT 'O'
AS IN SECTION A-A WILL BE IDENTICAL TO SECTION A-A
FROM PT. 'J' TO PT. 'K'. (SEE P 2.1)

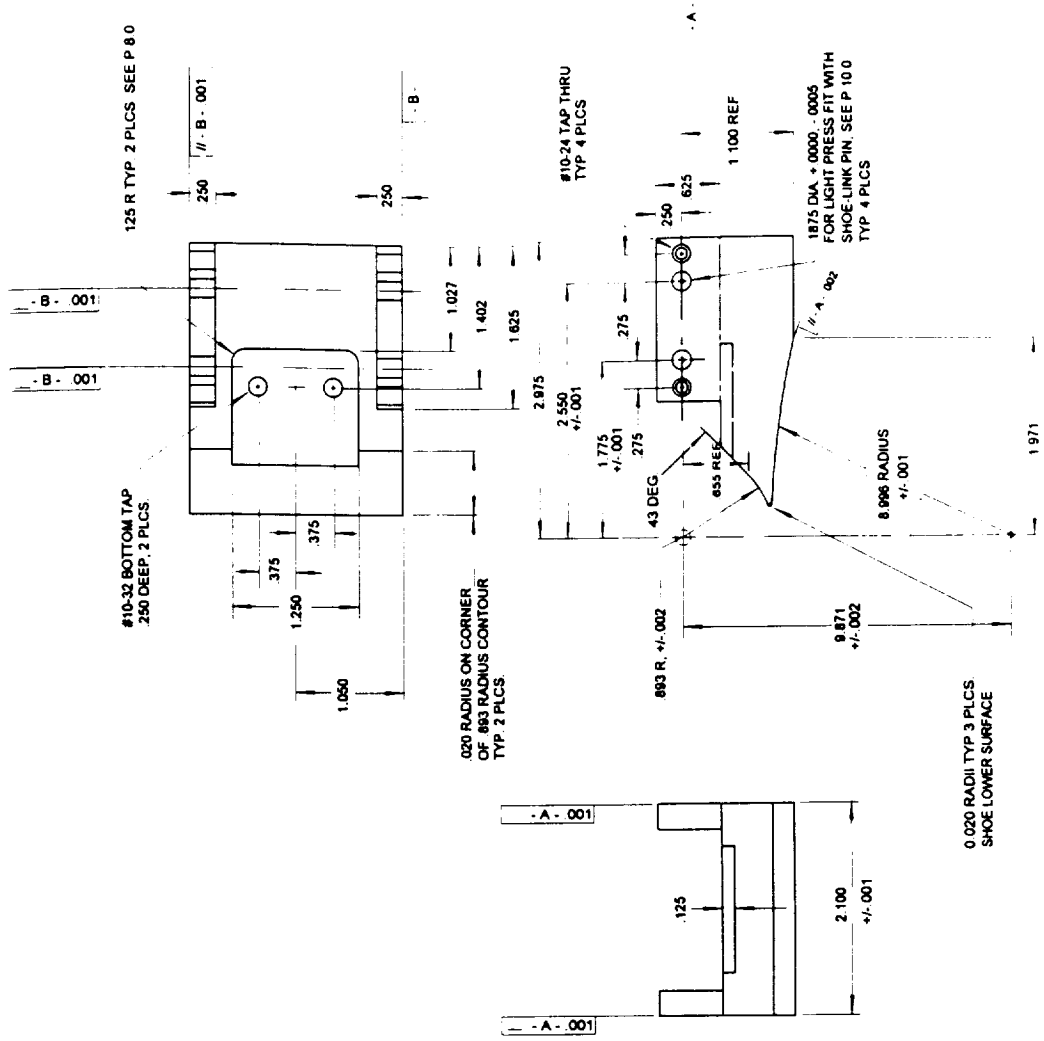

18 INCH HOOP SHOE

QUANTITY: 1

MATERIAL: 17-4 STAINLESS

TOLERANCES: +/-.005 UOS

SURFACE FINISH: 32 RMS MIN. ALL SURFACES

B. HULCHER EXT 44286

BREAK ALL CORNERS AND SHARP EDGES .030 MAX. UOS

18 INCH FLAT SHOE

QUANTITY: 1
MATERIAL: 17-4 STAINLESS
SURFACE FINISH: 32 RMS MIN. ALL SURFACES
TOLERANCES: +/-.005 UOS
[illegible]

B. HULCHER EXT. 44289

BREAK ALL CORNERS AND SHARP EDGES .030 MAX. UOS

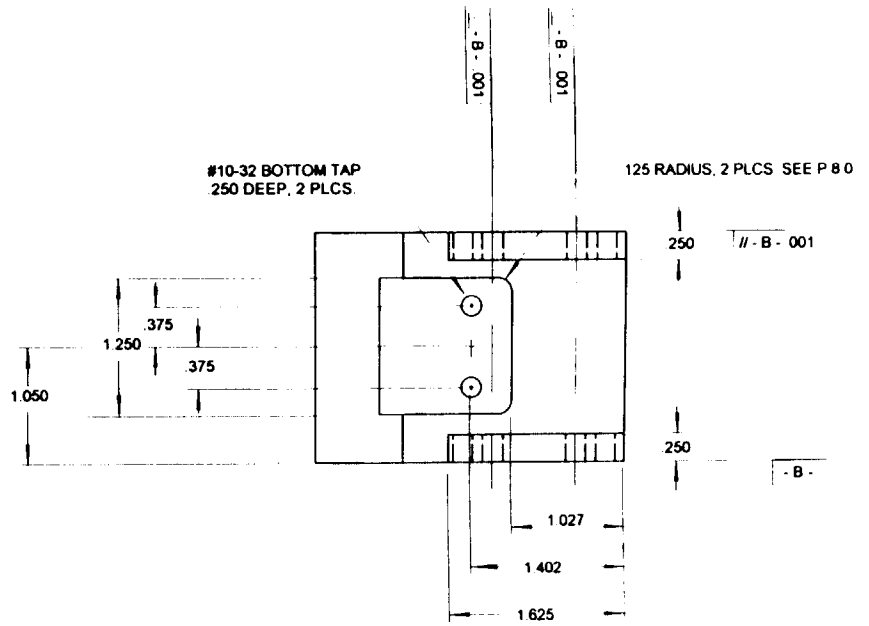

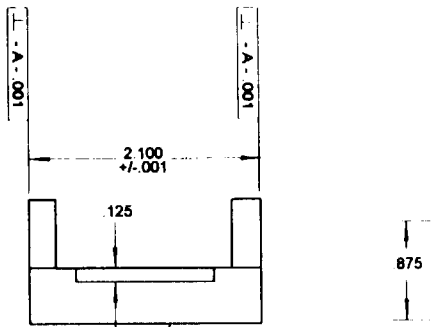

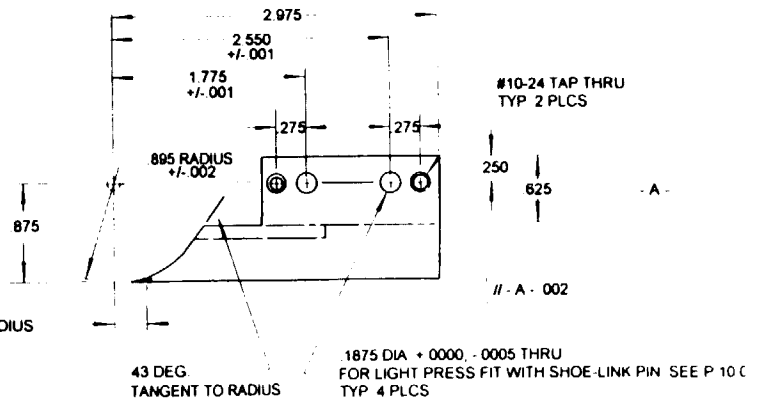

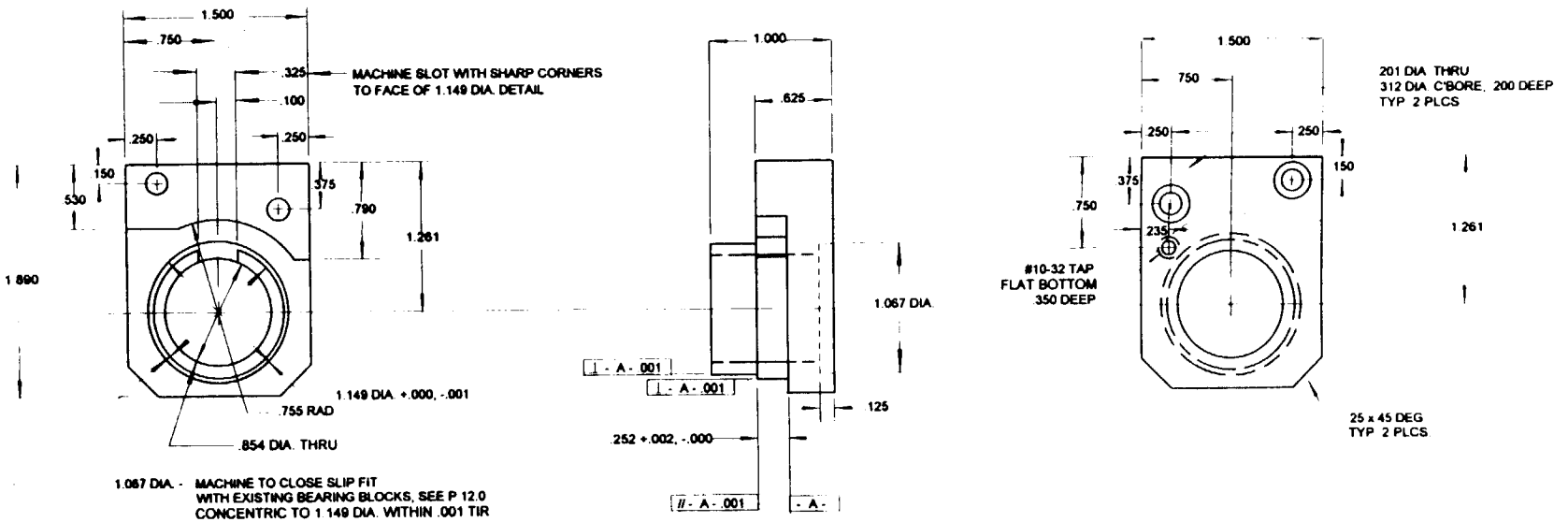

BEARING CAP

QUANTITY REQUIRED: 2 -ONE AS SHOWN
ONE OPPOSITE HAND

MATERIAL: 17-4 STAINLESS

SURFACE FINISH: 32 RMS MIN. ALL SURFACES

TOLERANCES: +/-.005 UOS

filename: 18incap.dw2

B. HULCHER EXT. 44289

BREAK ALL CORNERS AND SHARP EDGES .030 MAX.

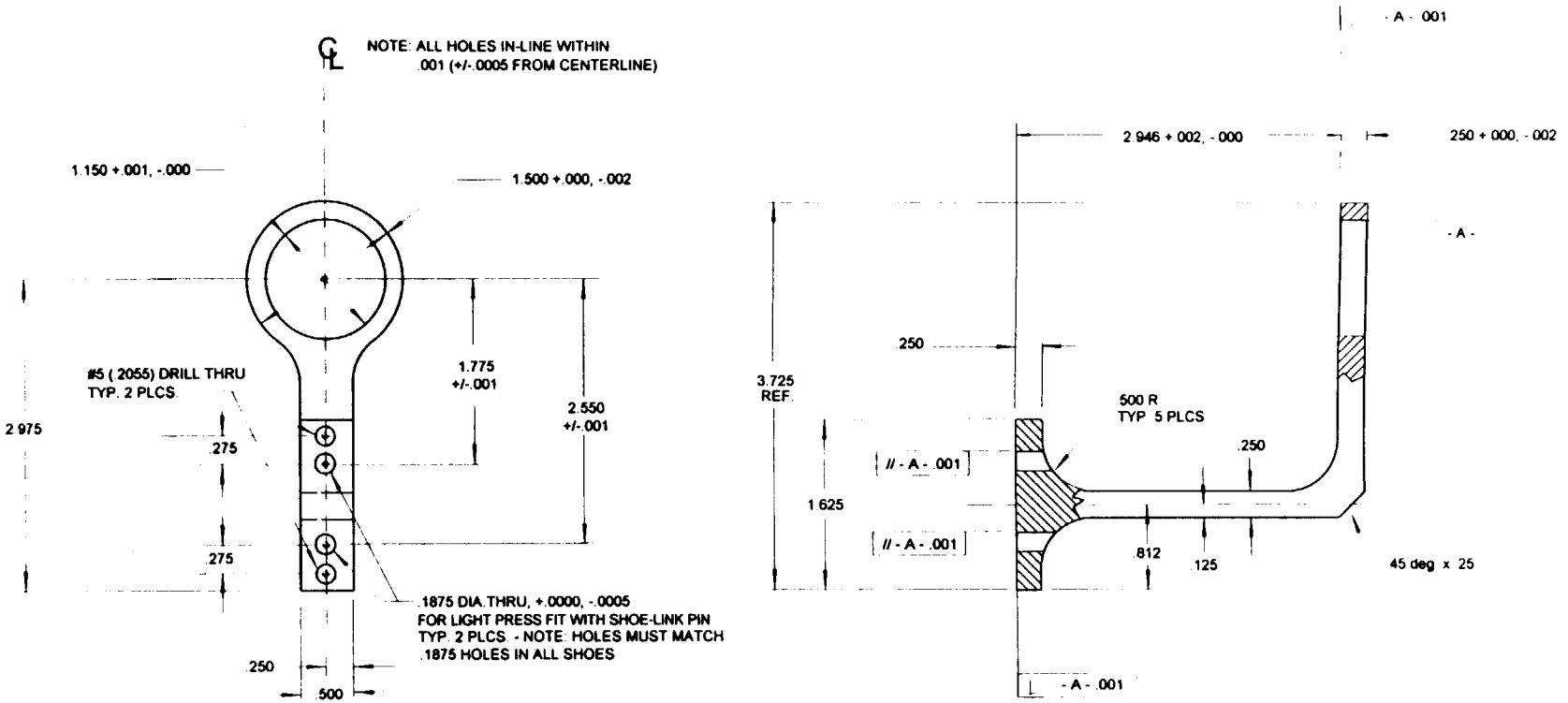

LINK

QUANTITY REQUIRED: 2
MATERIAL: 17-4 STAINLESS
SURFACE FINISH: 32 RMS MIN. ALL SURFACES
TOLERANCES: +/-.005 UOS

filename: 18link.dw2

B HULCHER EXT 44289

BREAK ALL CORNERS AND SHARP EDGES .030 MAX.

CYLINDER MOUNT

QUANTITY: 1

MATERIAL: 17-4 STAINLESS

SURFACE FINISH: 32 RMS MIN. ALL SURFACES

TOLERANCES: +/-.005 UOS

filename: 18cylmnt.dw2

B. HULCHER EXT. 44289

BREAK ALL CORNERS AND SHARP EDGES .030 MAX.

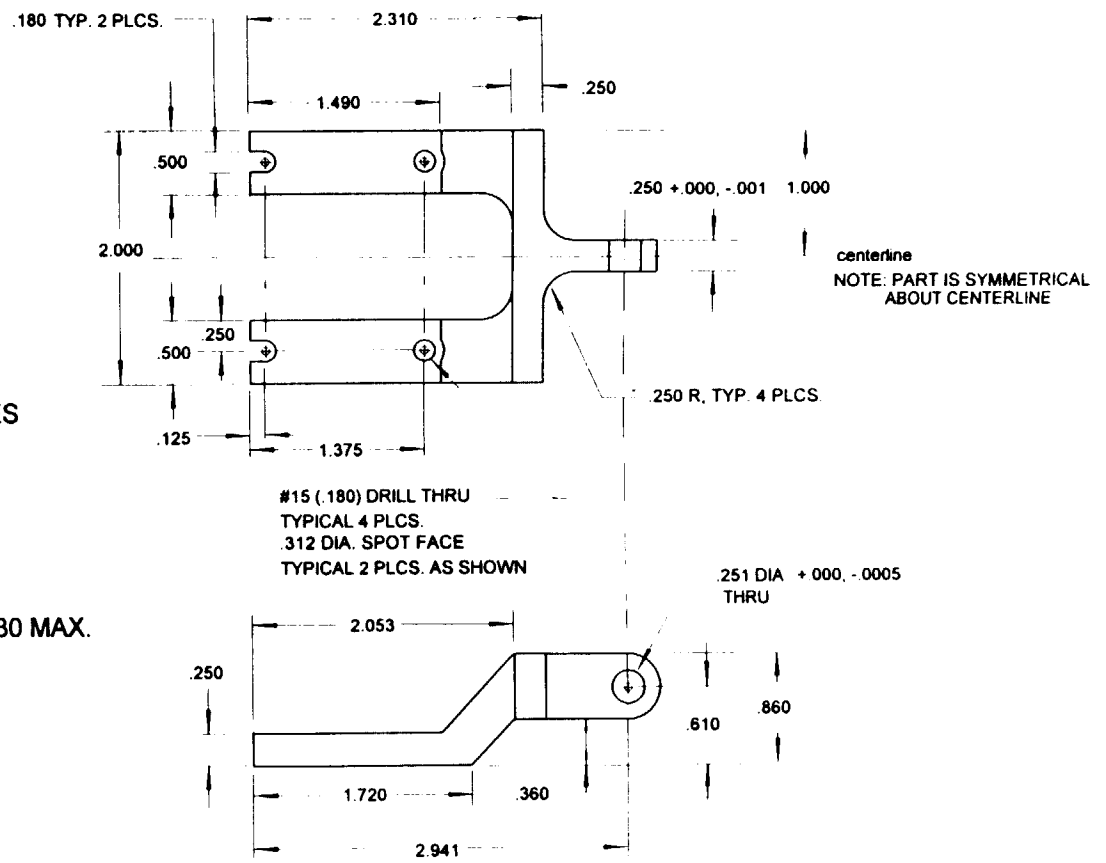

APPENDIX C

HYDROGEN PERMEABILITY PROPERTIES OF SELECTED COMPOSITE MATERIALS

C.1 Introduction

Extensive use of composite materials is necessary in such applications as advanced reusable launch vehicles where mass (i.e., specific strength) considerations are of great importance. The development of such structures for use in large cryogenic fuel tank applications requires that data on the permeability of these materials to liquid hydrogen be obtained. McDonnell Douglas Corporation, as part of its work on the National Aerospace Plane project (NASP), and as part of their Internal Research and Development activities (IRAD), conducted studies to characterize several materials for cryogenic applications. Tests were performed under both thermal and mechanical cycling in an attempt to simulate possible in-flight loading conditions [23].

C.2 Permeability and Tensile Strength Test Results

The test specimens used in the study were disks of 2 inches in diameter. The disks were placed in a sealed fixture and put into a dewar of liquid nitrogen or helium so that the desired temperature could be reached during testing. Hydrogen gas was introduced on one side of the specimen at 20-psig. The far side of the specimen was evacuated by a vacuum pump and a residual gas analyzer (RGA) was connected. The limit, or minimal detectable permeation rate, of this experimental set-up was approximately 2×10^{-6} standard cubic centimeters per second per square inch (scc/in^2). Several materials were

chosen for initial permeability testing at 78K (liquid nitrogen temperatures) with thermal cycling only; further testing was conducted on materials showing no detectable permeation during the first round. The second set of tests was conducted under both thermal and mechanical cycling at 4K (liquid helium temperatures). The results of this set are given in Tables C.1.

Tensile tests were also conducted, both prior to, and after, thermal and mechanical cycling on the same materials at 4K. The results indicate no significant decrease in the strengths of these materials within the limits of the data scatter. The results of these tests are presented in Table C.2 [23].

Table C.1 Summary of permeation tests with both thermal and mechanical cycling [23].

Material System	Material Type[4]	Uncycled Permeation @ 4K (scc/s/in^2)	Permeation at 4 K after thermal cycling[1] (scc/s/in^2)	Permeation at 4Kafter thermal and mechanical cycling[2] (scc/s/in^2)	Material Layup
IM6/APC-2 (PEEK)	T/P	$< 2 \times 10^{-6}$	$< 2 \times 10^{-6}$	$< 2 \times 10^{-6}$	[+45, -45, 0, 0, 0, -45, +45]
AS4/8551-7	T/S	$< 2 \times 10^{-6}$	$< 2 \times 10^{-6}$	$< 2 \times 10^{-6}$	[+45, -45, 0, 0, -45, +45]
IM6/18271-E	T/S	$< 2 \times 10^{-6}$	$< 2 \times 10^{-6}$	$< 2 \times 10^{-6}$	[+45, -45, 0, 0, +45, +45]
IM6/1827	T/S	$< 2 \times 10^{-6}$	$< 2 \times 10^{-6}$	$< 2 \times 10^{-6}$	[+45, 0, -45, +45, 0, +45]
T40/9405[3]	T/S	$< 2 \times 10^{-6}$	$< 2 \times 10^{-6}$	$< 6 \times 10^{-4}$	[0, 90, FM1000, 90, 0]

Note 1: Thermal cycling consisted of 150 cycles from room temperature to 4K.
Note 2: Mechanical cycling consisted of 150 cycles at 4K from 0 to 43-ksi.
Note 3: Specimens with FM1000 epoxy film interleaf layer.
Note 4: T/P = thermoplastic, T/S = thermoset.

Table C.2 Summary of tensile tests with and without thermal and mechanical cycling [23].

Material System	Material Type[6]	Uncycled Tensile at RT (ksi)	Uncycled Tensile at 4 K (ksi)	Tensile at 4 K after thermal cycling[3] (ksi)	Tensile at 4 K after thermal and mechanical cycling[4] (ksi)	Material Layup
IM6/APC-2 (PEEK)	T/P	145.2 (2)[1]	153.0 (4) SD[2] = 24.4	172.8 (4) SD = 27.8	172.2 (6) SD = 13.1	[+45, -45, 0, 0, 0, -45, +45]
AS4/8551-7	T/S	-	152.0 (4) SD = 3.3	-	164.6 (4) SD = 7.0	[+45, -45, 0, 0, -45, +45]
IM6/18271-E	T/S	-	127.2 (4) SD = 4.9	-	116.6 (2)	[+45, -45, 0, 0, +45, +45]
IM6/1827	T/S	-	100.4 (4) SD = 8.4	-	109.8 (2)	[+45, 0, -45, +45, 0, +45]
T40/9405[5]	T/S	-	94.8 (2)	-	121.0 (2)	[0, 90, FM1000, 90, 0]

Note 1: Numbers in parentheses indicate quantity of specimens tested.
Note 2: SD represents the standard deviation.
Note 3: Thermal cycling consisted of 150 cycles from room temperature to 4 K.
Note 4: Mechanical cycling consisted of 150 cycles at 4 K from 0 to 43-ksi.
Note 5: Specimens with FM1000 epoxy film interleaf layer.
Note 6: T/P = thermoplastic, T/S = thermoset.